Feasibility of irreversible electroporation for pulmonary vein isolation

Master's thesis Technical Medicine
Medical Sensing and Simulation

by

Marijn Groen

April, 2018

Graduation committee

Prof. Dr. Slump
Dr. R.J. Hassink
Dr. R. Van Es
Dr.ir. T. Heida
Drs. R. Haarman

UNIVERSITY OF TWENTE.

UMC Utrecht

Index

Chapter 1 1-4

Introduction

Chapter 2 2-13

In vitro analysis of the origin and characteristics of gaseous micro-emboli during catheter mediated electroporation ablation

Chapter 3 3-24

In vivo analysis of the origin and characteristics of gaseous micro emboli during catheter mediated irreversible electroporation

Chapter 4 4-34

Qualitative temperature measurements during catheter IRE-ablation, using Schlieren imaging.

Chapter 5 5-41

Difference in lesion depth between monophasic anodal and cathodal pulses using irreversible electroporation ablation

Chapter 6 6-46

Determination of the arcing threshold for anodal and cathodal IRE-pulses

Chapter 7 7-51

Difference between biphasic and monophasic pulse using irreversible electroporation ablation

Chapter 8 8-56

Discussion

Chapter 9 9-61

Conclusion

Chapter 10 10-62

Acknowledgements

Appendix A 11-63

JoVE manuscript

1. Introduction

1.1. Atrial fibrillation

Atrial fibrillation (AF) is the most common cardiac arrhythmia, which increases in prevalence with advancing age and comorbidities such as hypertension, obesity, diabetes mellitus, coronary artery disease, chronic kidney disease and valvular heart diseases[1–3]. AF results in a fast and insufficient atrial contraction and an irregular ventricular contraction. AF increases the risk of atrial thrombi, stroke, dementia, left ventricular dysfunction that can ultimately lead to heart failure and mortality[1]. AF often has a large impact on the quality of life of AF-patients, with symptoms varying from complaints of palpitations, fatigue, hypotension and dyspnea[1,4]. AF is divided into three types, depending on the duration of the AF periods: paroxysmal AF, which is self-terminating AF in <7 days; persistent AF, in which AF sustained for >7 days; and long-standing persistent AF, in which AF sustained for >12 months[1].

1.1.1. Electrical conduction

Normal contraction of the heart is induced by electrical stimuli and regulated by the autonomic nerves of the peripheral nerves system. The electric stimulus is generated by the sinoatrial (SA) node in the high right atrium (**Figure 1.1A**). This pulse causes the atria to contract and continues through the atrioventricular (AV) node, located in the middle between the atria and ventricles. In the AV node the pulse is delayed for 120-200 milliseconds, to allow the atria to fully contract. Then, the electrical signal continues through to the bundle of His, through the two bundle branches (left and right) down the septum, through the Purkinje fibers into the left and right ventricle causing the ventricles to contract.

With AF, rapidly firing ectopic foci constantly activate the atria at a rate of 400-600 beats per second, leading to a chaotic atrial contraction (**Figure 1.1B**). One of the properties of the AV node is decremental conduction; when the AV is stimulated more frequently, the AV node conduction

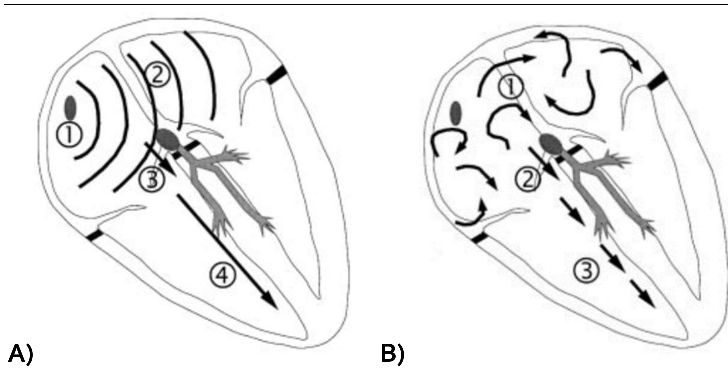

Figure 1.1 Conduction system of the heart. **A)** Normal pathway: starting at SA (1), leading to atrial contraction (2), leading through the AV-node (3) to ventricular contraction (4). **B)** Abnormal pathway causing AF: starting at random signals in the atria (1) leading through the AV-node (2) to fast ventricular contraction (3). Images obtained from a paper of Waktare[5].

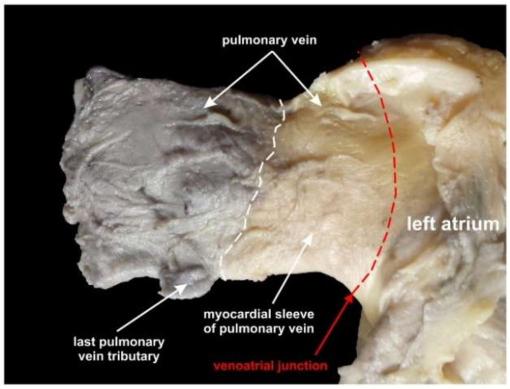

Figure 1.2 Left superior pulmonary vein with a myocardial sleeve. Obtained from Klimek-Piotrowskat *et al.*[6].

becomes slower. Therefore, not all of the chaotic signals from the atria are propagated to the ventricles, resulting in an fast and irregular ventricular rhythm. The pulmonary veins are often the origin of erratic electrical signals, and therefore play an important role in the cause and maintaining of AF (**Figure 1.2**)[6,7].

1.2. Treatment

At first, AF is medically treated by lowering the ventricular rate for rate control, with the use of for example beta blockers or calcium channel blockers. Depending on different patient characteristics e.g. degree of symptoms, presence of a structural heart disease, type of AF etc., in addition on, or as an alternative for rate control, rhythm control strategies are preferred[4]. Rhythm control can be achieved by electrical or pharmacological cardioversion, or by catheter ablation by the means of a pulmonary vein isolation (PVI).

1.2.1. Pulmonary vein isolation

The aim of PVI is to electrically isolate the pulmonary veins (PV) from the left atrium (LA), thereby preventing the electrical impulses originating at the pulmonary veins from reaching the LA. During this procedure a sheath is inserted via the right femoral vein. A trans septal puncture is performed, to gain access to the LA with the ablation catheter. Isolation of the PVs is accomplished by creating a continuous circumferential lesion in the antrum of each PV. Isolation of the PVs is confirmed by either confirmation of an entrance block in the PVs by using a circular mapping catheter, or by confirmation of an exit block by confirmation of no atrial capture after stimulation in the PVs[8].

1.2.2. Radiofrequency ablation

The most commonly used method for PVI is radiofrequency (RF) ablation[9]. With RF-ablation, an alternating high frequency electrical current is used to create thermal lesion formation by tissue heating of ≥50°C. The long-term success remains limited and often multiple procedures are required, particularly in longstanding persistent AF[10–14]. In addition, several complications can occur as a result of the thermal energy used with RF-ablation[15,16]. Blood clots can be formed by protein aggregation and may lead to neurological complications[17,18]. Excessive heating may cause collateral damage to surrounding tissue, e.g. causing damage to the phrenic nerves[19], coronary arteries[20], esophagus[15,21,22] and can lead to PV stenosis[16,23]. Furthermore, lesion formation with RF-ablation is influenced by blood flow by means of a heat sink effect, limiting lesion size[17,24]. A comprehensive description on lesion formation during RF-ablation was published by Wittkampf *et al.*[25].

1.2.3. Cryothermal ablation

Unlike damage by heating with RF ablation, cryoenergy ablation uses freezing of tissue to create hypothermic tissue injury[26–28]. Temperatures below -80ºC are used to freeze target tissue, thereby creating lesions. For cryoablation a catheter with an inflatable balloon is used, which can be inflated inside the PVs. Correct placement of the cryoballoon is confirmed by means of fluoroscopic images and contrast injection, which might induce a prolonged fluoroscopy time compared to RF-ablation[29]. Possible complications of cryothermal ablation are PV stenosis, phrenic nerve injury, and stroke[28]. Long-term efficacy and safety of cryothermal ablation compared to RF ablation appears to be similar[26,30,31].

1.2.4. Direct-current ablation

Up until the development of RF-ablation in the early 1990s, direct current (DC) catheter ablation was commonly used to perform cardiac ablations[32]. With DC-ablation, a large current was applied between a standard single electrode pacing catheter and a skin plate. Lesion formation was mainly attributed to the generation of pressure waves caused by arcing at the catheter electrode[33]. However, severe complications related to barotrauma due to the arcing and a high pressure shock wave occurred. Ahsan *et al.* developed low-energy DC ablation, which resulted in adequate lesion formation while decreasing the number of complications[34–36]. Even though low-energy DC-ablation was successful, it was abandoned after the introduction of RF-ablation.

1.2.5. Irreversible electroporation ablation

Recently, irreversible electroporation (IRE), low-energy DC, was reinvestigated as an alternative method for PVI[37]. With IRE a high current is applied between a multi-electrode circular catheter and a skin electrode, using a monophasic defibrillator[37]. IRE ablation is based on changes in the membrane potential and subsequent permeabilization in the lipid bilayers[38–42]. Depending on the electric field strength, pulse duration, pulse shape, frequency and polarity the permeabilization can be reversible or irreversible[41]. With IRE ablation, the electric field strength is high around the catheter, resulting in electroporation of the cells near the catheter. The so-called nanopores cause a disrupted cell homeostasis and subsequently the cell will go into apoptosis. The myocardial cells will be replaced by fibrosis, causing electrical isolation of the PVs. IRE is capable of producing permanent damage to tissue within a fraction of a second[40]. Over the past years, the feasibility of IRE was investigated in multiple porcine studies, using circular multi-electrode catheters[20,23,37,43,44]. These studies demonstrated the feasibility of using a circular catheter for performing PVI using IRE[37], the possibility of creating a continuous lesion depth of >4mm[44] and the absence of complications associated with RF ablation as for example nerve injury, PV stenosis and damage to arteries[20,43,45]. Although the low susceptibility to electroporation of certain tissue types is previously documented, the exact reason is unknown.

1.3. PVI using IRE ablation

At the moment, an external monophasic defibrillator (Lifepak 9, Physio Control, Redmond, WA) is used to deliver the high direct current, between a multi-electrode catheter and an indifferent skin patch[37]. In **Appendix A** – JoVE manuscript, an extensive description of the procedural steps during an animal experiment with PVI using IRE ablation, including a schematic overview of all used equipment, is given.

To produce an IRE-ablation, the defibrillator is used to deliver a current between the catheter and the indifferent skin patch. The defibrillator consists of a capacitor (54.2 µF), an inductor (40 mH) and a power source (**Figure 1.3A**). Using the monophasic defibrillator, a specific energy can be selected. Depending on the total system resistance of the patient, this energy will result in a specific delivered current and voltage (**Figure 1.4A**). To measure the delivered voltage and current waveforms, an oscilloscope (Tektronix TDS 2002B) in combination with a hall sensor and a voltage divider is used

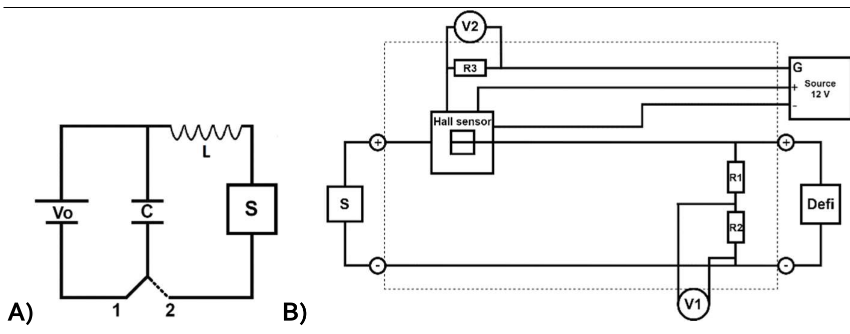

Figure 1.3 A) Simplified scheme of a defibrillator with a power source (Vo), a capacitor (C), an inductor (L) and the subject (S) with catheter and skin patch. The capacitor is charged by connecting the power source in series (circuit 1). For pulse delivery, the capacitor is discharged through an electrical circuit between the catheter, the subject and the indifferent patch (circuit 2). **B)** Scheme of the current and voltage measurement box (dotted line). Two resistances are placed in series (R1 and R2) to measure the voltage (V1) using the oscilloscope. The ratio in resistance between R1/R2 is 1/999, indicating the measured V1 should be multiplied by 1000 to determine the total voltage. The hall sensor is connected to a power source and results in a output voltage which is measured (V2).

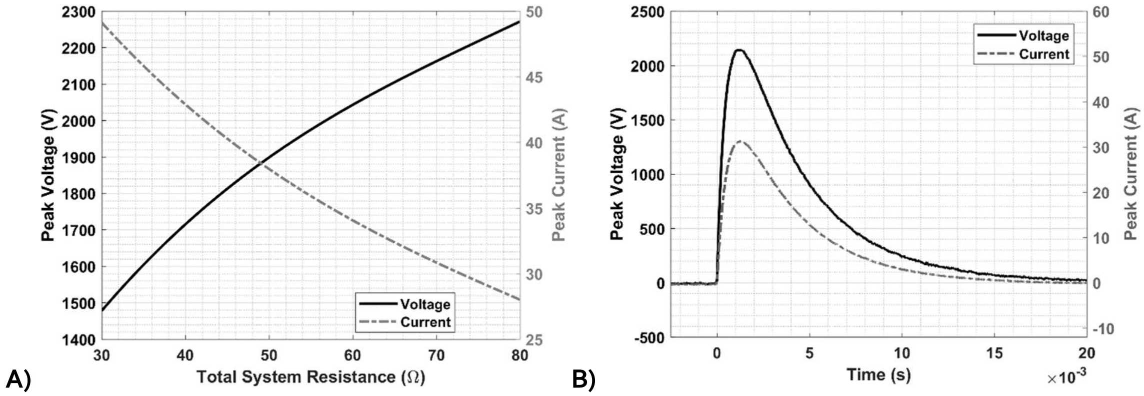

Figure 1.4 A) Resulting peak voltage and current of 200 J IRE-pulses using different system resistances. **B)** Example of the voltage and current waveform (200 J, cathodal IRE-pulse).

(**Figure 1.3B**). Previous work showed that cathodal IRE-pulses of 200 J were able to create lesions deep enough for PV isolation, without arcing at the electrodes[44]. A total system resistance of 65 Ω using 200 J will result in ±33 A and ±2100 V (**Figure 1.4B**).

1.3.1. Catheter

A custom 7F multi-electrode circular catheter (Abbott, St. Paul, MN, USA) with a variable hoop diameter is used (**Figure 1.5**). The catheter consists of 14 electrodes of 2.5 mm, spaced 3.5 mm apart, resulting in a total electrode surface of 256 mm^2. Due to this larger total electrode surface, the current density at the same energy level will be lower for a multi-electrode catheter compared to the single electrode DC-ablation. Therefore, IRE-pulses can be produced without arcing, but still leading to a sufficient lesion depth[37,40]. The hoop of the catheter is adjustable between 16-mm and 27-mm, to match the variable diameter of the human pulmonary veins ostia.

1.4. Aim of this thesis

Although IRE seems to be a safe method for PVI, a few aspects need to be studied before the technique can be used during human studies.

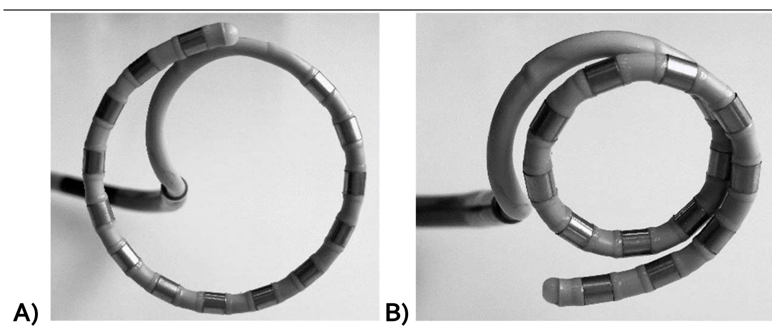

Figure 1.5 A 14-electrode catheter with a variable hoop diameter with **A)** a large diameter of 27-mm and **B)** a small diameter of 16-mm.

I. Bubble formation

The delivery of a current through an solution containing electrolytes, e.g. blood, will induce a chemical reaction at the electrodes, resulting in the formation of gas. This process is called electrolysis.

The generation of gaseous micro emboli (GME) during cardiac catheter ablations may be hazardous.[46] GME may obstruct blood flow in capillary vessels resulting in neurological ischemia and tissue damage, e.g. causing stroke[47]. GME may also embolize the coronary arteries; only 0.1-0.2 mL of gas is thought to be sufficient to cause myocardial damage[46].

The main cause of gas formation at the electrode surface is thought to be electrolysis, driven by the delivered charge. Oxygen (O_2) collects at the positive (anodal) electrode while hydrogen (H_2) collects at the negative (cathodal) electrode. Therefore, we expect that the polarity of the catheter influences the bubble formation. Besides pulse polarity, hoop diameter may affect the current distribution at the metal electrode surface and may thus affect electrolysis.

Both an *in vitro* set up (**chapter 2**) and an *in vivo* set up (**chapter 3**) are used to investigate the influence of the delivered charge, the polarity of the catheter and the catheter hoop diameter on bubble gas formation during IRE-ablation.

II. Temperature measurements

IRE-ablation is thought to be a non-thermal modality to create tissue damage, since cell damage is based on ultra-short delivery of electrical pulses [40,48]. However, some studies suggest that application of IRE-ablation will result in a temperature rise due to Joule heating[49–51]. Since an important advantage of IRE-ablation over the current ablation techniques is thought to be the lack of thermal damage, we need to investigate temperature development during IRE-ablation. Earlier research of Bos *et al.*[50], showed that temperature changes during IRE are influenced by e.g. voltage, pulse length and electrode-electrode distance. However, in their study they used a single electrode for IRE, and therefore these results are not directly translatable to our IRE set up.

An *in vitro* set up (**chapter 4**) is used to research the effect of delivered charge, polarity and catheter hoop diameter on temperature changes during IRE-ablation, using color Schlieren imaging; a method to visualize temperature changes.

III. Comparison of lesion depth; anodal versus cathodal IRE-pulses

Based on the results found in **chapter 2** and **3**, it might be beneficial to use anodal IRE-pulses instead of cathodal IRE-pulses. However, all previous efficacy studies were based on cathodal IRE-pulses[44,52,53]. No difference in lesion depth is expected, since the only difference is the direction of the current. However, no studies have been performed to confirm this assumption. Therefore, the lesion depth as created by anodal IRE-pulses is compared with the lesion depth as created by cathodal IRE-pulses in an *in vivo* set up (**chapter 5**).

IV. Comparison of lesion depth; anodal versus cathodal IRE-pulses

As explained before, IRE-ablation is based on non-arcing delivery of IRE-pulses. However, previous studies were not conclusive about the difference in arcing threshold between anodal and cathodal IRE-pulses[34,35,37,54]. To ensure safe application of the IRE-pulses, we need to determine the arcing threshold for both anodal and cathodal IRE-pulses. Therefore, the arcing threshold for anodal IRE-pulses is compared with cathodal IRE-pulses in an *in vivo* set up (**chapter 6**).

V. Comparison of lesion depth: monophasic versus biphasic IRE-pulses

In the current IRE set up, a monophasic defibrillator is used, as based on the previous DC-ablation method (**section 1.2.4**). However, nowadays the use of a biphasic waveform is recommended for defibrillation by the European Resuscitation Council Guidelines[55]. Therefore, the use of a monophasic waveform is outdated and almost all monophasic defibrillator are replaced by biphasic defibrillators. Subsequently we might be interested in replacing the monophasic defibrillator by a biphasic defibrillator, to increase the availability of our ablation modality. Although biphasic pulses are more successful for defibrillation, several studies are ambiguous about the actual cell damage as created by biphasic defibrillation[56–59]. None of these studies focused on cell damage as created by single monophasic and biphasic pulses, therefore we are interested in the difference in lesion depth between the two modalities in our set up. In an *in vivo* set up (**chapter 7**) the lesion depth and width as created by monophasic and biphasic IRE-pulses are compared.

1.5. References

1. Kirchhof Kolh Kirchhof, P., Benussi, S., Kotecha, D., Ahlsson, A., Atar, D. & Casadei, B. 2016 ESC Guidelines for the management of atrial fibrillation developed in collaboration with EACTS. Eur. Heart J. 18 (11), 1609–1678 (2016).
2. Langenberg, M., Hellemons, B. S., van Ree, J. W., Vermeer, F., Lodder, J., Schouten, H. J., et al. Atrial fibrillation in elderly patients: prevalence and comorbidity in general practice. BMJ Br. Med. J. 313 (7071), 1534 (1996).
3. Vermond, R. A., Geelhoed, B., Verweij, N., Tieleman, R. G., Van Der Harst, P., Hillege, H. L., et al. Incidence of Atrial Fibrillation and Relationship With Cardiovascular Events, Heart Failure, and Mortality A Community-Based Study From the Netherlands. J. Am. Coll. Cardiol. 66 (9), 1000–1007 (2015).
4. January, C. T., Samuel Wann, L., Alpert, J. S., Field, M. E., Calkins, H., Murray, K. T., et al. 2014 AHA/ACC/HRS Guideline for the Management of Patients With Atrial Fibrillation. Circulation 129 , (2014).
5. Waktare, J. E. P. Atrial fibrillation. Circulation 106 (1), 14–16 (2002).
6. Klimek-Piotrowska, W., Hołda, M. K., Piątek, K., Koziej, M. & Hołda, J. Normal distal pulmonary vein anatomy. PeerJ 4 , e1579 (2016).
7. Haïssaguerre, M., Jaïs, P., Shah, D. C., Takahashi, A., Hocini, M., Quiniou, G., et al. Spontaneous Initiation of Atrial Fibrillation by Ectopic Beats Originating in the Pulmonary Veins. N. Engl. J. Med. 339 (10), 659–666 (1998).
8. Gerstenfeld, E. P., Dixit, S., Callans, D., Rho, R., Rajawat, Y., Zado, E., et al. Utility of exit block for identifying electrical isolation of the pulmonary veins. J. Cardiovasc. Electrophysiol. 13 (10), 971–9 (2002).

9. Cappato, R., Calkins, H., Chen, S. A., Davies, W., Iesaka, Y., Kalman, J., et al. Updated worldwide survey on the methods, efficacy, and safety of catheter ablation for human atrial fibrillation. Circ. Arrhythmia Electrophysiol. 3 (1), 32–38 (2010).
10. Rostock, T., Salukhe, T. V., Steven, D., Drewitz, I., Hoffmann, B. A., Bock, K., et al. Long-term single- and multiple-procedure outcome and predictors of success after catheter ablation for persistent atrial fibrillation. Hear. Rhythm 8 (9), 1391–1397 (2011).
11. Katritsis, D., Wood, M. A., Giazitzoglou, E., Shepard, R. K., Kourlaba, G. & Ellenbogen, K. A. Long-term follow-up after radiofrequency catheter ablation for atrial fibrillation. Europace 10 (4), 419–424 (2008).
12. Bertaglia, E., Tondo, C., De Simone, A., Zoppo, F., Mantica, M., Turco, P., et al. Does catheter ablation cure atrial fibrillation? Single-procedure outcome of drug-refractory atrial fibrillation ablation: A 6-year multicentre experience. Europace 12 (2), 181–187 (2010).
13. Kumar, S., Barbhaiya, C. R., Balindger, S., John, R. M., Epstein, L. M., Koplan, B. A., et al. Better lesion creation and assessment during catheter ablation. J. Atr. Fibrillation 8 (3), (2015).
14. Teunissen, C., Kassenberg, W., Van Der Heijden, J. F., Hassink, R. J., Van Driel, V. J. H. M., Zuithoff, N. P. A., et al. Five-year efficacy of pulmonary vein antrum isolation as a primary ablation strategy for atrial fibrillation: A single-centre cohort study. Europace 18 (9), 1335–1342 (2016).
15. Scanavacca, M. I., D'Ávila, A., Parga, J. & Sosa, E. Left atrial-esophageal fistula following radiofrequency catheter ablation of atrial fibrillation. J. Cardiovasc. Electrophysiol. 15 (8), 960–962 (2004).
16. Saad, E. B., Marrouche, N. F., Saad, C. P., Ha, E., Bash, D., White, R. D., et al. Pulmonary Vein Stenosis after Catheter Ablation of Atrial Fibrillation: Emergence of a New Clinical Syndrome. Ann. Intern. Med. 138 (8), 634–638+I41 (2003).
17. Yokoyama, K., Nakagawa, H., Wittkampf, F. H. M., Pitha, J. V., Lazzara, R. & Jackman, W. M. Comparison of electrode cooling between internal and open irrigation in radiofrequency ablation lesion depth and incidence of thrombus and steam pop. Circulation 113 (1), 11–19 (2006).
18. Sauren, L. D., Van Belle, Y., De Roy, L., Pison, L., La Meir, M., Van Der Veen, F. H., et al. Transcranial measurement of cerebral microembolic signals during endocardial pulmonary vein isolation: Comparison of three different ablation techniques. J. Cardiovasc. Electrophysiol. 20 (10), 1102–1107 (2009).
19. Sacher, F., Monahan, K. H., Thomas, S. P., Davidson, N., Adragao, P., Sanders, P., et al. Phrenic Nerve Injury After Atrial Fibrillation Catheter Ablation. Characterization and Outcome in a Multicenter Study. J. Am. Coll. Cardiol. 47 (12), 2498–2503 (2006).
20. Du Pré, B. C., Van Driel, V. J., Van Wessel, H., Loh, P., Doevendans, P. A., Goldschmeding, R., et al. Minimal coronary artery damage by myocardial electroporation ablation. Europace 15 (1), 144–149 (2013).
21. Pappone, C., Oral, H., Santinelli, V., Vicedomini, G., Lang, C. C., Manguso, F., et al. Atrio-esophageal fistula as a complication of percutaneous transcatheter ablation of atrial fibrillation. Circulation 109 (22), 2724–2726 (2004).
22. Doll, N., Borger, M. A., Fabricius, A., Stephan, S., Gummert, J., Mohr, F. W., et al. Esophageal perforation during left atrial radiofrequency ablation: Is the risk too high? J. Thorac. Cardiovasc. Surg. 125 (4), 836–842 (2003).
23. Van Driel, V. J. H. M., Neven, K. G. E. J., Van Wessel, H., Du Pré, B. C., Vink, A., Doevendans, P. A. F. M., et al. Pulmonary vein stenosis after catheter ablation electroporation versus radiofrequency. Circ. Arrhythmia Electrophysiol. 7 (4), 734–738 (2014).
24. Meo, J. P., Scanavacca, M., Sosa, E., Correia, A., Hachul, D., Darrieux, F., et al. Atrial coronary arteries in areas involved in atrial fibrillation catheter ablation. Circ. Arrhythmia Electrophysiol. 3 (6), 600–605 (2010).
25. Wittkampf, F. H. M. & Nakagawa, H. RF catheter ablation: Lessons on lesions. PACE - Pacing Clin. Electrophysiol. 29 (11), 1285–1297 (2006).
26. Reissmann, B., Metzner, A. & Kuck, K. H. Cryoballoon ablation versus radiofrequency ablation for atrial fibrillation. Trends Cardiovasc. Med. 27 (4), 271–277 (2017).
27. Khairy, P., Chauvet, P., Lehmann, J., Lambert, J., Macle, L., Tanguay, J. F., et al. Lower incidence of thrombus formation with cryoenergy versus radiofrequency catheter ablation. Circulation 107 (15), 2045–2050 (2003).
28. Packer, D. L., Kowal, R. C., Wheelan, K. R., Irwin, J. M., Champagne, J., Guerra, P. G., et al. Cryoballoon ablation of pulmonary veins for paroxysmal atrial fibrillation: First results of the North American arctic front (STOP AF) pivotal trial. J. Am. Coll. Cardiol. 61 (16), 1713–1723 (2013).
29. Tse, H. F., Reek, S., Timmermans, C., Lai-Fun Lee, K., Geller, J. C., Rodriguez, L. M., et al. Pulmonary vein isolation using transvenous catheter cryoablation for treatment of atrial fibrillation without risk of pulmonary vein stenosis. J. Am. Coll. Cardiol. 42 (4), 752–758 (2003).
30. Kuck, K.-H., Brugada, J., Fürnkranz, A., Metzner, A., Ouyang, F., Chun, K. R. J., et al. Cryoballoon or Radiofrequency Ablation for Paroxysmal Atrial Fibrillation. N. Engl. J. Med. 374 (23), 2235–2245 (2016).
31. Chen, Y.-H., Lu, Z.-Y., Xiang, Y.-, Hou, J.-W., Wang, Q., Lin, H., et al. Cryoablation vs. radiofrequency ablation for treatment of paroxysmal atrial fibrillation: a systematic review and meta-analysis. EP Eur. 19 (5), 784–794 (2017).
32. Gallagher, J. J., Svenson, R. H., Kasell, J. H., German, L. D., Bardy, G. H., Broughton, A., et al. Catheter Technique for Closed-Chest Ablation of the Atrioventricular Conduction System. N. Engl. J. Med. 306 (4), 194–200 (1982).
33. Bardy, G. H., Coltorti, F., Stewart, R. B., Greene, H. L. & Ivey, T. D. Catheter-mediated electrical ablation: The relation between current and pulse width on voltage breakdown and shock-wave generation. Circ. Res. 63 (2), 409–414 (1988).

34. Ahsan, A. J., Cunningham, D., Rowland, E. & Rickards, a F. Catheter ablation without fulguration: design and performance of a new system. Pacing Clin. Electrophysiol. 12 (9), 1557–61 (1989).
35. Rowland, E., Cunningham, D., Ahsan, A. & Rickards, A. Transvenous ablation of atrioventricular conduction with a low energy power source. Br. Heart J. 62 (5), 361–366 (1989).
36. Ahsan, A. J., Cunningham, D. & Rowland, E. Low energy catheter ablation of right ventricular outlfow tract tachycardia. Br. Heart J. 65 (3), 231–233 (1991).
37. Wittkampf, F. H., Van Driel, V. J., Van Wessel, H., Vink, A., Hof, I. E., Gründeman, P. F., et al. Feasibility of electroporation for the creation of pulmonary vein ostial lesions. J. Cardiovasc. Electrophysiol. 22 (3), 302–309 (2011).
38. Yarmush, M. L., Golberg, A., Serša, G., Kotnik, T. & Miklavčič, D. Electroporation-Based Technologies for Medicine: Principles, Applications, and Challenges. Annu. Rev. Biomed. Eng. 16 (1), 295–320 (2014).
39. TOVAR, O. & TUNG, L. Electroporation of Cardiac Cell Membranes with Monophasic or Biphasic Rectangular Pulses. Pacing Clin. Electrophysiol. 14 (11), 1887–1892 (1991).
40. Lavee, J., Onik, G., Mikus, P. & Rubinsky, B. A novel nonthermal energy source for surgical epicardial atrial ablation: Irreversible electroporation. Heart Surg. Forum 10 (2), 96–101 (2007).
41. Bilska, A. O., Debruin, K. A. & Krassowska, W. Theoretical modeling of the effects of shock duration, frequency, and strength on the degree of electroporation. Bioelectrochemistry Bioenerg. 51 (2), 133–143 (2000).
42. Davalos, R. V., Mir, L. M. & Rubinsky, B. Tissue ablation with irreversible electroporation. Ann. Biomed. Eng. 33 (2), 223–231 (2005).
43. Van Driel, V. J. H. M., Neven, K., Van Wessel, H., Vink, A., Doevendans, P. A. F. M. & Wittkampf, F. H. M. Low vulnerability of the right phrenic nerve to electroporation ablation. Hear. Rhythm 12 (8), 1838–1844 (2015).
44. Wittkampf, F. H. M., Van Driel, V. J., Van Wessel, H., Neven, K. G. E. J., Gründeman, P. F., Vink, A., et al. Myocardial lesion depth with circular electroporation ablation. Circ. Arrhythmia Electrophysiol. 5 (3), 581–586 (2012).
45. Neven, K., Van Driel, V., Van Wessel, H., Van Es, R., Doevendans, P. A. & Wittkampf, F. Myocardial Lesion Size After Epicardial Electroporation Catheter Ablation After Subxiphoid Puncture. Circ. Arrhythmia Electrophysiol. 7 (4), 728–733 (2014).
46. Bardy, G. H., Coltorti, F., Ivey, T. D., Alferness, C., Rackson, M., Hansen, K., et al. Some factors affecting bubble formation with catheter-mediated defibrillator pulses. Circulation 73 (3), 525–538 (1986).
47. Barak, M. & Katz, Y. Microbubbles: Pathophysiology and clinical implications. Chest 128 (4), 2918–2932 (2005).
48. Golberg, A. & Yarmush, M. L. Nonthermal irreversible electroporation: Fundamentals, applications, and challenges. IEEE Trans. Biomed. Eng. 60 (3), 707–714 (2013).
49. Davalos, R. V., Rubinsky, B. & Mir, L. M. Theoretical analysis of the thermal effects during in vivo tissue electroporation. Bioelectrochemistry 61 (1–2), 99–107 (2003).
50. Van Den Bos, W., Scheffer, H. J., Vogel, J. A., Wagstaff, P. G. K., De Bruin, D. M., De Jong, M. C., et al. Thermal Energy during Irreversible Electroporation and the Influence of Different Ablation Parameters. J. Vasc. Interv. Radiol. 27 (3), 433–443 (2016).
51. Van Gemert, M. J. C., Wagstaff, P. G. K., De Bruin, D. M., Van Leeuwen, T. G., Van Der Wal, A. C., Heger, M., et al. Irreversible electroporation: Just another formof thermal therapy? Prostate 75 (3), 332–335 (2015).
52. Neven, K., Van Driel, V., Van Wessel, H., Van Es, R., Doevendans, P. A. & Wittkampf, F. Epicardial linear electroporation ablation and lesion size. Hear. Rhythm 11 (8), 1465–1470 (2014).
53. Neven, K., Driel, V. Van, Wessel, H. Van, Es, R. Van, Pré, B. Du, Doevendans, P. A., et al. Safety and feasibility of closed chest epicardial catheter ablation using electroporation. Circ. Arrhythmia Electrophysiol. 7 (5), 913–919 (2014).
54. Lee, R. C., Zhang, D. & Hannig, J. Biophysical Injury Mechanisms in Electrical Shock Trauma. Annu. Rev. Biomed. Eng. 2 (1), 477–509 (2000).
55. Soar, J., Nolan, J. P., Böttiger, B. W., Perkins, G. D., Lott, C., Carli, P., et al. European Resuscitation Council Guidelines for Resuscitation 2015. Section 3. Adult advanced life support. Resuscitation 95 , 100–147 (2015).
56. Kotnik, T., Mir, L. M., Flsar, K., Puc, M. & Miklavcic, D. Cell membrane electropermeabilization by simmetrical bipolar rectangular pulses. Part I. Increased efficiency of permeabilization. Bioelectrochemistry 54 , 83–90 (2001).
57. Zhou, X., Smith, W. M., Justice, R. K., Wayland, J. L. & Ideker, R. E. Transmembrane potential changes caused by monophasic and biphasic shocks. Am. J. Physiol. 275 (5 Pt 2), H1798-807 (1998).
58. Ibey, B. L., Ullery, J. C., Pakhomova, O. N., Roth, C. C., Semenov, I., Beier, H. T., et al. Bipolar nanosecond electric pulses are less efficient at electropermeabilization and killing cells than monopolar pulses. Biochem. Biophys. Res. Commun. 443 (2), 568–573 (2014).
59. Bardy, G. H., Ivey, T. D., Allen, M. D., Johnson, G., Mehra, R. & Greene, H. L. A prospective randomized evaluation of biphasic versus monophasic waveform pulses on defibrillation efficacy in humans. J. Am. Coll. Cardiol. 14 (3), 728–733 (1989).

2. In vitro analysis of the origin and characteristics of gaseous micro-emboli during catheter mediated electroporation ablation.

2.1. Introduction

As described in the introduction, main cause of gas formation is thought to be electrolysis. Oxygen (O_2) collects at the positive (anodal) electrode while hydrogen (H_2) collects at the negative (cathodal) electrode. However, the results of Bardy *et al.* showed that electrolysis could not account for all gas formation during ablation. They suggested that bubble formation was also a result of cavitation, a high-pressure shockwave that extrudes dissolved gasses from the solution[1]. In their study, all produced DC-pulses were arcing, which might explain the large contribution of cavitation.

In the present in-vitro study, the generation of gas during non-arcing IRE-ablation pulses was visually studied using a high-speed camera (FASTCAM-APX RS, Photron USA, Inc., San Diego, USA) and measured with a bubble counter (BCC200, GAMPT, Zappendorf, Germany). The purpose was to investigate the influence of electrode polarity and catheter hoop size on bubble size and gas volume produced during non-arcing IRE-ablation pulses.

2.2. Methods

2.2.1. Direct volume measurements

A basin was filled with 2.4 g/L sodium chloride solution to obtain an impedance similar to blood[2]. A circular 7F, 14-electrode catheter with a variable hoop diameter ranging from 16 to 27-mm was positioned inside the basin underneath a transparent funnel, which was attached to a 1 mL syringe (**Figure 2.1A**). Cathodal and anodal IRE-pulses of 50, 100 and 200 Joules (J) were delivered using an external monophasic defibrillator (Lifepak 9, Physio-Control, Redmond, WA), while performing voltage and current measurements using an oscilloscope (Tektronix TDS 2002b, Beaverton, OR).

Depending on the energy level, a total of 20-50 IRE-pulses were delivered for each measurement (**Table 2.1**). Measurements were repeated 3 times per energy level with a catheter hoop diameter of 27-mm, resulting in 18 measurements. To compare absolute volumes between the small and large diameter hoops, measurements were repeated for 200 J with a catheter hoop diameter of 16-mm. The surface area of the indifferent electrode was adjusted to ensure a total system impedance of 65 Ohm (Ω) for the 27-mm diameter catheter setting. The same surface area of the indifferent electrode was used for the 16-mm catheter hoop diameter. Total gas volume per IRE-pulse, and the voltage and current curves were stored.

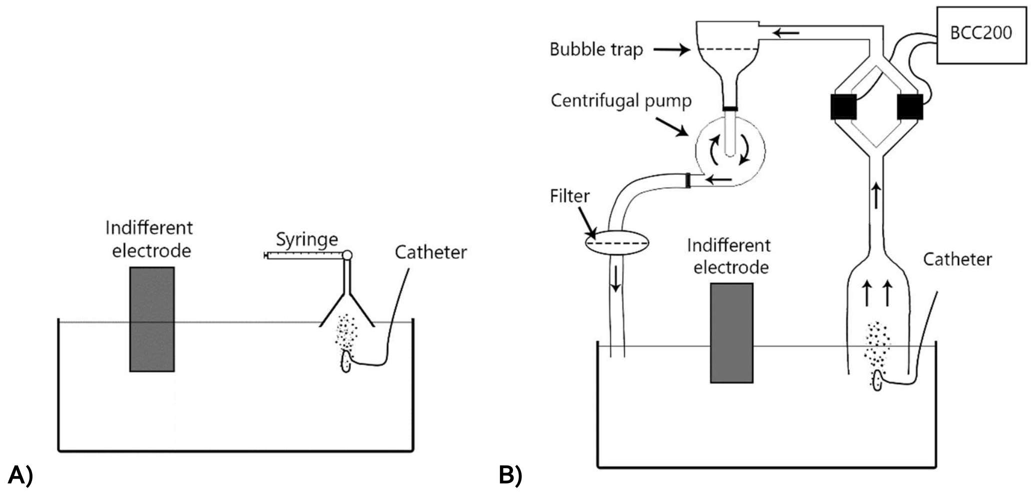

Figure 2.1 A) Set up as used for direct volume measurements. The catheter was placed underneath a funnel, which was attached to a 1 mL syringe. The indifferent electrode was positioned 20 cm from the catheter. **B)** Flow set up as used for BCC200 measurements. The catheter was placed underneath a cylinder and connected to a parallel tubing system. A flow of 1 L/min was created by a centrifugal pump, which was placed between a bubble trap and an air filter. The indifferent electrode was positioned 20 cm from the catheter.

2.2.2. Bubble counter measurements

A basin was filled with 2.4 g/L sodium chloride solution. The same circular catheter was placed inside the basin underneath a transparent cylinder (**Figure 2.1B**). The cylinder was connected to an Y-piece to create a parallel tubing circuit, on which two ultrasonic probes (Gampt, Zappendorf, Germany) were fixed. The bubble counter (BCC200) measures the amount and diameter of microbubbles with a diameter ranging from 10-500 µm. Using the number of bubbles and diameter, total bubble volume was calculated. Bubbles with a diameter >500 µm were marked as overrange volume, while exceptionally large bubbles were marked as bolus volume[3]. Cathodal and anodal IRE-pulses of 5, 10, 20, 30, 50, 100 and 200 J were delivered using the external defibrillator, while performing voltage and current measurements using an oscilloscope (Tektronix TDS 2002b, Beaverton, OR). Every measurement was repeated 5 times using a 27-mm catheter hoop diameter, resulting in a total of 70 measurements. To compare the 16-mm and 27-mm catheter hoop diameter, measurements were repeated at 20 J with a catheter hoop diameter of 16-mm. The surface area of the indifferent electrode was adjusted to ensure a total system impedance of 65 Ω for the 27-mm catheter hoop diameter setting. The same surface area of the indifferent electrode was used for the 16-mm catheter hoop diameter. Per setting, mean bubble size was calculated as the average gas volume divided by the number of gas bubbles. Total bubble volume, number of bubbles, mean bubble size, maximum bubble size, overrange number and volume, bolus volume and the voltage- and current curves were stored for every pulse.

2.2.3. High speed analysis

A plastic basin was filled with a 2.4 g/L sodium chloride solution. The same circular catheter was positioned in the basin, approximately 10 cm from the indifferent electrode. The catheter hoop was recorded with a high-speed camera (FASTCAM-APX RS, Photron USA, Inc., San Diego, USA) with a framerate of 10,000 frames per second and a resolution of 512 by 512 pixels. Recordings were synchronized with the voltage and current measurements using an oscilloscope (Tektronix DPO3014). Three 200 J IRE-pulses were applied, with the catheter serving as either the anode or cathode. The size of the largest gas bubbles was measured at 500 frames (5 ms) after the pulse by 2 independent investigators. The largest value of both measurements was used for further calculation.

2.2.4. Statistical analysis

All continuous variables are expressed as mean±SD. Data was analyzed using Matlab (2017a, The Mathworks, Natick, MA, USA). Cathodal versus anodal IRE-pulses and small versus large catheter hoop diameter were compared. High speed camera recordings and the direct volume measurements were analyzed using a two-sample t-test. The bubble counter recordings were analyzed using the Mann-Whitney U test. Regression analysis was performed to determine the linear correlation between volume and delivered charge. A p-value of $p<0.05$ was considered statistically significant.

2.3. Results

All IRE-pulses resulted in smooth voltage waveforms, suggesting the absence of arcing during all measurements[1] (e.g. **Figure 1.5B**).

2.3.1. Direct volume measurements

A total of 24 measurements were analyzed. For all energy levels, volume per IRE-pulse was significantly higher for cathodal IRE-pulses than for anodal IRE-pulses ($p < 0.001$) (**Table 2.1, Figure 2.2A**). The ratio between cathodal and anodal IRE-pulse volumes ranges from 4.7 to 6.3. For

Table 2.1 Cathodal vs anodal: 50J $p<0.001$, 100J <0.001, 200J $p<0.001$, **16 vs 27-mm** cathodal $p=0.0913$ and anodal $p=0.0686$

Catheter Polarity	Hoop diameter (mm)	Energy (J)	Number of IRE-pulses	Volume per IRE-pulse (µl)	Peak Voltage (V)	Peak Current (A)	Resistance (Ω)	Delivered charge (mC)
Cathode	27	50	50	8.47±0.61	1053±5	16.5±0.1	64.0±0.7	73±0
	27	100	30	13.33±1.20	1520±0	23.1±0.2	65.9±0.7	106±0
	27	200	20	19.17±0.29	2107±12	32.7±0.1	64.4±0.6	153±0
	16	200	20	18.00±0.87	2270±12	30.6±0.2	72.1±0.8	151±0
Anode	27	50	50	1.67±0.12	1051±5	16.5±0.1	63.8±0.6	72±0
	27	100	50	2.13±0.12	1513±12	23.4±0.2	64.7±0.7	106±0
	27	200	30	4.11±0.19	2107±12	32.5±0.1	64.6±0.7	152±0
	16	200	30	4.89±0.51	2187±12	30.5±0.23	71.8±0.5	151±1

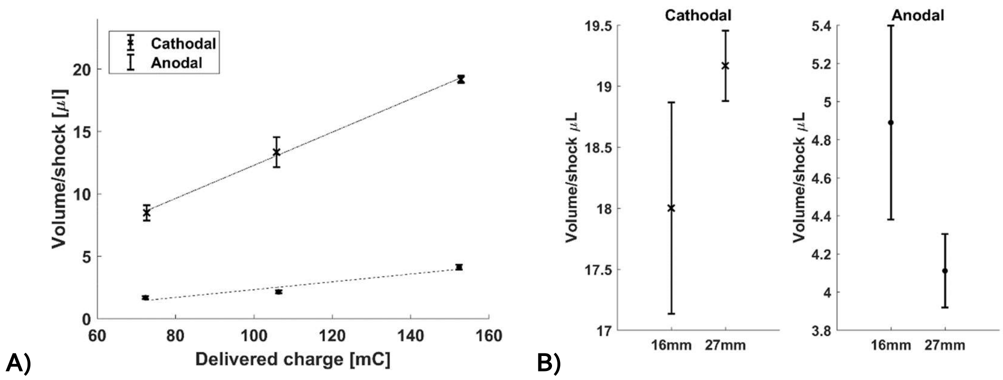

Figure 2.2 Direct volume measurements A) Mean volume per IRE-pulse vs. delivered charge (milli-coulombs). A significant difference is seen for all energy levels between cathodal and anodal IRE-pulses. For both cathodal and anodal IRE-pulses a strong positive relation was seen, with a slope of 0.133 μL/mC and 0.031 μL/mC, respectively. **B)** Volume per IRE-pulse for both 16-mm and 27-mm, for cathodal (B1) and anodal (B2) IRE-pulses.

both cathodal and anodal IRE-pulses a strong positive linear correlation was observed between the delivered charge and bubble volume: r=0.99 ($p<0.001$) and r=0.96 ($p<0.001$), respectively (**Figure 2.2A**). For both cathodal and anodal IRE-pulses, no significant difference in volume was found between 16-mm and 27-mm hoop diameter: p=0.0913 and p=0.0686, respectively (**Table 2.1, Figure 2.2B**). A single cathodal IRE-pulse produced 18.00±0.87 μl and 19.17±0.29 μl, while an anodal IRE-pulse produced 4.89±0.51 μl and 4.11±0.19 μl, for the 16-mm hoop diameter compared to the 27-mm hoop diameter, respectively.

2.3.2. Bubble counter measurements

A total of 80 measurements were analyzed. Cathodal IRE-pulses resulted in a significant larger volume for all energy levels (**Table 2.2, Figure 2.3A**). The ratio between cathodal and anodal IRE-pulse volumes ranged from 2.1 to 44.2. For cathodal IRE-pulses, a strong positive linear correlation (r=0.92, $p<0.001$) was found between delivered charge and gas volume. At higher energy levels, a large

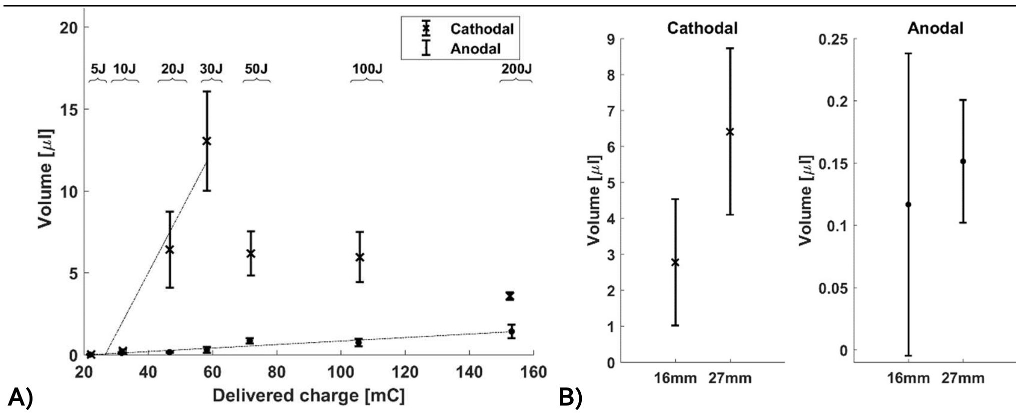

Figure 2.3 Bubble counter measurements A) Volume (μL) for cathodal IRE-pulses and anodal IRE-pulses versus delivered charge (milli-coulombs). Difference between cathodal and anodal IRE-pulses were significant for all energy levels. For both cathodal and anodal IRE-pulses a strong positive relation was seen, with a slope of 0.373 μL/mC and 0.011 μL/mC , respectively. **B)** Difference in volume (μL) for 16-mm hoop diameter and 27-mm hoop diameter for both cathodal (crosses) and anodal (dots) IRE-pulses of 20J. Differences between 16-mm and 27-mm hoop diameter were not significant.

Table 2.2 Volume per IRE-pulse, cathodal vs anodal: 5J p = 0.0079, 10J p = 0.0317, 20J p = 0.0079, 30J p = 0.0079, 50J p = 0.0079, 100J p = 0.0079, 200J p = 0.0079. **16 vs 27-mm:** Cathodal p = 0.0317, anodal p = 0.695. * = Bolus volume was detected, † = unreliable measurement

Catheter Polarity	Energy level (J)	Hoop diameter (mm)	Volume per IRE-pulse (µl)	Number per IRE-pulse	Mean bubble size (µm)	Max bubble size (µm)	Over-range number	Peak Voltage (V)	Peak Current (A)	Resistance (Ω)	Delivered charge (mC)
Cathode	5	27	0.01±0.0	195±40	29±18	150±35	0±0	332±0	5.12±0.0	64.8±0.0	22±0
	10	27	0.23±0.1	1387±303	44±33	239±44	0±0	472±0	7.26±0.0	65.0±0.3	32±0
	20	27	6.41±2.2	4736±395	90±69	472±20	1±1	664±0	10.16±0.0	65.4±0.0	47±0
	30	27	13.04±3.0	5230±492	110±88	496±5	8±6	816±0	12.51±0.0	65.2±0.2	58±0
	50†	27	6.18±1.3	4449±482	93±69	481±18	2±3	1064±0	16.40±0.0	64.9±0.0	72±0
	100†	27	5.96±1.5	4538±350	84±68	495±4	15±5	1524±9	23.48±0.1	64.9±0.3	106±0
	200†*	27	3.58±0.2	3378±266	67±61	494±5	53±4	2136±9	33.00±0.0	64.7±0.3	153±0
	20	16	2.79±1.8	3649±401	71±5	417±52	1±1	696±0	9.38±0.0	74.4±0.3	46±0
Anode	5	27	0.00±0.0	39±6	23±11	110±19	0±0	332±0	5.10±0.0	65.0±0.3	22±0
	10	27	0.11±0.0	369±67	35±25	345±85	0±0	472±0	7.26±0.0	65.0±0.3	32±0
	20	27	0.15±0.0	910±159	41±30	268±37	0±0	664±0	10.24±0.0	64.8±0.0	47±0
	30	27	0.30±0.2	1230±635	46±35	324±86	0±0	819±4	12.56±0.0	65.2±0.3	58±0
	50	27	0.85±0.2	2480±275	54±42	360±58	0±0	1056±0	16.40±0.0	64.4±0.0	72±0
	100	27	0.74±0.2	2166±214	50±40	384±55	1±1	1528±11	23.28±0.1	65.6±0.7	106±0
	200	27	1.42±0.4	2897±209	60±47	435±42	1±1	2140±0	32.80±0.0	65.2±0.0	153±1
	20	16	0.18±0.1	704±561	40±8	268±115	0±0	664±0	9.36±0.0	75.4±0.0	46±0

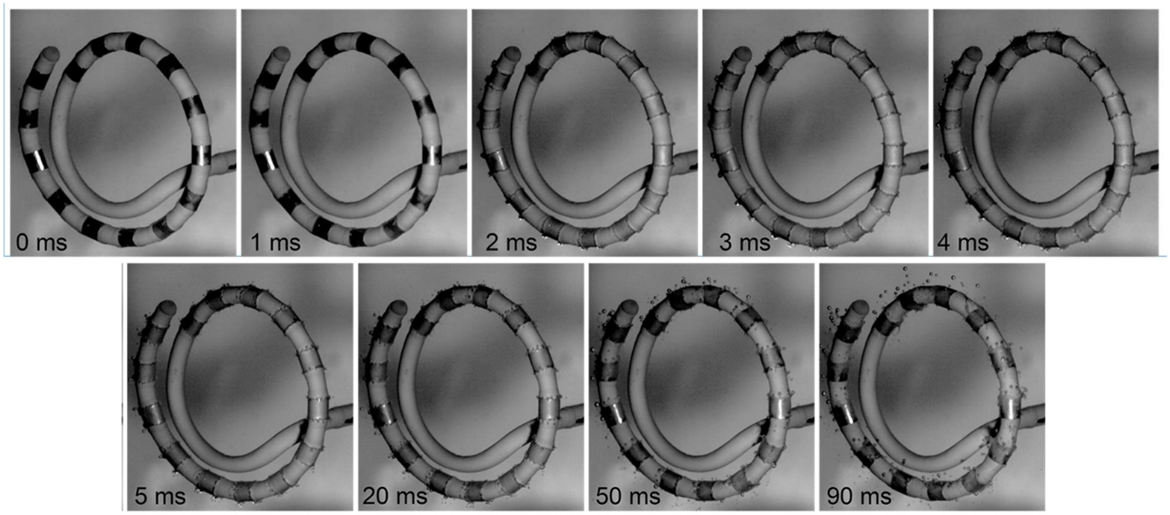

Figure 2.4 Example of the high speed images after different time frames of a cathodal IRE-pulse of 200 J.

decrease in volume per IRE-pulse was observed (**Figure 2.3A;** 50, 100 and 200 J). For anodal IRE-pulses a strong positive linear correlation was observed between the delivered charge and gas volume across the entire range of delivered charges: r=0.89, p<0.001 (**Figure 2.3A**). Cathodal IRE-pulses produced a significant lower volume with the 16-mm hoop diameter than with the 27-mm hoop diameter (p=0.032). For anodal IRE-pulses, no significant difference was found between volume produced by the 16-mm and 27-mm hoop diameter (p=0.695) (**Table 2.2, Figure 2.3B**). No significant difference was found between maximum bubble size for both cathodal and anodal IRE-pulses between 16-mm and 27-mm hoop diameter (p=0.056 and p=0.389) (**Table 2.2**).

2.3.3. High speed analysis

A total of 12 IRE-pulses were analyzed (e.g. **Figure 2.4**). Anodal IRE-pulses led to a significantly smaller maximum bubbles size than cathodal IRE-pulses using both the small and large hoop diameter (p=0.017 and p=0.025, respectively) (**Table 2.3**). With anodal IRE-pulses, the 16-mm hoop produced a significantly larger maximum bubble size than the 27-mm hoop diameter (p=0.011). Cathodal IRE-pulses showed no significant difference in maximum bubble size between the 16-mm and 27-mm hoop diameter (p=0.054). A part of the produced bubbles tend to stick to the catheter (**Figure 2.4**).

Table 2.3 Maximum bubble diameter, cathodal vs anodal: 16-mm p=0.017, 27mm p=0.025, 16 vs 27-mm: anodal p=0.011, cathodal p=0.054.

Catheter Polarity	Catheter Hoop diameter (mm)	Maximum Bubble (µm)	Peak Voltage (V)	Peak Current (A)	Resistance (Ω)
Cathode	16	781±77	2188±4	31.3±0.1	69.9±0.3
	27	601±86	2024±4	35.9±0.1	56.4±0.2
Anode	16	520±30	2126±6	33.0±0.2	64.4±0.6
	27	368±44	1956±9	38.2±0.2	51.2±0.5

2.4. Discussion

In this study, we investigated the influence of electrode polarity and catheter hoop size on gas formation during IRE. Both the direct volume and bubble counter measurements showed significantly larger volumes for cathodal IRE-pulses compared to anodal IRE-pulses. No significant difference in gas volume was measured between the 16-mm and 27-mm hoop diameter, except during the bubble counter measurements: Cathodal IRE-pulses with the 16-mm catheter hoop diameter produced less volume compared to cathodal IRE-pulses with the 27-mm catheter hoop diameter. A strong linear relationship was found between delivered charge and volume. High speed measurements showed a significantly larger maximum bubble size for cathodal IRE-pulses than anodal IRE-pulses. The 16-mm hoop diameter showed a significantly larger maximum bubble size for anodal IRE-pulses than the 27-mm hoop diameter.

2.4.1. Ratio cathodal-/anodal IRE-pulses

Overall results of this study showed a larger bubble volume and bubble size for cathodal IRE-pulses than for anodal IRE-pulses. This finding is in compliance with theory, since electrolysis is thought to be the main cause of gas creation during non-arcing IRE pulses. Reduction of H_2O produces O_2-gas at the anode, and H_2-gas at the cathode, according to **equation 1**.

$$2\ H_2O\ (l) + 4\ e^- \rightarrow 2\ H_2\ (g) + O_2\ (g) \tag{1}$$

According to Faraday's law, delivered charge (Coulombs) directly relates with the generated gas volume. With the monophasic defibrillator used in this study, a specific energy level is selected (in Joules), then, depending on system resistance, this energy results in a delivered current (Ampere) and voltage. During our measurements, a constant resistance between the catheter and indifferent electrode was created by adjusting the surface area of the indifferent electrode. Therefore, delivered charge was the same for cathodal and anodal IRE-pulses. In theory, the gas volume of cathodal IRE-pulses should be twice the gas volume of anodal IRE-pulses for any given charge. For the direct volume and BCC200 measurements this ratio ranged from 4.7 to 6.3 and 2.1 to 44.2, respectively. The amount of gas observed in different experiments can therefore not only be attributed to electrolysis.

Direct volume measurements showed that the absolute volume was significantly higher for cathodal IRE-pulses than for anodal IRE-pulses. For 200 Joules the direct volume measurements resulted in 19.17±0.29 µL and 4.11±0.19 µL, respectively. The 200 J pulses delivered 153 mC, which should result in 35.5 µL and 17.75 µL for cathodal and anodal IRE-pulses, respectively, according to Faraday's law. In the studies of Holt *et al.*[4] and of Bardy *et al.*[1], the same test setup was used as for our direct volume measurements. Holt used anodal and cathodal pulses with energy levels ranging from 10 – 400 J, using a single electrode catheter. They concluded that anodal pulses produced significantly more volume as compared to cathodal pulses (up to 15-fold). However, from their voltage and current waveforms we may conclude that all of their pulses were arcing[4]. The same applies to the DC-pulses delivered during Bardy's experiments[1]. From gas composition analysis they concluded that part of the gas volume arose from dissolved gasses.[1] Their results also showed an increased ratio between cathodal and anodal volume (up to 50-fold). They concluded that the generated shock wave forced gas out of the solution. However, during our measurements, arcing did not occur. Therefore, shockwaves associated with arcing pulses cannot explain the different ratio in gas volume between cathodal and anodal IRE-pulses.

2.4.2. Ratio between delivered charge and total gas volume

The BCC200 measurements showed a linear relation between the delivered charge and volume per cathodal IRE-pulse of 5 – 30 J. Interestingly, the volume decreased at higher energy levels (**Figure 2.3A**). The BCC200 is able to measure bubbles with a minimal distance of 5000 µs between two bubbles, resulting in a theoretical maximum of 200 bubbles per second. If more bubbles are detected within 5000 µs, only the largest bubble will be counted while the other bubbles in that timeframe will be ignored. Therefore, the number of bubbles will be underestimated by the BCC counter. In order to prevent this limitation, we used a parallel flow set up, to reduce the number of bubbles per probe per second (**Figure 2.1B**). However, from our data we suspect that the number of bubbles still exceeded the maximal countable bubble concentration and therefore not all bubbles are counted. For cathodal IRE-pulses, the total volume and number of bubbles at 50, 100 and 200 J are lower than for the lower energy settings (**Table 2.2**). Therefore, these energy levels were excluded for regression analysis.

Although both the direct volume measurements and the BCC200 measurements showed a linear correlation between the delivered charge and the total gas volume, the slope between gas volume and delivered charge was different for both measurements (**Figure 2.2 & Figure 2.3**). The theoretical relation is 0.232 µL/mC and 0.116 µL/mC for cathodal and anodal IRE-pulses, respectively. However, for the direct volume measurements and the anodal bubble counter measurements, a lower volume per mC was produced (**Figure 2.2**). Cathodal bubble counter measurements showed a larger volume per mC compared to the theoretical value (**Figure 2.3**). An explanation might be that the produced gasses reacted with other components in the saline solution, or that the produced gasses dissolved in the solution. For the direct volume measurements, adhering of bubbles to the catheter or the funnel may explain a small factor of gas volume loss.

In an article by Segers *et al.*[5] the BCC200 was evaluated on accuracy. They stated that the BCC200 overestimates bubble diameter by a factor of 2 to 3, resulting in a volume overestimation of 8-27 times. However, during their measurements they used a flow rate of 4 L/min and a constant bubble size of 43 µm. We cannot predict whether these factors are the same for a lower flow rate (1 L/min) and variable bubble sizes. Therefore, the BCC200 may be unsuitable for absolute volume detection, but these results may rather be used as indication and to compare ratios between different measurements.

2.4.3. Comparison between 16-mm and 27-mm catheter hoop diameter

The BCC200 is able to count bubbles with a diameter ranging from 10-500 µm. Every bubble with a diameter larger than 500 µm is considered overrange and is counted separately. For the calculation of the overrange volume, the diameter of the overrange bubble is assumed to be 500 µm. This results in an underestimation of the overrange volume. Furthermore, if there are too many and too large bubbles, the BCC200 marks the volume as bolus volume. For the comparison between the 16-mm and 27-mm hoop diameter, we aimed at measurements without overrange and/or bolus volume and therefore chose a lower energy setting of 20 J IRE-pulses.

According to the high-speed camera measurements, the 16-mm hoop diameter produced bubbles with a larger maximum size than the 27-mm hoop diameter. It would be expected that total volume for the 16-mm hoop is therefore higher than for the 27-mm hoop. However, the bubble counter measurements showed a decreased volume for the 16-mm hoop compared to the 27-mm hoop. The anodal bubble counter measurements and both cathodal and anodal direct volume measurements showed no significant differences between the 16-mm and 27-mm catheter hoop in total gas volume. Cathodal IRE-pulses seems to show a trend towards a larger volume for the 27-mm hoop compared to the 16-mm hoop, while this trend is the other way around for the anodal IRE-pulses.

2.4.4. Clinical implications

Bubble size is thought to be an important factor for safe clinical use of IRE. Bubble distribution and dissolving time are dependent on the bubble size; ranging from a lifetime of 6 seconds for bubbles with a diameter of 18 µm to 1 hour for bubbles with a diameter of 500 µm[6]. BCC200 measurements showed a mean diameter 67±61 µm and 60±47 µm and a maximum diameter of 494±4.9 µm and 435±42 µm for cathodal and anodal IRE-pulses of 200J, respectively. The BCC200 is limited to a maximum bubble size of 500 µm. Therefore, the maximum diameter of cathodal IRE-pulses is unreliable. High speed analysis showed bubbles with a maximum diameter of 601±86 µm and 368±44 µm for cathodal and anodal IRE-pulses of 200J, respectively. In the study of Chung *et al.*, they found that microbubbles with a diameter <38 µm did not impair cerebral blood flow, but with every setting we used, this limit was exceeded. Other studies stated that a large stream of small gas bubbles will activate the inflammatory response and complement system, resulting in ischemic infarction[7,8].

Haines *et al.* found acute ischemic cerebral lesions with bubbles with a diameter of 20-200 µm or a minimal volume of 4 µL[9]. If the above mentioned cut-off values hold true for our experiments, then we cannot rule occurrence of acute ischemic cerebral lesions out. This would have to be investigated in future in-vivo studies.

2.4.5. Limitations

Our measurements were performed in a saline solution. However, gas composition as a result of electrolysis is expected to be different for saline and blood[1]. The temperature of the saline solution was room temperature and is therefore lower than the temperature of blood *in vivo*.

As observed during the high speed analysis, bubbles tend to stick to the catheter after the delivery of a pulse. This might influence the accuracy of our measurements, since not all of the produced bubbles can be counted (during the bubble counter and direct volume measurements).

We performed the BCC200 measurements in a flow set up to simulate the blood flow, however the blood flow in vivo is more complex and might influence the bubble distribution and size. As mentioned before, the absolute gas volumes as measured by the BCC200 are inaccurate[5], and therefore it is difficult to predict what the clinical impact of the produced gas will be. However, for in vivo measurements the BCC200 is still the most suitable instrument to measure bubble gas formation.

2.4.6. Comparison to RF ablation

To predict whether IRE-ablation is a safe alternative for RF ablation, a comparison should be made between bubble size and gas for IRE ablation and RF ablation. However, measuring bubble size and volume in vitro for RF-ablation is difficult, since RF ablation is based on heating of tissue under specific conditions. Bubble formation is dependent on electrode-tissue contact and heating of blood, which is difficult to be simulated in our in vitro set up. We recommend to perform in vivo measurements using both cathodal and anodal IRE-pulses as well as RF pulses, to make a founded comparison between these techniques.

2.5. Conclusion

Overall results showed a lower total gas volume for anodal IRE pulses than for cathodal IRE pulses. Differences in total gas volume between 16-mm and 27-mm catheter hoop diameters were inconclusive. A linear relationship was found between delivered charge and total gas volume. Although our results provide an indication of the characteristics of gas formation during catheter ablation using IRE, the results of this study cannot directly be translated into a clinical situation. We recommend to further investigate gas bubble formation in an in-vivo set up, to estimate safety of catheter ablation using IRE.

2.6. References

1. Bardy, G. H. *et al.* Some factors affecting bubble formation with catheter-mediated defibrillator pulses. *Circulation* **73,** 525–538 (1986).
2. Geddes, L. A. & Kidder, H. Specific resistance of blood at body temperature II. *Med. Biol. Eng.* **14,** 180–185 (1976).
3. Stehouwer, M. C. *et al.* Clinical evaluation of the air removal characteristics of an oxygenator with integrated arterial filter in a minimized extracorporeal circuit. *Int. J. Artif. Organs* **34,** 374–382 (2011).
4. Holt, P. M. & Boyd, E. G. C. A. Hematologic effects of the high-energy endocardial ablation technique. *Circulation* **73,** 1029–1036 (1986).
5. Segers, T., Stehouwer, M. C., de Somer, F. M. J. J., de Mol, B. A. & Versluis, M. Optical verification and in-vitro characterization of two commercially available acoustic bubble counters for cardiopulmonary bypass systems. *Perfus. (United Kingdom)* **33,** 16–24 (2018).
6. Chung, E. M. L. *et al.* Size distribution of air bubbles entering the brain during cardiac surgery. *PLoS One* **10,** 1–11 (2015).
7. Barak, M. & Katz, Y. Microbubbles: Pathophysiology and clinical implications. *Chest* **128,** 2918–2932 (2005).
8. Juenemann, M. *et al.* Impact of bubble size in a rat model of cerebral air microembolization. *J. Cardiothorac. Surg.* **8,** 1–8 (2013).
9. Haines, D. E. *et al.* Microembolism and catheter ablation I: A comparison of irrigated radiofrequency and multielectrode-phased radiofrequency catheter ablation of pulmonary vein ostia. *Circ. Arrhythmia Electrophysiol.* **6,** 16–22 (2013).

3. In vivo analysis of the origin and characteristics of gaseous micro emboli during catheter mediated irreversible electroporation

3.1. Introduction

The results from the *in vitro* study indicated cathodal IRE-pulses produce a significant higher gas volume compared to anodal IRE-pulses. A linear relationship was found between delivered charge and total gas volume. However, these results cannot directly be translated to a clinical situation.

Previous studies investigated bubble gas formation as a result from RF-ablation *in vivo*, in a porcine model[1,2]. They used an extra corporeal circulation loop and transesophageal echocardiography (TEE). In the present study we will investigate the generation of gas during non-arcing IRE-ablation pulses and RF ablation using a bubble counter on an extracorporeal loop and TEE in a porcine model. The purpose of this study was to characterize the influence of electrode polarity and catheter hoop size on bubble size and gas volume and to compare IRE- with RF-ablation.

3.2. Methods

All experiments were approved by the Animal Experimentation Committee of the University Medical Center Utrecht and were in compliance with the *Guide for the Care and Use of Laboratory Animals*[3].

3.2.1. Study procedure

This study was performed in seven 60-75 kg pigs (Topigs Norsvin). The animals were given 1200 mg/day amiodarone starting seven days before the procedure. Three days before the procedure antibiotics (amoxicillin/clavulanic acid, 12.5 mg/kg) were started. On the day of the procedure the animals were sedated, intubated and anesthetized according to a previously described protocol[4]. An indifferent patch electrode (7506, Valley Lab Inc, Boulder, CO, USA) was placed on a shaven area at the lower back and used as counter electrode. Intravenous heparin was administered to maintain an active clotting time of >350 seconds.

Under fluoroscopic guidance, transseptal puncture was performed using a deflectable sheath (Agilis, Abbott, Minnetonka, MN, USA) via the right femoral vein. For IRE ablation a 7F circular 14-electrode catheter with an adjustable hoop diameter of 16-27-mm was used (**Figure 1.4**). For RF ablation a 7F irrigated ablation catheter (TactiCath, Abbott, Minnetonka, MN, USA) was used.

3.2.2. Extracorporeal loop

An external loop was created between the left femoral artery and the left femoral vein, using 18F-20F cannulas and 3/8" inch tubing. A parallel circuit was created to attach two ultrasound probes from the

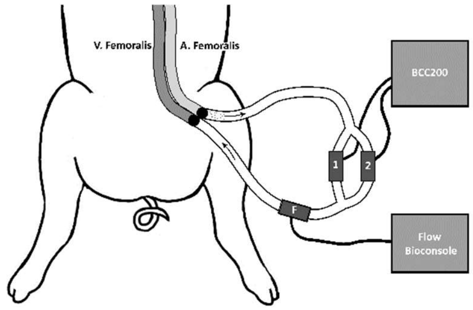

Figure 3.1 Schematic overview of the extracorporeal circuit on which two ultrasound probes (1 and 2) and a flow sensor (F) were attached to the bubble counter (BCC200) and flow Bioconsole, respectively.

BCC200 (**Figure 3.1**). An extra flow sensor (Medtronic Bioconsole, TX-40 flow transducer, Minneapolis, MN, USA) was attached to the external parallel circuit (**Figure 3.1**). The flow in the shunt was measured continuously and set to a constant flow of 1 L/min. The cardiac output (CO) was measured after every two sets of measurements during the experiments.

The number and size of gas bubbles over time, total gas volume and flow rate (volume/s) were measured and stored using the Bcc200.

3.2.3. Ablation settings

For IRE-ablation a monophasic external defibrillator (LifePak 9) was used to deliver the IRE-pulses. An oscilloscope (Tektronix TDS 2002B) was used to store the voltage and current waveforms. For both cathodal and anodal pulses an energy level of 50, 100 and 200 joules were used for the large (27-mm) hoop diameter. Cathodal and anodal pulses of 50 joules were used for the 16-mm catheter hoop diameter. Five IRE-pulses were applied for each setting at different locations in the LA. The total system resistance was adjusted by adding serial resistor of 10 Ω, to create a similar resistance of 55-65 Ω in all animals.

Point-by-point RF ablation was performed using a power setting of 40 W at a random position in the LA with good catheter-tissue contact, for 30 and 60 seconds. Saline irrigation was set at 30 mL/min. Measurements were repeated 5 times per setting.

3.2.4. Transesophageal echocardiography

A 2D-Echo machine (Philips IE33, Eindhoven, Netherlands) in combination with a 3-8 MHz TEE probe was used to record the microbubbles in the left atrium, left ventricle or proximal aorta. Every IRE- and RF-pulse was recorded separately. Afterwards, the images were scored based on the microbubble density by a blinded expert. Microbubble formation was compared to baseline microbubble density. The density of the microbubbles was categorized as one of four types; isolated bubbles were marked as "few", continuous but non-dense microbubbles were marked as "moderate", continuous and dense microbubbles were marked as "shower" and an intense change in density was marked as "abundant".

3.2.5. Statistical analysis

All continuous variables are expressed as mean±SD. Data was analyzed using Matlab (2017a, The Mathworks, Natick, MA, USA). Total gas volume and number of bubbles were corrected by the ratio between the flow rate in the external loop and the CO. Bubble volume as produced by cathodal versus anodal IRE-pulses, small versus large catheter hoop diameter and IRE-pulses compared to RF-pulses were compared using the Mann-Whitney U test. Regression analysis was performed to determine the linear correlation between volume and delivered charge. A p-value of $p<0.05$ was considered statistically significant.

3.3. Results

Measurements were successfully performed in 7 pigs. IRE-pulses that showed signs of arcing were excluded from analysis. A total of 248 measurements were analyzed. The median CO was 4.7 (interquartile range (IQR): 1.2) L/min.

3.3.1. IRE-ablation

Total volumes of cathodal IRE-pulses with the 27-mm hoop diameter were significantly higher compared to anodal IRE-pulses with the 27-mm hoop diameter for all energy settings ($p<0.0001$) (**Figure 3.2, Table 3.1**). Cathodal pulses were marked as 'shower' or 'abundant', while anodal pulses were marked as 'few' and 'moderate, indicating the volume measurements are consistent with TEE analysis (**Figure 3.3**).

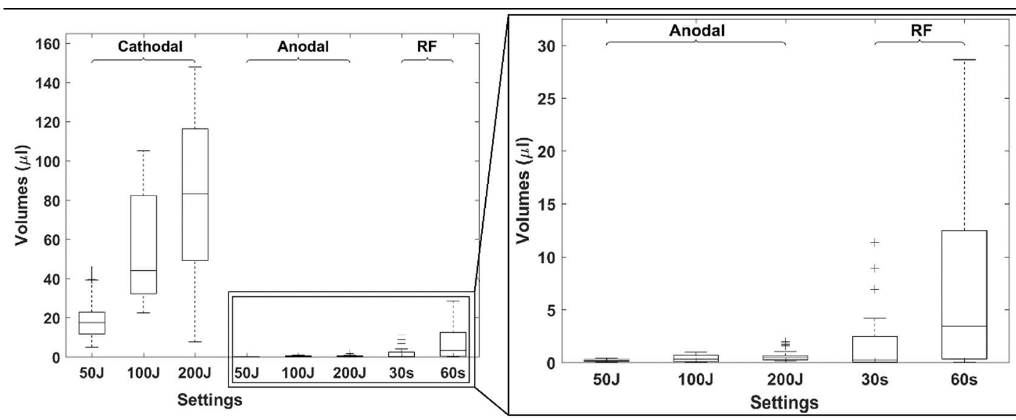

Figure 3.2 Boxplot of total volume per setting. Data point outside the 75th-percentile+1.5*IQR and 25th-percentile–1.5* IQR were marked as outliers. Cathodal and anodal pulses were delivered using the 27-mm hoop diameter. Cathodal IRE-pulses produce more gas volume than both anodal IRE-pulses or during RF-ablation (overview). Anodal-IRE pulses however produce a lower gas volume compared to 60s RF-ablation (zoom).

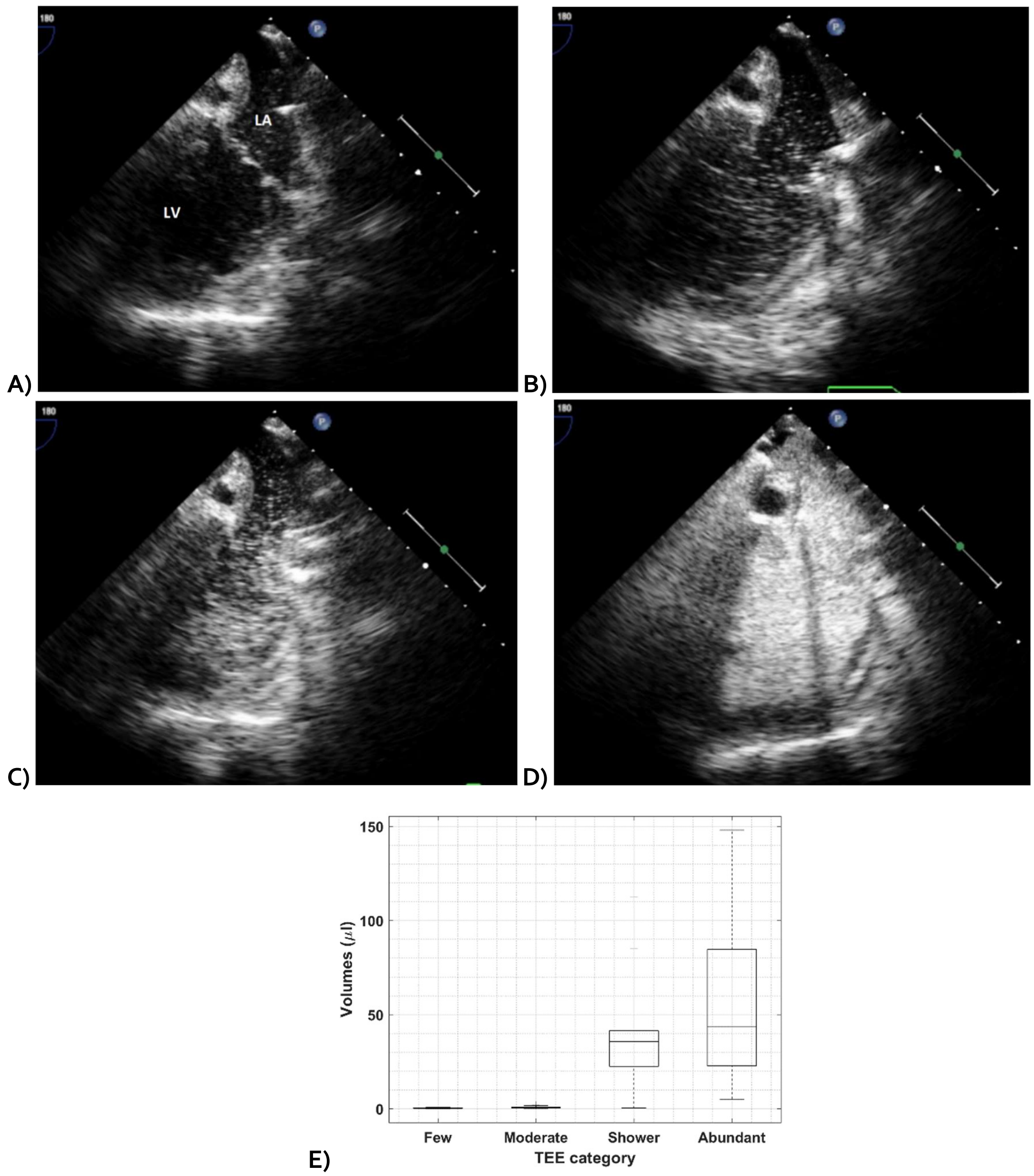

Figure 3.3 Example images showing different categories that were used for TEE analysis. **A)** Category 1, few isolated bubbles, **B)** Category 2, continuous but non-dense (moderate), **C)** Category 3, continuous and dense microbubbles (shower) and **D)** Category 4, an intense change in density (abundant). **E)** Total gas volume relating to the four TEE categories (produced by IRE-pulses using the large catheter hoop).

Mean bubble sizes of cathodal IRE-pulses with the 27-mm hoop diameter were significantly higher compared to anodal IRE-pulses with the 27-mm catheter hoop diameter for 50, 100 and 200 J ($p=0.0079$, $p=0.0079$ and $p=0.0012$, respectively). Total volume of cathodal IRE-pulses with the 16-mm catheter hoop diameter was significantly higher compared to anodal IRE-pulses with the 16-mm catheter hoop diameter ($p<0.0001$).

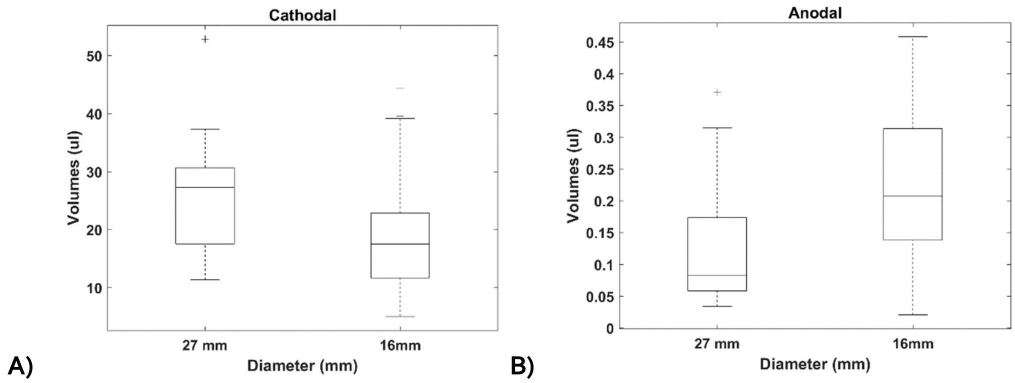

Figure 3.4 Boxplots of the comparison between 16-mm and 27-mm catheter hoop diameter. **A)** Total volume as produced by cathodal IRE-pulses of 50 J **B)** Total volume as produced by anodal IRE-pulses of 50 J. Note the difference in Y-axis between both figures.

Differences in total volume between 16-mm and 27-mm hoop diameter were not significant for both 50J cathodal and anodal IRE-pulses (p=0.0575 and p=0.7374, respectively) (**Figure 3.4, Table 3.1**). No significant differences in mean bubble size were found between 16-mm and 27-mm hoop diameter for cathodal and anodal IRE-pulses (p=0.5174 and p=0.5174, respectively). A linear relation was found between delivered charge and total volume for cathodal and anodal IRE-pulses delivered with the 27-mm catheter hoop diameter (**Figure 3.5**).

3.3.2. RF-ablation

Few bubbles were measured at the start of the RF-pulses, but the greater part of the produced volume arose at the end of the RF-pulses. TEE analysis showed RF-pulses are mostly categorized as 'few' or 'moderate' (**Figure 3.3**). RF-pulses of 60 s produced significantly more gas volume compared to RF-pulses of 30 s (p=0.0017). Cathodal IRE-pulses of 200 J produced significantly more volume compared to RF-pulses of both 30 and 60 seconds (both p<0.0001) (**Figure 3.2, Table 3.2**). Anodal IRE-pulses of 200 J produced significantly less volume compared to RF-pulses of 60 seconds (p=0.0015), however no

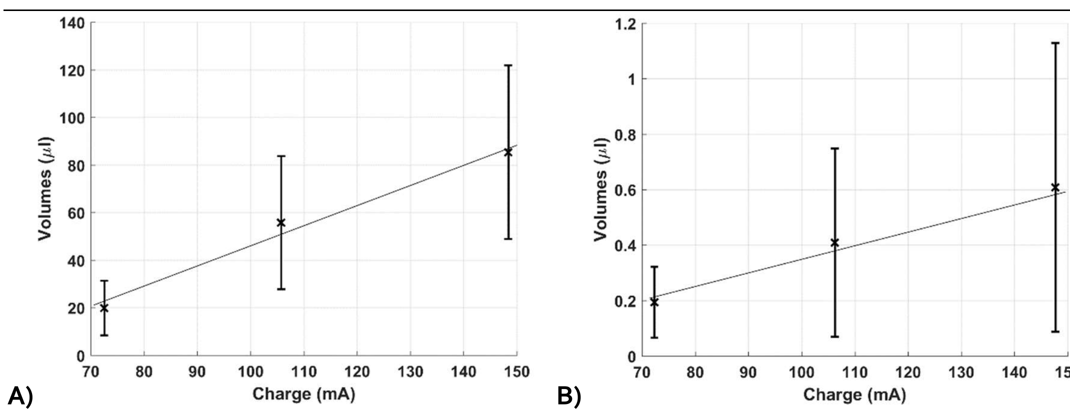

Figure 3.5 Regression analysis between delivered charge in mA and total volume. **A)** Cathodal IRE-pulses, with a slope 0.7797 μL/mA and **B)** Anodal IRE-pulses with a slope of 0.0049 μL/mA. Note the different scale on the y-axis.

Table 3.1 Results of the bubble counter measurements, corrected with cardiac output. Cathodal IRE-pulses produced a significantly larger volume and larger bubbles compared to anodal IRE-pulses. No significant difference in volume and bubble size was measured between the 16-mm and 27-mm catheter hoop diameter for anodal and cathodal IRE-pulses.

Catheter Polarity	Hoop diameter (mm)	Energy (J)	Volume (µl)	Number	Mean bubble size (µm)	Peak Voltage (V)	Peak Current (A)	Resistance (Ω)	Delivered charge (mC)
Cathodal	16	50	25.9±10.3	15656±3189	95±14	1065±12	15.7±0.2	68.6±0.9	72±0
	27	50	19.9±11.5	15112±2451	86±18	1047±22	16.2±0.5	66.4±1.9	73±1
	27	100	55.8±28.0	19758±2143	108±17	1468±5	24.1±0.1	66.6±12.2	106±1
	27	200	85.4±36.5	24011±3458	117±17	2053±47	33.7±1.2	62.6±8.5	148±2
Anodal	16	50	0.18±0.12	1041±498	34±4	1055±14	15.9±0.3	67.5±4.5	72±0
	27	50	0.19±0.13	1582±1058	31±5	1037±28	16.4±0.7	66.3±8	72±1
	27	100	0.41±0.34	2149±1654	35±6	1456±13	24.5±0.3	62.5±6.6	106±1
	27	200	0.61±0.52	2732±1973	41±6	2015±34	34.9±0.9	57.9±2.4	148±1

Table 3.2 Results of RF-pulses of 30 and 60 seconds. RF-pulses of 60 s produced a significant larger volume compared to RF-pulses of 30 s.

	Energy (Watt)	Duration (s)	Volume (µl)	Number	Mean bubble size (µm)
RF-ablation	40	30	1.6 ±2.8	4717±4878	43±13
	40	60	6.6±7.5	16665±12594	55±11

significant difference was found between anodal IRE-pulses of 200 J compared to RF-pulses of 30 seconds (p=0.2165) (**Figure 3.2**).

No significant difference was measured in mean bubble size for RF-pulses of 30s compared to RF-pulses of 60 s (p=0.1797). Mean bubble size produced by cathodal IRE-pulses of 200 J were significantly larger compared to RF-ablation of 30 and 60 s (both p=0.0022, respectively). Anodal IRE-pulses of 200 J produced significantly smaller bubbles compared to RF-pulses of 60 s (p=0.0140), while no significant difference was found between anodal IRE-pulses of 200 J and RF-ablation of 30 s in mean bubble size.

3.4. Discussion

The purpose of this study was to investigate the influence of polarity and catheter hoop diameter on gas formation and to compare gas formation during IRE-ablation with gas formation during RF-ablation.

We found that cathodal IRE-pulses produced significantly more volume than anodal IRE-pulses both using the 27-mm catheter hoop diameter and for all energy levels. No significant difference in total volume was found between 16-mm and 27-mm catheter hoop for cathodal and anodal IRE-pulses. A linear relation was found between delivered charge and the produced volume.

Cathodal IRE-pulses of 200 J produced significantly more volume and a larger mean bubble size compared to RF-pulses of 30 and 60 s. No significant difference in total volume and mean bubble size was found between anodal IRE-pulses of 200 J and RF-pulses of 30 s, while anodal IRE-pulses of 200 J produced significantly less volume and smaller mean bubble size compared to RF-pulses of 60 s.

3.4.1. Relation between cathodal and anodal IRE-pulses

The mechanism of electrolysis is explained in chapter 2. The theoretical ratio between cathodal and anodal gas production is 2:1. For our measurements, this ratio for 200 J IRE-pulses is 85.4:0.61 µL, resulting in ≈140 times more volume for cathodal IRE-pulses compared to anodal IRE-pulses. This difference is even higher as compared to the ratio found during the *in vitro* measurements (up to 44-fold). According to Faraday's law, the 200 J IRE-pulses (with ≈148 mC delivered charge) should theoretically result in 34.3 µL and 17.2 µL for cathodal and anodal IRE-pulses, respectively. This indicates that our volume measurements for cathodal IRE-pulses are more than twice the theoretical value, while the volumes for anodal IRE-pulses is approximately 28 times smaller than predicted. The difference in volume produced by cathodal IRE-pulses might partly be explained by the overestimation of the BCC200[5], however the difference in volume produced by anodal IRE-pulses cannot simply be explained by a measuring error. As explained in chapter 2, anodal IRE-pulses produce O_2-gas at the electrode. A possible explanation for the smaller volume might be that O_2 is likely to react with other components in the blood, or can be bound to hemoglobin.

3.5. RF-pulses

Takami *et al.*[1] compared 30 W and 50 W point-by-point RF-pulses, resulting in a median of 36 (IQR:122) nL and 62 (IQR: 183) nL per RF-pulse without steam pops. Their results suggest RF-pulses produce less volume than we measured during our experiments. Possible explanations might be that they did not correct for the CO, resulting in an underestimation of the total volume produced at the catheter. They do not distinguish between 30s and 60s RF-pulses, but they excluded RF-pulses which produced steam pops. We did not correct for the occurrence of steam pops, which might resulted in the higher total volume.

3.5.1. Limitations

As mentioned in **chapter 2**, the absolute volume as measured by the BCC200 is thought to be inaccurate[5]. Therefore, no firm conclusions can be drawn regarding the produced gas volume. However, relative differences in total volume can be compared and will provide an indication of the clinical impact of the total gas volume as produced by the different ablation modalities and settings. Besides, there is no other suitable method to measure gas bubbles in blood.

We measured cardiac output and flow rate in the external loop and corrected the total gas volume and number of bubbles with this ratio. Theoretically this would approximate the total amount of gas volume produced at the catheter. However, the bubbles might not distribute evenly over the transversal plane vessel at every bifurcation. Bubbles with a diameter of 20-60 µm will distribute based on blood flow, because they have no buoyancy in flowing blood[6]. However, during our measurements, also bubbles with a larger diameter were observed. This might cause an over- or underestimation of the total bubble volume produced at the catheter. Also, the cardiac output was not constant throughout the procedures, resulting in different correction factors for the different measurements. It is unknown what the influence of the CO is on the solubility and distribution of the bubbles.

In our study the produced volume of one IRE-pulse of 200 J was compared with the produced volume of RF-pulses of both 30 and 60 seconds. However, in a clinical setting RF-pulses will not be exactly 30 or 60s during the whole procedure. Our results showed a larger gas volume produced by 60s RF-pulses compared to 30s RF-pulses. One of the factors which influence bubble formation by RF-ablation is the amount of heat. Excessive heating of tissue and blood may induce larger gas volumes. This explains that the greater part of the produced bubbles were formed at the end of the RF-pulses. The average ablation time during PVI procedures using RF-ablation is 1885 s (1510–2450 s)[7], but no univocal data is available about the duration per RF-pulse. It is expected that RF-pulses that exceed 60 s will produce even a larger volume, due to elevated temperatures.

3.5.2. Clinical implications

No significant differences in total volume were measured between the 16-mm and 27-mm catheter hoop diameter. For cathodal pulses a trend towards less total volume for the small catheter hoop diameter was seen. This might be beneficial for the intended therapy (PVI ablation), since human PVs are irregular in size and shape. Therefore, the catheter can be adjusted to fit in the antrum of the PVs, without producing more gas volume during delivering of the IRE-pulse.

The result of this study indicate that the use of anodal IRE-pulses should be preferred over cathodal IRE-pulses, since the produced volume and bubbles size are less for anodal IRE-pulses compared to cathodal IRE-pulses. Delivered charge is directly related to the total gas volume, and therefore it is recommended to use the lowest energy setting as possible. Earlier research focused on lesion depth as created by cathodal IRE-pulses and concluded that 200 J IRE-pulses are needed to create sufficient lesion depth. For anodal IRE-pulses this relation has not yet been established, but it is expected that the relation between energy level and lesion depth is the same for cathodal and anodal IRE-pulses.

Anodal IRE-pulses of 200 J produced the same gas volume as RF-pulses of 30 s and even less gas volume as compared with RF-pulses of 60 s. However, to investigate which of these modalities produces the least gas volume during a PVI-ablation we need to correct for the total amount of IRE-pulses and total RF-time during a procedure. Assuming 1885 seconds for PVI-ablation using RF-pulses of 60 s (mean of 6.6 µL per RF-pulse), total produced volume will be ≈207 µL. A total PVI-ablation using IRE-pulses is thought to require ≈2.3 IRE-pulses of 200 J per PV[8] (mean of 0.61 µL per IRE-pulse), which would result in 5.5 µL total produced volume. Based on this data, it might be beneficial to use anodal IRE-pulses instead of RF-ablation for PVI-ablation. An important note on this is the speed at which the bubbles are developed. IRE-pulses lasts for 6 ms, therefore the flow rate of the bubble produced by IRE-pulses is 101 µL/second. Bubble formation during RF-pulses lasts for approximately 40 seconds, resulting in a flow rate of 0,14 µL/second. We cannot be certain about the influence of the difference in flow rate between the two modalities.

Clinical relevance of the produced gas bubbles is difficult to predict. Several studies were performed to investigate the influence of total volume of injected air or the influence of bubble size on clinical outcome, mostly focusing on cerebral damage. Haines *et al.* found acute ischemic cerebral lesions with bubbles with a diameter of 20-200 µm or a minimal volume of 4 µL[2]. Chung *et al.* found that microbubbles with a diameter <38 µm did not impair cerebral blood flow[9]. Helps *et al.* stated that injection of 25 µL declines cerebral blood flow in a rabbit model[10]. Michell *et al*. stated that large bubble might directly impair blood flow and cause ischemia, however small bubble will redistribute and might induce transient ischemia and damage to the endothelial wall[11]. Taken all these studies together, no univocal conclusion can be drawn.

3.6. Conclusion

These results suggest that, considering total gas volume and bubble sizes, anodal IRE-pulses are preferred over cathodal IRE-pulses. Considering the different diameter of PVs in human anatomy, it might be beneficial to use the adjustable catheter hoop. Our results indicate that there is no difference in total gas volume between the 16-mm and 27-mm catheter, and therefore both modalities might be used for PVI using IRE-ablation. Comparing the total volume of produced gas between anodal IRE-ablation and RF-ablation during a total PVI procedure, anodal IRE-ablation is thought to produce less gas. Therefore, anodal IRE-ablation might be a suitable replacement for RF-ablation.

3.7. References

1. Takami, M., Lehmann, H. I., Parker, K. D., Welker, K. M., Johnson, S. B. & Packer, D. L. Effect of left atrial ablation process and strategy on microemboli formation during irrigated radiofrequency catheter ablation in an in vivo model. Circ. Arrhythmia Electrophysiol. 9 (1), (2016).
2. Haines, D. E., Stewart, M. T., Ahlberg, S., Barka, N. D., Condie, C., Fiedler, G. R., et al. Microembolism and catheter ablation I: A comparison of irrigated radiofrequency and multielectrode-phased radiofrequency catheter ablation of pulmonary vein ostia. Circ. Arrhythmia Electrophysiol. 6 (1), 16–22 (2013).
3. Council, N. R. Guide for the Care and Use of Laboratory Animals: Eighth Edition. (The National Academies Press, 2011). doi:10.17226/12910
4. Wittkampf, F. H., Van Driel, V. J., Van Wessel, H., Vink, A., Hof, I. E., Grundeman, P. F., et al. Feasibility of electroporation for the creation of pulmonary vein ostial lesions. J. Cardiovasc. Electrophysiol. 22 (3), 302–309 (2011).
5. Segers, T., Stehouwer, M. C., de Somer, F. M. J. J., de Mol, B. A. & Versluis, M. Optical verification and in-vitro characterization of two commercially available acoustic bubble counters for cardiopulmonary bypass systems. Perfusion 26765911772259 (2017). doi:10.1177/0267659117722595
6. De Somer, F. M. J. J., Vetrano, M. R., Beeck, J. P. A. J. Van & Nooten, G. J. Van. Extracorporeal bubbles: a word of caution. Interact. Cardiovasc. Thorac. Surg. 10 , 995–1002 (2010).
7. Teunissen, C., Clappers, N., Kassenberg, W., Hassink, R. J., Van Der Heijden, J. F. & Loh, P. Time matters: Adenosine testing immediately after pulmonary vein isolation does not substitute a waiting period. Europace 19 (7), 1140–1145 (2017).
8. van Es, R., van Driel, V. J. H. M., Neven, K., van Wessel, H., Doevendans, P. A. F. M. & Wittkampf, F. H. M. Feasibility of multi-electrode contact measurement as a predictor of long-term success with circular pulmonary vein electroporation ablation (abstract). Eur. J. Clin. Invest. 47 (Supplement S1), (2017).
9. Chung, E. M. L., Banahan, C., Patel, N., Janus, J., Marshall, D., Horsfield, M. A., et al. Size distribution of air bubbles entering the brain during cardiac surgery. PLoS One 10 (4), 1–11 (2015).
10. Helps, S. C., Meyer-Witting, M., Reilly, P. L. & Gorman, D. F. Cerebral Blood Flow in Rabbits. Stroke 21 , 1340–1346 (1990).
11. Mitchell, S. & Gorman, D. The pathophysiology of cerebral arterial gas embolism. J. Extra. Corpor. Technol. 34 (1), 18–23 (2002).

4. Qualitative temperature measurements during catheter IRE-ablation, using Schlieren imaging.

4.1. Introduction

Measuring absolute temperature changes during IRE-ablation is challenging. The IRE-pulse has a duration of only 6 ms, making fiber optic sensors unsuitable, due to their insufficient response time. Non-optic sensors on the other hand will be hindered by the electromagnetic interference of the IRE-pulses. Schlieren imaging is a method to visualize temperature changes for qualitative temperature analysis[1]. Schlieren imaging allows visualization of relative temperature changes in a transparent medium, by visualization of changes in optical density caused by temperature changes or local stress[1,2]. A parallel light beam is send through a transparent medium and focused on a high speed camera (**Figure 4.1A**). Changes in optical density and thus refractory index will cause deflection of the light rays. A rainbow filter is used to color code the degree of deflection of the light rays (**Figure 1B**). The center of the filter is black and therefore nondeflected rays are blocked. Because the background light is blocked, the contrast of the images is enhanced. The circles around the center of the filter are gradually shifting from blue to red, corresponding with a shift from colder to warmer temperatures.

The purpose of this study was to obtain qualitative data about the influence of catheter hoop diameter, energy level and polarity on temperature changes during IRE-ablation.

4.2. Methods

4.2.1. Experimental set up

A Perspex basin of was filled with a saline solution. An indifferent electrode was placed in such position the total system resistance was 60 Ω. A parallel light source was placed behind the basin, and focused towards the camera. A high-speed camera (Photron Fastcam Mini UX50, Motion Engineering, Westfield, IN) was used to capture the Schlieren images. Focused IRE-pulses were produced using

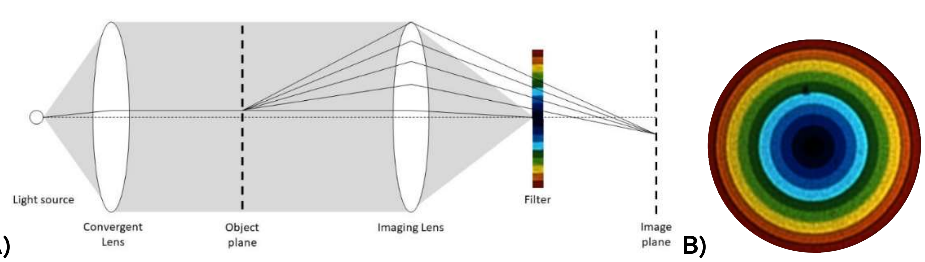

A) B)

Figure 4.1 A) Set up Schlieren imaging. Image obtained from Verdaasdonk[1]. **B)** Rainbow filter as used in our set up.

the monophasic defibrillator (Lifepak 9, Physio-control) using the 7F multi-electrode circular catheter with adjustable diameter. An oscilloscope (Tektronix MDO3014) was used to save the current and voltage waveforms.

IRE-pulses of 20, 50, 100 and 200 J were produced, both with the catheter as cathode and anode and with a catheter hoop diameter of 16, 22 and 27-mm. All measurements were repeated three times. Both overview images of the whole catheter as close-up images focusing on one electrode were produced, using a 6.75 mm and 9 mm filter, respectively. For images of the whole catheter, a framerate of 2000 fps with a resolution of 1280x1024, while for close-up images a framerate of 5000 fps was used with a resolution of 1280x488.

4.2.2. Data analysis

The obtained images were visually analyzed. The different energy settings, cathodal and anodal and different catheter hoop diameters were compared.

4.3. Results

A total of 72 measurements were performed using the different settings. Current and voltage waveforms were smooth, indicating no arcing occurred during the measurements. Different settings and the accompanying IRE-pulses characterizations are shown in **Table 4.1** . A smaller catheter hoop diameter resulted in a higher system resistance and subsequently in a lower peak current.

4.3.1. Ablation settings

A clear difference was seen between the different energy levels; a higher energy level shows a larger change in colors indicating more heat developed during these IRE-pulses (e.g. **Figure 4.2A** vs**. Figure 4.2C**).

Only a slight difference in color changes could be observed between cathodal and anodal IRE-pulses (**Figure 4.2**, left versus right images). A clear difference in the formation of gas bubbles between cathodal and anodal IRE-pulses was seen. During cathodal IRE-pulses larger bubble were observed, which tend to stay longer visible on the images as compared to bubbles during anodal IRE-pulses.

The intensity of the color changes during IRE-pulses using the 16-mm catheter hoop diameter seems to be higher as compared to the intensity during IRE-pulses using the 27-mm catheter hoop diameter (**Figure 4.2**).

Table 4.1 Characterization of the IRE-pulses for all the different settings

	Energy (J)	Peak voltage (V)			Peak Current (A)			Peak resistance (Ω)			Delivered charge (mA)		
		27mm	22mm	16mm	27mm	22mm	16mm	27mm	22mm	16mm	27mm	22mm	16mm
Cathodal	20	633 ± 1	662 ± 1	674 ± 1	11.0 ± 0	9.8 ± 0	9.4 ± 0	58 ± 0	68 ± 0	71 ± 0	53 ± 0	46 ± 0	46 ± 0
	50	1001 ± 0	1052 ± 1	1073 ± 1	17.2 ± 0	15.7 ± 0	15.2 ± 0	58 ± 0	67 ± 0	71 ± 0	82 ± 0	82 ± 0	82 ± 0
	100	1432 ± 1	1492 ± 8	1518 ± 2	24.6 ± 0	22.5 ± 0	21.7 ± 0	58 ± 0	66 ± 0	70 ± 0	116 ± 0	114 ± 0	115 ± 0
	200	1981 ± 1	2084 ± 3	2160 ± 5	34.7 ± 0	31.7 ± 0	30.6 ± 0	57 ± 0	66 ± 0	71 ± 0	167 ± 2	164 ± 1	165 ± 1
Anodal	20	631 ± 1	663 ± 0	674 ± 1	10.7 ± 0	9.8 ± 0	9.5 ± 0	59 ± 0	68 ± 0	71 ± 0	46 ± 0	46 ± 0	46 ± 0
	50	1002 ± 1	1053 ± 1	1068 ± 1	17.2 ± 0	15.7 ± 0	15.2 ± 0	58 ± 0	67 ± 0	70 ± 0	82 ± 1	81 ± 0	81 ± 0
	100	1436 ± 1	1500 ± 1	1517 ± 0	24.7 ± 0	22.4 ± 0	21.7 ± 0	58 ± 0	67 ± 0	70 ± 0	119 ± 1	115 ± 0	115 ± 0
	200	1990 ± 1	2088 ± 4	2116 ± 1	34.6 ± 0	31.8 ± 0	30.7 ± 0	58 ± 0	66 ± 0	69 ± 0	167 ± 1	166 ± 1	166 ± 1

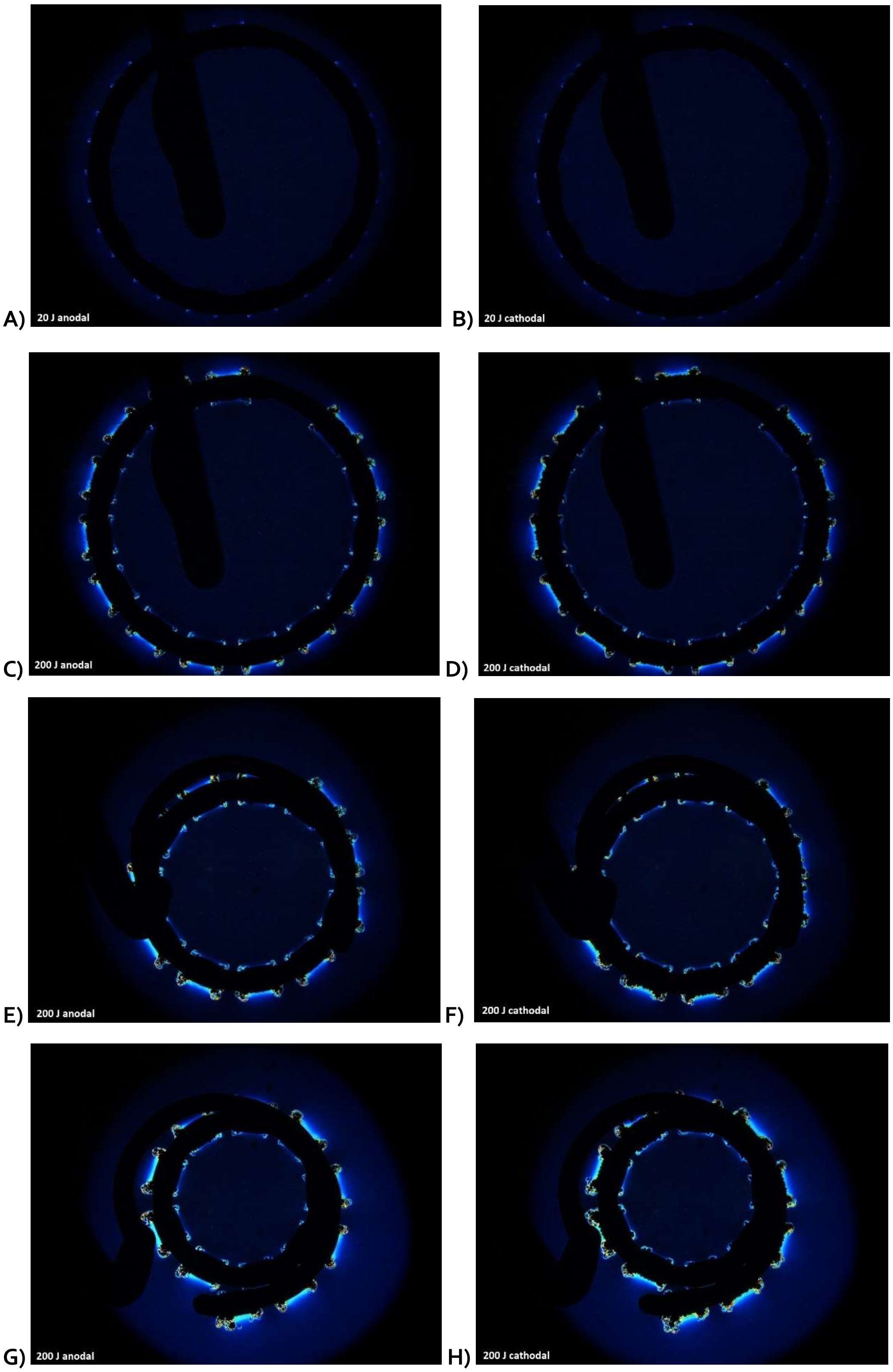

Figure 4.2 Representative Schlieren-images of IRE-pulses using different settings, taken at 12.5 ms after the start of the IRE-pulse. Images of IRE-pulses using the 27-mm catheter hoop diameter: A) 20 J anodal, B) 20 J cathodal, C) 200 J anodal, D) 200 J cathodal. Images of IRE-pulses using the 22-mm catheter hoop diameter: E) 200 J anodal, F) 200 J cathodal. Images of IRE-pulses using the 16-mm catheter hoop diameter: G) 200 J anodal and H) 200 J cathodal.

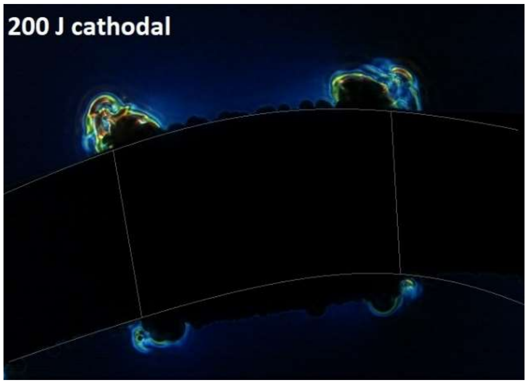

Figure 4.3 Schlieren-image focused on a single electrode.

4.3.2. Location

Based on the overview images, a clear difference was observed between temperature changes on the inside of the catheter compared to the outside of the catheter. The outside of the catheter shows more intense color changes.

Focusing on one electrode, it was observed that the development of heat was higher at the edges of the electrode, while in the center of the electrode only small color changes were observed (**Figure 4.3**). The amount of bubble produced was higher at the edges of the electrodes.

4.4. Discussion

In this study we visualized temperature changes during delivery of IRE-pulses using different settings using color Schlieren imaging. We observed a relation between the used energy level and the amount of heat development, were a higher energy level resulted in a larger change in temperature. No differences were observed between cathodal and anodal IRE-pulses. A smaller catheter hoop diameter seems to produce a larger change in temperature. Development of heat is higher at the edges compared to the center of the electrodes, and higher on the outside of the catheter compared to the inside of the catheter.

The relation between a higher energy level and a larger change in temperature can be explained by joule heating. A higher energy level will lead to a higher current density (**Table 4.1**), which subsequently will lead to more heating.

IRE-pulses produced using the small catheter hoop diameter seem to produce higher temperatures compared to the large catheter hoop diameter. This finding cannot be explained by the current density, since the current density is lower or similar for the small- compared to the large catheter hoop diameter due to a larger resistance (**Table 4.1**). A possible explanation might be the interference of the different electrodes on the light rays. In the small catheter hoop diameter setting, the electrodes overlap each other and produce an image in which the light rays are exposed to multiple electrodes. Therefore, these images show possibly more deflection than actually produced by one electrode.

The fact that the edges of the electrode seem to produce more heat than the center of the electrode can also be explained by the higher current density at the edges of the electrode[3,4]. At the transition from the electrode surface to the catheter, the electric field is higher[3]. The higher current density will also increase the amount of produced gas bubbles, as can be confirmed by our images. A more uniform distribution of the current density along the electrode might decrease the temperature rise. Therefore, future studies should focus on improvement of the electrode design.

4.4.1. Limitations

Temperature visualization using Schlieren imaging is based on changes in refractory index. The refractory index is influenced by temperature changes, but also by changes in local stress. During our experiments, bubbles were formed at the electrode surface, which might have influenced the images. During cathodal IRE-pulses, more and larger bubbles were developed, suggesting that during these measurements a larger effect can be expected. These results are in agreement with the findings described in **chapter 2** and **3**. Although the bubbles might have influenced the Schlieren images, still no clear difference was observed between cathodal and anodal IRE-pulses.

Our measurements were performed in a saline solution at room temperature. Although this gave us an indication about temperature changes and distribution, these results are not directly translatable to a clinical situation.

4.4.2. Clinical implications

During a PVI, the outside of the catheter will be in contact with tissue while the inside of the catheter will be in contact with blood. This might influence the heat development and distribution. The blood flow on the inside of the catheter will decrease the temperature. Since the efficacy of IRE-ablation is at least to a large extent dependent on the changes in the electric field across the cell, cooling by blood will not influence IRE-ablation. The blood flow will decrease the produced temperature, possibly protecting the tissue from thermal damage.

The Schlieren images confirm that the current is directed towards the outside of the catheter, indicating a higher current density on the outside of the catheter. This fact might be beneficial for PVI using IRE-ablation, since a higher current is related to deeper myocardial lesions.

Although the Schlieren images suggest that the duration of the temperature rise is very short, we cannot make statements about the absolute temperature changes. Denaturation of protein in human cells develops at 43–45°C, which is a relative small temperature rise[5]. Several studies focused on temperature changes during IRE-ablation, however these studies are producing more and/or longer IRE-pulses[2,6,7]. Although previous studies did not focus on thermal damage, visual examination showed no clear signs of thermal damage using IRE-ablation[8,9].

4.5. Conclusion

These results suggest that there is no difference in temperature rise as produced by anodal or cathodal IRE-pulses. A higher energy level is related to a higher temperature rise. Improvement of the electrode design will improve the distribution of the current density at the electrode surface. This might lead to an even distribution of heat development the electrode, possibly resulting in a lower peak temperature. This hypothesis should be investigated by future studies.

4.6. References

1. Verdaasdonk, R. in *Handbook of physics in medicine and biology* (ed. Robert Splinter) 1–10 (2010).
2. Van Den Bos, W., Scheffer, H. J., Vogel, J. A., Wagstaff, P. G. K., De Bruin, D. M., De Jong, M. C., *et al.* Thermal Energy during Irreversible Electroporation and the Influence of Different Ablation Parameters. *J. Vasc. Interv. Radiol.* **27** (3), 433–443 (2016).
3. Ahsan, A. J., Cunningham, D., Rowland, E. & Rickards, a F. Catheter ablation without fulguration: design and performance of a new system. *Pacing Clin. Electrophysiol.* **12** (9), 1557–61 (1989).
4. Pour Aryan, N. Primary Current Distribution and Electrode Geometry. *Electr. Comput. Eng.* **78** , (2015).
5. Yarmush, M. L., Golberg, A., Serša, G., Kotnik, T. & Miklavčič, D. Electroporation-Based Technologies for Medicine: Principles, Applications, and Challenges. *Annu. Rev. Biomed. Eng.* **16** (1), 295–320 (2014).
6. Van Gemert, M. J. C., Wagstaff, P. G. K., De Bruin, D. M., Van Leeuwen, T. G., Van Der Wal, A. C., Heger, M., *et al.* Irreversible electroporation: Just another formof thermal therapy? *Prostate* **75** (3), 332–335 (2015).
7. Faroja, M., Ahmed, M., Appelbaum, L., Ben-David, E., Moussa, M., Sosna, J., *et al.* Irreversible Electroporation Ablation: Is All the Damage Nonthermal? *Radiology* **266** (2), 462–470 (2013).
8. Wittkampf, F. H. M., Van Driel, V. J., Van Wessel, H., Neven, K. G. E. J., Gründeman, P. F., Vink, A., *et al.* Myocardial lesion depth with circular electroporation ablation. *Circ. Arrhythmia Electrophysiol.* **5** (3), 581–586 (2012).
9. Neven, K., Van Es, R., Van Driel, V., Van Wessel, H., Fidder, H., Vink, A., *et al.* Acute and Long-Term Effects of Full-Power Electroporation Ablation Directly on the Porcine Esophagus. *Circ. Arrhythmia Electrophysiol.* **10** (5), e004672 (2017).

5. Difference in lesion depth between monophasic anodal and cathodal pulses using irreversible electroporation ablation

5.1. Introduction

The results as described in **chapter 2, 3** and **4** suggest that anodal IRE-pulses are preferred over cathodal IRE-pulses, considering bubble gas formation and temperature. So far, all feasibility studies were performed using cathodal IRE-pulses[1–3], therefore it is not certain that anodal IRE-pulses are just as effective. In this non-inferiority study, we will focus on long-term cardiac cell damage, by comparing lesion depth in a porcine model. A follow up period of three weeks will allow lesion formation by replacement of cardiomyocytes by fibroblasts with loose collagen fibers[1], which can be histologically identified.

5.2. Methods

This study was performed with prior approval from the Animal Experimentation Committee of the University Medical Center Utrecht and were in compliance with the *Guide for the Care and Use of Laboratory Animals*[4].

5.2.1. Study protocol

This study was performed in ten pigs (weight 60-70 kg, Topigs Norsvin). Antibiotics (amoxicillin/clavulanic acid, 12.5 mg/kg) was started three days before the procedure. The animals were given amiodarone starting 1 week before the procedure (1200 mg daily). The animals were sedated, intubated and anesthetized according to standard procedures[5]. A patch electrode (7506, Valley Lab Inc, Boulder, CO, USA) was placed on a shaven area at the lower back and used as counter electrode. The thorax was opened using a median sternotomy and the peripheral sac was opened. A custom made linear suction cup electrode was used, which consisted of a 35-mm-long and 6-mm-

A)
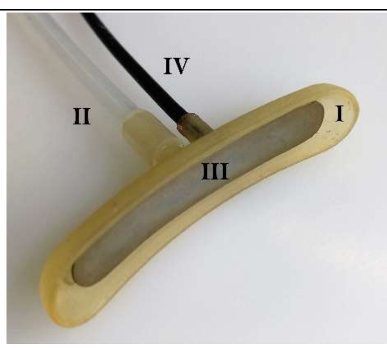

B)
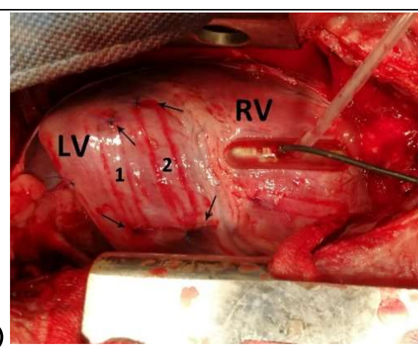

Figure 5.1 A) Linear suction cup electrode consisting of a plastic suction cup (42x7mm, I) connected to a vacuum system (II) and an electrode (35x6 mm, III) which is connected to the defibrillator with a cable (IV). Obtained from Neven et al.[2] **B)** Example of the placement of the electrode at the RV. On the LV two lesions can be identified, with at both ends sutures (arrows).

wide linear electrode inside a 42-mm-long and 7-mm-wide plastic suction cup (**Figure 5.1A**). A constant negative pressure was used to fixate the electrode to the desired locations at the left ventricle (LV) and right ventricle (RV) (**Figure 5.1B**). A monophasic defibrillator (Lifepak 9, Physio-Control, Inc, Redmond, WA) was used to create lesions at random positions on the LV and RV. Four lesions were created on the LV, using 50 and 100 J for both anodal and cathodal IRE-pulses. Two lesions were created on the RV, using 30 J for both anodal and cathodal IRE-pulses. After each ablation, the ablation side was marked using sutures at both ends of the electrode position. Voltage and current waveforms were recorded and stored using an oscilloscope (Tektronix TDS 2002B). Resistance was calculated by dividing the peak voltage by the peak current.

After three weeks survival the animals were euthanized and the heart was removed for histological analysis. Tissue was fixated in formaldehyde and each section was cut into 5-6 segments perpendicular to the lesion and embedded in paraffin. The segments were stained using hematoxylin and eosin (H&E) and Elastic - Van Gieson (EvG).

All segments were digitized to measure lesion depth and width. Lesion depth was measured conform protocol of a previous study[2]. Lesion width was measured at 50% of the total depth of the lesion. The median lesion depth and width were calculated per lesion, after which the mean depth and width for each setting was calculated.

5.3. Data analysis

All variables were expressed as mean±SD. Voltage and current waves were analyzed using Matlab (2017a, The Mathworks, Natick, MA, USA). Lesion depth and width was analyzed using cellSens (Olympus, Tokyo, Japan). Lesion depth and width for anodal and cathodal IRE-pulses were compared.

5.4. Preliminary results

Two of the animals died before the follow up period was ended. One of the animals died the first day after the procedure, presumably due to procedure related arrhythmias and/or heart failure. The other

Table 5.1 Mean lesion depth and width for all different settings.

	Location	Energy (J)	Peak voltage (V)	Peak current (A)	Resistance (Ω)	Delivered charge (mC)	Lesion depth (mm)	Lesion width (mm)	Trans-mural (n/total)
Cathodal	RV	30	930±23	8.8±0.7	106±11	56±1	5.1±0.4	8.1±1.1	4/4
	LV	50	1212±31	10.9±0.9	111±12	72±3	5.4±2.2	7.6±1.4	3/4
	LV	100	1753±16	15.5±0.6	113±5	101±2	6.5±2.2	10.4±0.8	3/4
Anodal	RV	30	934±19	8.7±0.5	108±8	56±1	5.9±0.9	8.2±0.7	4/4
	LV	50	1226±7	10.5±0.3	117±4	72±3	6.4±0.6	7.2±1.9	3/4
	LV	100	1751±11	15.6±0.2	112±2	100±2	7.7±1.3	10.5±2.0	3/4

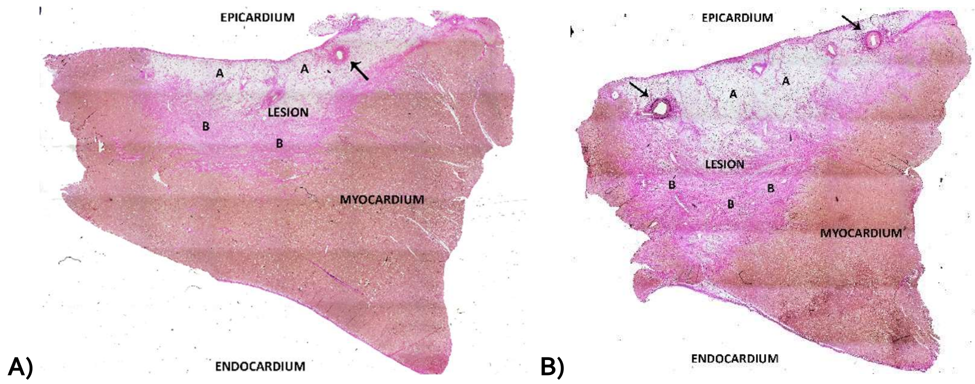

Figure 5.2 Representative images of **A)** cathodal and **B)** anodal lesions of 100 J. The maturation of the lesion is different in different regions of the lesions. In regions A loose connective tissue can be identified, where the myocardium is not totally replaced by collagen fibers. In regions B the myocardial cells are replaced by collagen fibers produced by fibroblasts. Coronary arteries are marked by the arrows.

animal died the second day after the procedure, due to a volvulus and subsequent an ischemic bowel. A volvulus is a rare but known complication of general anesthesia. Both animals were excluded from analysis. So far, four animals were included for the analysis.

All voltage and current waveform were smooth, indicating no arcing occurred. In two cases, the heart went into ventricular fibrillation (VF) after delivery of the IRE-pulse; in one case after a 50 J anodal IRE-pulse and in one case after 100 J cathodal IRE-pulse. Sinus rhythm was restored after two 10 J- and two 10 J plus one 20 J internal defibrillator shocks using sterile paddles, respectively.

For all energy levels (30, 50 and 100 J), anodal IRE-pulses resulted in at least as deep and wide lesions as compared to cathodal IRE-pulses, p=0.068, p=0.273 and p=0.273, respectively (**Table 5.1**). No significant difference in lesion width was seen between anodal and cathodal IRE-pulses of 30, 50 and 100 J, p=1.000, p=0.465 and p=1.00, respectively.

5.5. Discussion

We focused on lesion formation during epicardial IRE-ablation, to compare difference in lesion size between cathodal and anodal IRE-pulses. Anodal IRE-pulses produced at least the same lesion depth and width as compared to cathodal IRE-pulses.

Theoretically, no difference in lesion depth is expected, since the only difference would be the direction of the current. Some studies focused of the influence of the direction of the current on electroporation of a single cell and found a difference in cell damage between cells which were orientated parallel or perpendicular to the current[6]. However, we are not interested in the damage of a single cell, but in overall damage in tissue with different orientated cells. Therefore, we expect that the direction of the current would not influence the overall effect of electroporation.

In previous work of Neven et al.[2], the same set up was used to determine the lesion depth and width of monophasic IRE-ablation application of 30, 100 and 300 J. We can directly compare our measurements of cathodal IRE-pulses of 30 and 100 J, to verify the measurement method. They found a lesion depth of 3.2±0.7 and 6.3±1.8 mm, compared to 5.1±0.4 and 6.5±2.2 mm in our study, for 30 and 100 J IRE pulses respectively. The lesion depth as created by IRE-pulses of 100 J are comparable between the two studies. In our study, the lesion depth as created by IRE-pulses of 30 J are higher as compared to the lesion depth they measured. A possible explanation might be the location of the ablations, since in the study of Neven et al. only positions at the left ventricle were used, while our 30 J applications were positioned at the right ventricle. All of our 30 J lesions were transmural, while only 25% of their lesions were transmural. Another difference is the follow up term, which is 3 months in their study compared to three weeks in our study.

In two cases VF was developed after application of the IRE-pulse. Although sinus rhythm could be restored, development of VF is undesirable. All animals received anti-arrhythmic drugs before the start of the procedure (**section 5.2.1**). An explanation of the development of VF might be that the delivery of the IRE-pulse could not always be synchronized with the heart rhythm of the animal[7]. During clinical procedures, delivery of IRE-pulses should be synchronized to prevent the development of VF due to the IRE-pulse.

5.5.1. Limitations

So far, only four out of eight animals could be included for the analysis. Therefore, these results should be interpreted with caution. A more elaborate analysis should confirm our results.

In this study we used three energy settings (30, 50 and 100 J), while the clinically relevant energy setting is thought to be 200 J[5]. Therefore, we are not sure what the exact effects of 200 J IRE-pulses will be. Since this study was a non-inferiority study and lesion depth is related to the amount of delivered charge[2], it is expected that these results may be extrapolated to 200 J IRE-pulses.

In our setup epicardial IRE-pulses were delivered using a suction cup electrode, while in the clinical setting endocardial lesions are created using a multi-electrode circular catheter. Our set up provides comparable electrode-tissue contact between the different settings, which improves the reliability of our results. However, the measured lesion depth and width might not directly be translatable to endocardial ablations. We expect that the current density for the circular multi-electrode will be lower compared to the suction cup electrode, since the current may leak into surrounding tissue e.g. blood. Therefore, we expect that the lesion depth and width might be lower for the circular multi-electrode catheter.

5.5.2. Clinical implications

The results of this study suggest that anodal IRE-pulses produce at least the same lesion depth and width as cathodal IRE-pulses. Based on this results and the results from **chapter 2, 3 and 4**, anodal IRE-pulses should be preferred over cathodal IRE-pulses. Anodal IRE-pulses are thought to be just as effective as cathodal IRE-pulses, however a lower total gas volume and a less number of gas bubbles is developed during anodal IRE-pulses. Further studies are needed to investigate the difference in arcing threshold between anodal and cathodal IRE-pulses.

5.6. Conclusion

Anodal and cathodal IRE-pulses result in the same lesion depth and width, indicating anodal IRE-pulses are non-inferior to cathodal IRE-pulses.

5.7. References

1. Wittkampf, F. H. M., Van Driel, V. J., Van Wessel, H., Neven, K. G. E. J., Gründeman, P. F., Vink, A., et al. Myocardial lesion depth with circular electroporation ablation. Circ. Arrhythmia Electrophysiol. 5 (3), 581–586 (2012).
2. Neven, K., Van Driel, V., Van Wessel, H., Van Es, R., Doevendans, P. A. & Wittkampf, F. Epicardial linear electroporation ablation and lesion size. Hear. Rhythm 11 (8), 1465–1470 (2014).
3. Neven, K., Van Driel, V., Van Wessel, H., Van Es, R., Doevendans, P. A. & Wittkampf, F. Myocardial Lesion Size After Epicardial Electroporation Catheter Ablation After Subxiphoid Puncture. Circ. Arrhythmia Electrophysiol. 7 (4), 728–733 (2014).
4. Council, N. R. Guide for the Care and Use of Laboratory Animals. (The National Academies Press, 2011). doi:10.17226/12910
5. Wittkampf, F. H., Van Driel, V. J., Van Wessel, H., Vink, A., Hof, I. E., Gründeman, P. F., et al. Feasibility of electroporation for the creation of pulmonary vein ostial lesions. J. Cardiovasc. Electrophysiol. 22 (3), 302–309 (2011).
6. Knisley, S. B. & Grant, A. O. Asymmetrical electrically induced injury of rabbit ventricular myocytes. J. Mol. Cell. Cardiol. 27 (5), 1111–1122 (1995).
7. Wojtaszczyk, A., Caluori, G., Pešl, M., Melajova, K. & Stárek, Z. Irreversible electroporation ablation for atrial fibrillation. J. Cardiovasc. Electrophysiol. (2018). doi:10.1111/jce.13454

6. Determination of the arcing threshold for anodal and cathodal IRE-pulses

6.1. Introduction

As described in **chapter 1**, an advantage of IRE-ablation using a circular catheter is that it is possible to produce sufficient lesion depth without arcing at the catheter. Previous studies were inconclusive about the difference in arcing threshold for cathodal and anodal IRE-pulses[1–4]. The arcing threshold is an important factor for the safety of IRE-ablation, since arcing is likely to induce barotrauma and thereby may cause severe complications[5,6]. In this study, the arcing threshold for anodal and cathodal IRE-pulses was determined in an *in vivo* porcine model.

6.2. Methods

All experiments were approved by the Animal Experimentation Committee of the University Medical Center Utrecht and were in compliance with the *Guide for the Care and Use of Laboratory Animals*[7].

6.2.1. Study procedure

This study was performed in three 60-75 kg pigs (Topigs Norsvin). The animals were given 1200 mg/day amiodarone starting seven days before the procedure. Three days before the procedure antibiotics (amoxicillin/clavulanic acid, 12.5 mg/kg) were started. On the day of the procedure the animals were sedated, intubated and anesthetized according to a previously described protocol[4]. An indifferent patch electrode (7506, Valley Lab Inc, Boulder, CO, USA) was placed on a shaven area at the lower back and used as counter electrode. The animals were heparinized.

Under fluoroscopic guidance, transseptal puncture was performed using a deflectable sheath (Agilis, Abbott, Minnetonka, MN, USA) via the right femoral vein. A 7F circular 14-electrode catheter with an adjustable hoop diameter of 16-27-mm was used. The catheter was introduced into the left atrium, and positioned in a floating position. After each delivery of the IRE-pulses, the catheter was pulled into the sheath and flushed with saline, to remove the produced bubbles from the catheter.

6.2.2. Ablation settings

For IRE-ablation a monophasic external defibrillator (LifePak 9) was used to deliver the IRE-pulses. An oscilloscope (Tektronix TDS 2002B) was used to store the voltage and current waveforms. For both cathodal and anodal pulses an energy level of 200 and 300 joules were used, using the 16-mm and 27-mm catheter hoop diameter.

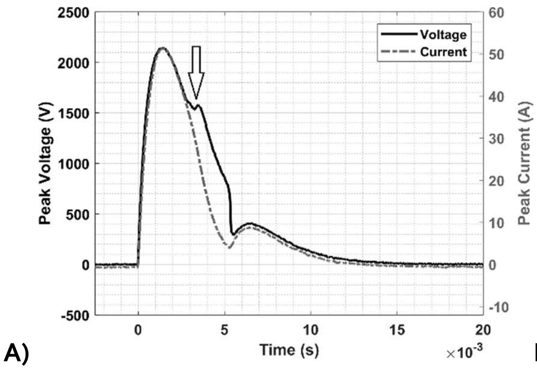

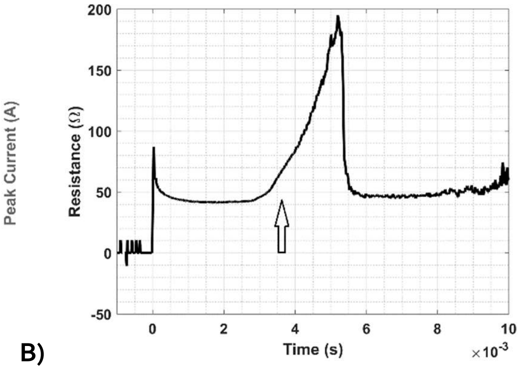

Figure 6.1 Example of a voltage and current waveform which shows clear signs of arcing. **A)** The voltage curve shows a sudden rise, while the current shows a decline (arrow). **B)** Image of the resistance waveform, focused on the sudden ride in resistance (arrow).

6.2.3. Data analysis

Data was analyzed using Matlab (2017a, The Mathworks, Natick, MA, USA). Impedance was calculated by dividing the voltage waveform by the current waveform. Three observers scored the impedance waveforms on the occurrence of arcing, based on a sudden rise in resistance (e.g. **Figure 6.1**). Three categories were used: no-arc, a possible arc and definitely arc. This data was compared and consensus was achieved.

6.3. Results

Measurements were successfully performed in three pigs. A total of 258 IRE-pulses were delivered, of which 78 IRE-pulses were marked as arcing, 24 IRE-pulses were marked as possibly arcing and 156 IRE-pulses were marked as non-arcing (**Figure 6.2**).

Anodal IRE-pulses resulted in a higher arcing threshold compared to cathodal IRE-pulses using the 27-mm catheter hoop diameter; 51.2 A and 45.2 A, respectively. Pulses produced by the 16-mm catheter hoop diameter resulted in a lower arcing threshold as compared to pulses produced using the 27-mm catheter hoop diameter. Anodal IRE-pulses using the 16-mm catheter hoop diameter, resulted in a arcing threshold of 37.4 A. Four IRE-pulses below this threshold were marked as a possible arc (34.7 A). Cathodal IRE-pulses resulted in a threshold of 36.8 A using the 16-mm catheter hoop diameter.

6.4. Discussion

These results showed a higher arcing threshold for anodal IRE-pulses compared to cathodal IRE-pulses for the 27-mm catheter hoop diameter. The smaller catheter hoop diameter resulted in a lower arcing threshold as compared to the larger catheter hoop diameter, for both anodal and cathodal IRE-pulses. For the 16-mm catheter hoop diameter, the arcing threshold for anodal IRE-pulses was 37.4 A

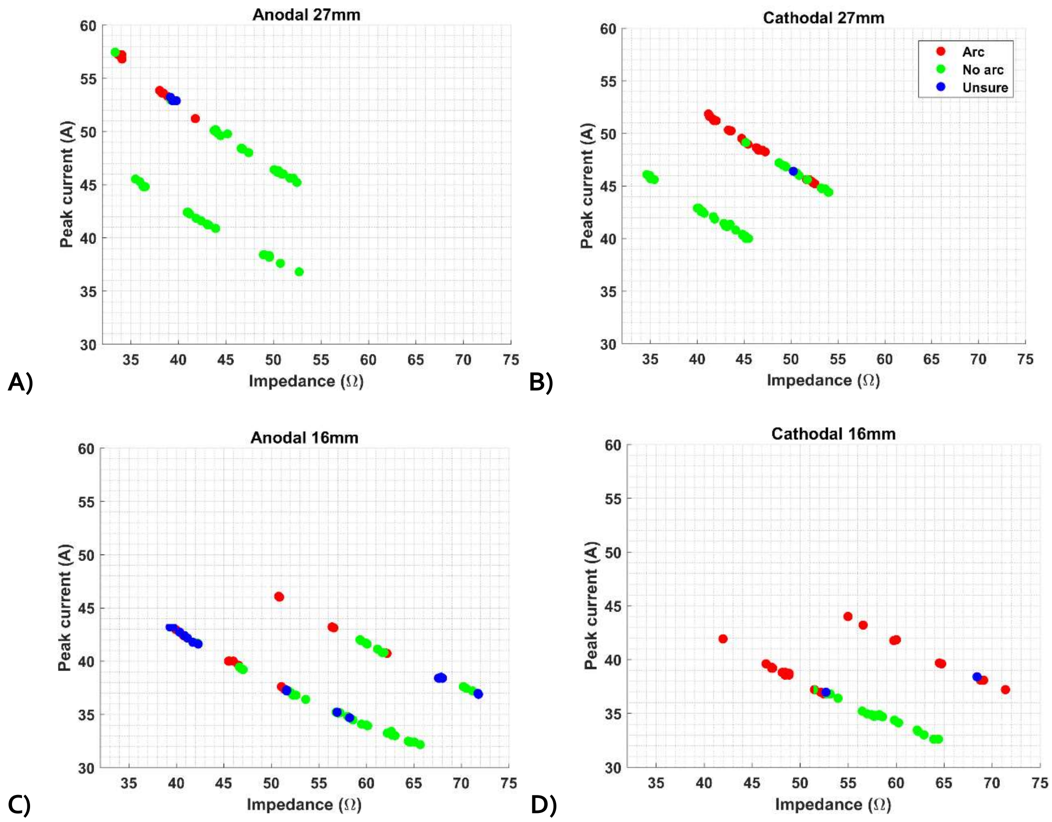

Figure 6.2 Delivered peak current for the different settings. In all graphs, the upper row of IRE-pulses are 300 J deliveries, while the lower row are 200 J deliveries. **A)** Anodal IRE-pulses using the 27-mm catheter hoop diameter. **B)** Cathodal IRE-pulses using the 27-mm catheter hoop diameter. **C)** Anodal IRE-pulses using the 16-mm catheter hoop diameter. **D)** Cathodal IRE-pulses using the 16-mm catheter hoop diameter.

for the definitive arcs, however four IRE-pulses were marked as possible arcs (lowest at 34.7 A). The arcing threshold for cathodal IRE-pulses using the 16-mm catheter hoop diameter was 36.8 A. These results indicate that there is no definite difference in arcing threshold for anodal and cathodal IRE-pulses for the 16-mm catheter hoop diameter.

The difference in arcing threshold between anodal and cathodal IRE-pulses might be explained by the development of gas bubbles (**chapter 2** and **3**). Since cathodal IRE-pulses are thought to produce significantly more gas bubbles as compared to anodal IRE-pulses, the electrodes might be insulated faster as compared to anodal IRE-pulses. A previous study of Ahsan *et al.*[1] showed similar results. They also stated that during their study set up the occurrence of arcing during anodal IRE-pulses rather occurred on the surface on the formed bubbles than at the electrode surface.

Another factor which might influence the arcing threshold is the catheter and electrode design[1]. The electrode design which is used for the circular catheter results in a higher current density at the edge of the electrode. A different electrode design might result in a more even current density around the electrode, which might result in an even higher arcing threshold. This theory might be confirmed in future studies: these studies should focus on the location of arcing at the electrode (or at the bubble surface) using the circular catheter.

The difference between the 16-mm and 27-mm catheter hoop diameter might be explained by the position of the electrode. If the catheter hoop diameter is small, several electrode overlap each other. This might influence the current density, resulting in a lower arcing threshold for the small catheter hoop diameter. Another possible explanation might be the formation of gas bubbles. The bubbles of neighboring electrodes (due to the small catheter hoop) might influence the occurrence of arcing.

6.4.1. Limitations

The occurrence of an arc cannot be scored objectively. The arcing threshold is thought to be different in saline and blood, therefore no visible confirmation of the arc can be used. In this study the resistance curves were visually scored by three observers and compared afterwards. Some of the curves were not clearly arcing, however a small bump in the resistance curve was observed. These curves were marked as 'possible arc'. However, there is no clinical evidence of the damage of such small arcs. Future studies should focus on the distinguishing between harmful arcs and safe IRE-pulses.

6.4.2. Clinical implications

The arcing threshold for anodal IRE-pulses is higher as compared to cathodal IRE-pulses, indicating that it would be safer to use anodal IRE-pulses. For a safe application of the IRE-current a safety margin of at least 5 percent should be added. This results in an arcing threshold for anodal IRE-pulses using the 27-mm catheter hoop diameter of 48.7 A, which is way above the current which is needed to produce a deep enough lesion. The arcing threshold for anodal IRE-pulses using the 16-mm catheter hoop diameter was 33.0 A, which is thought to be still above the current needed for a sufficient lesion depth. Therefore, no arcing is expected during IRE-ablation procedures. However, during this study the catheter was cleaned after every application by means of pulling the catheter in the sheath and flushing using saline. A suitable cleaning procedure should be development, which can be used during a clinical IRE-ablation procedure.

6.5. Conclusion

In this study we found a higher arcing threshold for IRE-pulses as delivered by the large catheter hoop diameter compared to the small catheter hoop diameter. During an IRE-ablation procedure it is important to monitor the total system resistance and add an extra serial resistance if needed to produce IRE-pulses which are below the arcing threshold.

6.6. References

1. Ahsan, A. J., Cunningham, D., Rowland, E. & Rickards, a F. Catheter ablation without fulguration: design and performance of a new system. *Pacing Clin. Electrophysiol.* **12** (9), 1557–61 (1989).
2. Lee, R. C., Zhang, D. & Hannig, J. Biophysical Injury Mechanisms in Electrical Shock Trauma. *Annu. Rev. Biomed. Eng.* **2** (1), 477–509 (2000).
3. Rowland, E., Cunningham, D., Ahsan, A. & Rickards, A. Transvenous ablation of atrioventricular conduction with a low energy power source. *Br. Heart J.* **62** (5), 361–366 (1989).
4. Wittkampf, F. H., Van Driel, V. J., Van Wessel, H., Vink, A., Hof, I. E., GrÜndeman, P. F., *et al.* Feasibility of electroporation for the creation of pulmonary vein ostial lesions. *J. Cardiovasc. Electrophysiol.* **22** (3), 302–309 (2011).
5. Bardy, G. H., Coltorti, F., Stewart, R. B., Greene, H. L. & Ivey, T. D. Catheter-mediated electrical ablation: The relation between current and pulse width on voltage breakdown and shock-wave generation. *Circ. Res.* **63** (2), 409–414 (1988).6. Lemery, R., Talajic, M., Roy, D., Coutu, B., Lavoie, L., Lavaliée, E., *et al.* Success, safety, and late electrophysiological outcome of low-energy direct-current ablation in patients with the Wolff-Parkinson-White syndrome. *Circulation* **85** (3), 957–962 (1992).
7. Council, N. R. *Guide for the Care and Use of Laboratory Animals*. (The National Academies Press, 2011). doi:10.17226/12910

7. Difference between biphasic and monophasic pulse using irreversible electroporation ablation

7.1. Introduction

To investigate whether the biphasic defibrillator may be a suitable replacement for the old-fashioned monophasic defibrillator, we compare lesion formation between single pulse monophasic and biphasic IRE ablation. We will focus on long-term cardiac cell damage, by comparing lesion depth in a porcine model. A follow up period of three weeks will allow lesion formation by replacement of cardiomyocytes by fibroblasts with loose collagen fibers[1], which can be histologically identified.

7.2. Methods

This study was performed with prior approval from the Animal Experimentation Committee of the University Medical Center Utrecht and were in compliance with the *Guide for the Care and Use of Laboratory Animals*[2].

7.2.1. Study protocol

This study was performed in seven pigs (weight 60-70 kg, Topigs Norsvin). Antibiotics (amoxicillin/clavulanic acid, 12.5 mg/kg) was started three days before the procedure. The animals were given amiodarone starting 1 week before the procedure (1200 mg daily). The animals were sedated, intubated and anesthetized according to standard procedures[3]. A patch electrode (7506, Valley Lab Inc, Boulder, CO, USA) was placed on a shaven area at the lower back and used as counter electrode. The thorax was opened using a median sternotomy and the peripheral sac was opened. The custom made linear suction cup electrode was used, which consisted of a 35-mm-long and 6-mm-wide linear electrode inside a 42-mm-long and 7-mm-wide plastic suction cup (**Figure 5.1**). A constant negative pressure was used to fixate the electrode to the desired locations at the left ventricle (LV). A monophasic defibrillator (Lifepak 9, Physio-Control, Inc, Redmond, WA) and a biphasic defibrillator (Philips Heartstart XL, Eindhoven, Netherlands) were used to create lesions at random positions on the LV. For both defibrillation modalities energy levels of 30 and 100 joules were used, resulting in a total of four lesions per heart. The catheter was used as cathode for the monophasic pulses, while the indifferent skin patch was used as anode. The biphasic pulses were initially cathodal. After each ablation, the ablation side was marked using sutures at both ends of the electrode position. Voltage and current waveforms were recorded and stored using an oscilloscope (Tektronix TDS 2002B). Resistance was calculated by dividing the peak voltage by the peak current.

After three weeks survival the animals were euthanized and the heart was removed for histological analysis. Tissue was fixated in formaldehyde and each section was cut into 5-6 segments perpendicular to the lesion and embedded in paraffin. The segments were stained using hematoxylin and eosin (H&E) and Elastic - Van Gieson (EvG).

All segments were digitized to measure lesion depth and width. Lesion depth was measured conform protocol of a previous study[4]. Lesion width was measured at 50% of the total depth of the lesion. The median lesion depth and width were calculated per lesion, after which the mean depth and width for each setting was calculated.

7.3. Statistical analysis

All variables were expressed as mean±SD. Voltage and current waves were analyzed using Matlab (2017a, The Mathworks, Natick, MA, USA). Lesion depth and width was analyzed using cellSens (Olympus, Tokyo, Japan). Lesion depth and width for both monophasic and biphasic IRE-pulses were compared using Wilcoxon signed rank test. Statistical significance was defined as $p \leq 0.05$.

7.4. Results

All animals survived both the index procedure and the three week survival. During one monophasic IRE-pulse of 30J the voltage and current waveforms were not smooth, indicating this IRE-pulse arced[5]. This data was excluded from analysis. The other waveforms were smooth and therefore no arcing is expected (**Figure 7.1**). Monophasic IRE-pulses of 30 and 100 J resulted in 7.9±0.3 and 16±0.8 A peak current, respectively, while biphasic IRE-pulses of 30 and 100 J resulted in 6.2±0.4 and 13.4±1.3 A peak current, respectively (**Table 7.1**). Peak resistance was 122±8 and 109±7 Ω for monophasic IRE-pulses of 30 and 100 J, respectively, and 132±12 and 111±11 Ω for biphasic IRE-pulses of 30 and 100 J, respectively. Monophasic IRE-pulses of 100 J resulted in significantly deeper lesions compared to monophasic IRE-pulses of 30 J (p=0.028). No significant difference in lesion depth was found between

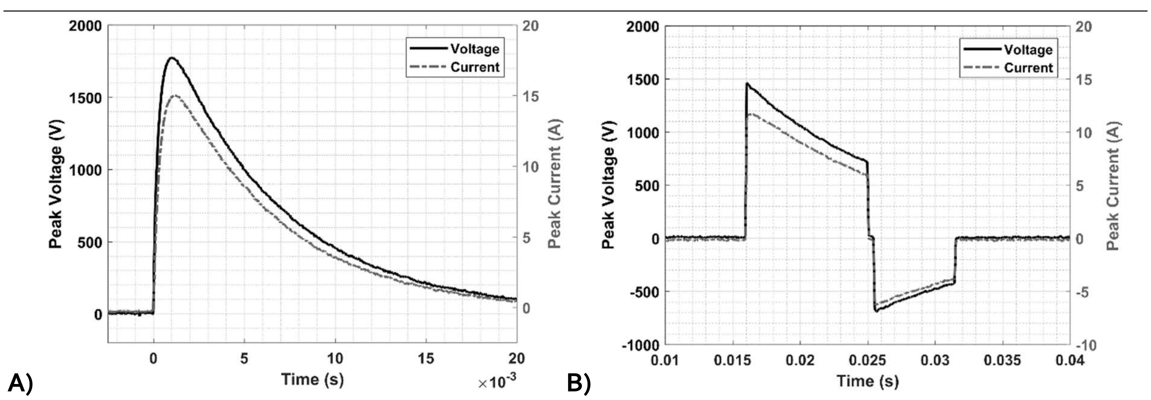

Figure 7.1 Example of the voltage and current waveforms. **A)** Representative 100 J monophasic IRE-pulse. **B)** Representative 100 J biphasic IRE-pulse.

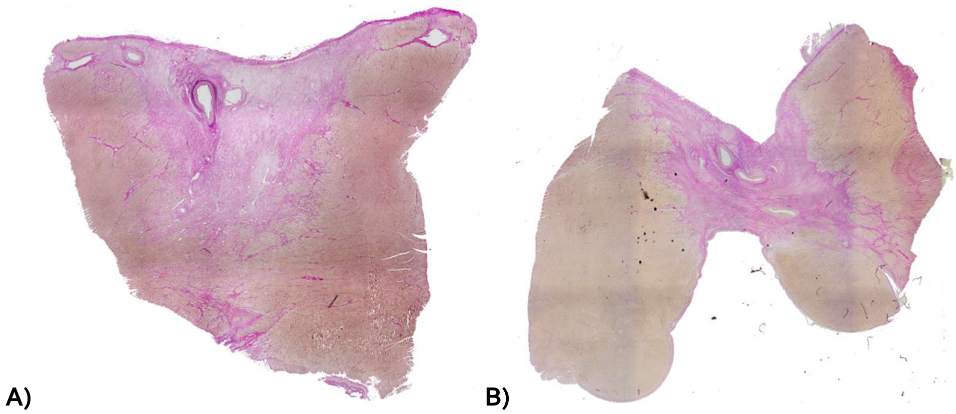

Figure 7.2 Example of lesions using EvG staining. **A)** Non-transmural lesion, **B)** Transmural lesion with extensive tissue shrinking.

biphasic IRE-pulses of 30 and 100 J (p=0.128). No significant difference in lesion depth was measured between monophasic and biphasic IRE-pulses of both 30 and 100J (p=0.345 and p=0.866, respectively).

No significant difference in lesion width was found between biphasic IRE-pulses of 30 and 100 J (p=1.000) and monophasic and biphasic IRE-pulses of 30 J (p=0.753). Monophasic IRE-pulses of 100 J were significantly wider than monophasic IRE-pulses of 30 J (p=0.043). Monophasic IRE-pulses of 100 J were significantly wider than biphasic IRE-pulses (p=0.028).

7.5. Discussion

In this study we focused on lesion formation by IRE using either a monophasic or biphasic IRE-pulse, by comparing lesion depth an width. No significant difference in lesion depth between monophasic and biphasic IRE-pulses was measured. Lesion depth of monophasic IRE-pulses of 100 J were significantly larger than monophasic IRE-pulses of 30 J. For biphasic pulses no significant difference in lesion depth was found between 30 and 100 J. Monophasic IRE-pulses of 100 J resulted in wider lesions compared to monophasic IRE-pulses of 30 J and biphasic IRE-pulses of 100 J. No difference in lesion width was measured between biphasic IRE-pulses of 30 and 100 J. These results indicate that there is no difference in lesion depth between IRE-ablation with monophasic or biphasic defibrillators.

Table 7.1 Mean lesion depth and width for all different settings

	Energy (J)	Peak voltage (V)	Peak current (A)	Resistance (Ω)	Delivered charge (mC)	Lesion depth (mm)	Lesion width (mm)	Trans-mural (n/total)
Mono phasic	30	966±20	8.0±0.0	122±8	54±3	5.1±1.1	5.7±1.0	1/7
	100	1744±27	16.0±0.8	109±7	102±3	7.6±4.0	10.6±1.7	4/7
Bi phasic	30	816±23	6.2±0.4	132±12	66±4	4.8±2.9	5.5±1.5	1/7
	100	1473±11	13.4±1.3	111±11	118±5	7.5±2.2	5.7±0.8	4/7

Previous studies investigated differences between monophasic and biphasic IRE-pulses. A previous study of Bilska *et al.*[7] found no difference in fractional pore area between monophasic and biphasic electroporation pulses. Huang *et al.*[8] found no difference in defibrillation threshold and upper limit vulnerability during defibrillation with either a monophasic or biphasic shock. However, these studies were not focused on irreversible cell damage.

In this study we used a linear suction cup electrode, to guarantee good electrode-tissue contact. The electrode is electrically isolated, resulting in delivery of the total current in the myocardial tissue. Therefore we are certain that there is no current leak to surrounding tissue.

As mentioned in **chapter 5**, in previous work of Neven *et al.*[4], the same set up was used to determine the lesion depth and width of monophasic IRE-ablation application of 30, 100 and 300 J. In their study they found a lesion depth of 3.2±0.7 and 6.3±1.8 mm, for 30 and 100 J IRE pulses respectively. These measurements are in the same range as our measured lesion depth (5.1±1.1 and 7.6±4.0 mm, respectively), although our measurements are consequently higher. The lesion width for 30 and 100 J were 10.1±0.8 and 15.1±1.5 mm, respectively. These measurements are larger than our measured lesion with (5.7±1.0 and 10.6±1.7 mm, respectively). This may be explained by the protocol for the measurement of the lesion width. In our study, we aimed for a standardized method for the measurement of lesion width to exclude subjective influences. Therefore we determined to measure the lesion width at 50% of the total lesion depth. However, this does not per se result in the maximum lesion width (e.g**. Figure 7.2**).

7.5.1. Limitations

In this study we only used two energy settings (30 and 100 J), while the clinically relevant energy setting is thought to be 200 J[3]. As mentioned in **chapter 5**, lesion depth is related to delivered charge and therefore these results can be extrapolated.

As mentioned in **chapter 5**, another limitation of this study might be the use of suction cup electrode. This electrode is different from the catheter which is going to be used during endocardial procedures. As explained before, current density will be lower using the circular catheter as compared to the suction cup electrode and therefore lesion depth are not directly translatable in to a clinical situation.

7.5.2. Clinical implications

Although the lesion depth as measured with the suction cup is not directly translatable to a lesion depth as created by the multi-electrode circular catheter, it is expected that the current density with the circular catheter towards the tissue is still high enough to create enough damage. In our study we used low energy levels (30 and 100 J), but we still found a lesion depth up to 7.6±4.0 mm. Transmural lesions were found in 4 out of 7 biphasic lesions.

Another factor which might influence the clinical relevance of biphasic IRE-pulses is the formation of gaseous microbubbles. As described in **chapter 2 and 3**, cathodal monophasic IRE-pulses will produce significantly more volume as compared to anodal monophasic IRE-pulses. The biphasic IRE-pulses consists of both a positive and negative part of the current waveform, indicating that biphasic IRE-pulses might produce more gas as compared to a single anodal IRE-pulses. Further research should be performed to investigate the formation of gas during biphasic IRE-pulses.

7.6. Conclusion

In this study we found that monophasic IRE-pulses and biphasic IRE-pulses with the same energy level will result in the similar lesion depth and width. In terms of efficacy, this indicates that it is possible to replace the monophasic defibrillator by a modern biphasic defibrillator. The availability of these devices is better and thereby the costs of the therapy might be decreased. Further studies should focus on endocardial ablations, on difference in polarity and on safety of IRE-ablation using biphasic IRE-pulses.

7.7. References

1. Wittkampf, F. H. M., Van Driel, V. J., Van Wessel, H., Neven, K. G. E. J., Gründeman, P. F., Vink, A., *et al.* Myocardial lesion depth with circular electroporation ablation. *Circ. Arrhythmia Electrophysiol.* **5** (3), 581–586 (2012).
2. Council, N. R. *Guide for the Care and Use of Laboratory Animals*. (The National Academies Press, 2011). doi:10.17226/12910
3. Wittkampf, F. H., Van Driel, V. J., Van Wessel, H., Vink, A., Hof, I. E., Gründeman, P. F., *et al.* Feasibility of electroporation for the creation of pulmonary vein ostial lesions. *J. Cardiovasc. Electrophysiol.* **22** (3), 302–309 (2011).
4. Neven, K., Van Driel, V., Van Wessel, H., Van Es, R., Doevendans, P. A. & Wittkampf, F. Epicardial linear electroporation ablation and lesion size. *Hear. Rhythm* **11** (8), 1465–1470 (2014)
5. Bardy, G. H., Coltorti, F., Ivey, T. D., Alferness, C., Rackson, M., Hansen, K., *et al.* Some factors affecting bubble formation with catheter-mediated defibrillator pulses. *Circulation* **73** (3), 525–538 (1986).
6. Knisley, S. B. & Grant, A. O. Asymmetrical electrically induced injury of rabbit ventricular myocytes. *J. Mol. Cell. Cardiol.* **27** (5), 1111–1122 (1995).
7. Bilska, A. O., Debruin, K. A. & Krassowska, W. Theoretical modeling of the effects of shock duration, frequency, and strength on the degree of electroporation. *Bioelectrochemistry Bioenerg.* **51** (2), 133–143 (2000).
8. Huang, J., KenKnight, B. H., Walcott, G. P., Rollins, D. L., Smith, W. M. & Ideker, R. E. Effects of transvenous electrode polarity and waveform duration on the relationship between defibrillation threshold and upper limit of vulnerability. *Circulation* **96** (4), 1351–1359 (1997).

8. Discussion

8.1. Overall results

In this thesis several safety aspects of IRE-ablation for PVI-isolation were investigated. In **chapter 2** and **3** the formation of gaseous micro-emboli as produced by IRE-ablation was studied. Both *in vitro* and *in vivo,* a comparison was made between cathodal versus anodal IRE-pulses, between different energy levels (50, 100 and 200 J), and between the 16-mm and 27-mm catheter hoop diameter. *In vivo*, a comparison between IRE-ablation and RF-ablation was added. Main outcome was that cathodal IRE-pulses produced up to 140 times more gas as compared to anodal IRE-pules. The mean bubble size produced during cathodal IRE-pulses was larger as compared to anodal IRE-pulses. Although it is difficult to predict the difference in clinical outcome regarding amount and size of gaseous bubbles, it is recommended to minimalize the amount of bubbles. For that matter, anodal IRE-pulses would be preferred over cathodal IRE-pulses.

Next, gas formation during anodal IRE-pulses of 200 J were compared with gas formation during RF-pulses of 30 and 60s, resulting in the same gas volume for 30s RF-pulses, but less volume for anodal IRE-pulses compared to 60s RF-pulses. We also attempted to extrapolate this data into a total PVI-procedure, which resulted in a prediction of approximately a 36 times lower volume for PVI-ablation using anodal IRE-pulses compared to PVI-ablation using RF-pulses. These results would support the use of anodal IRE-pulses for PVI-ablation.

In **chapter 4**, visualization of temperature changes during IRE-pulses was performed using color Schlieren imaging. Although this method cannot produce quantitative data or absolute temperature changes, it provides qualitative data about differences between the different modalities and settings. Main outcomes were the characteristic distribution of heating at the edges of the electrodes and the obvious difference between the inner and outer side of the catheter, indicating a higher current density towards the outside of the catheter. This may improve the efficacy of the IRE-pulses.

Chapter 5 and 6 are focused on differences between anodal and cathodal IRE-pulses. In **chapter 5**, the lesion depth was compared for anodal and cathodal IRE-pulses. No significant difference was measured between lesion depth between anodal and cathodal IRE-pulses. In **chapter 6** we focused on the arcing threshold for anodal and cathodal IRE-pulses and found that anodal IRE-pulses have a higher arcing threshold. Therefore, anodal IRE-pulses are less prone to produce arcing during the IRE-ablation procedure and therefore might be safer to use.

The efficacy of a different current modality, namely biphasic IRE-pulses, was investigated in **chapter 7**. Lesion depth was compared for monophasic and biphasic IRE-pulses of different energy levels, *in vivo.* Main outcome was that no significant difference was seen between biphasic and monophasic IRE-pulses, indicating it might be possible to replace the monophasic defibrillators by biphasic IRE-pulses. This feature might be useful for future application of IRE-ablation, however our focus should be on the implementation of IRE-ablation using the current monophasic modality.

8.2. Translation to in human study

Obviously, the main goal of all the previously described studies was to investigate and improve the safety and efficacy of IRE-ablation to a degree that IRE-ablation can be used for the treatment of patients. The intended therapy is PVI-ablation, for which RF-ablation is the current golden standard[1]. Multiple *in vitro* and *in vivo* studies were performed, all focusing on specific safety and efficacy issues, as described in **chapter 1**[2–11].

In vivo studies were performed using a porcine model, since the anatomy and size of the pig heart resembles the human heart[12]. Based on these studies, assumptions were made about the optimal settings and techniques to perform a PVI-procedure using IRE-ablation. One of the outcomes of these studies was that cathodal pulses of 200 J were able to create sufficient lesion depth to induce PV isolation. However, the peak current is dependent on the system resistance . Therefore, it is important to adjust the total system resistance so the current is high enough to create enough lesion depth, but below the arcing threshold.

First objective of the patient study should be to confirm the safety and feasibility of IRE-ablation for PVI. Since a new catheter design and ablation set up is used, study parameters should include the handling of the new circular catheter, occurrence of acute complications initiated by the catheter design and/or ablation set up and the feasibility to produce PV ablations. The procedural complications should be monitored. Based on these outcomes, catheter design and ablation set up should be optimized for a larger scale patient study in which the efficacy of IRE-ablation can be investigated. Besides efficacy of the IRE-ablation, which can be based on e.g. ability to create complete PV isolation and the recurrences rates, different parameters such as procedure duration and fluoroscopy duration can be monitored for a comparison with the current RF-ablation procedures.

8.3. Future outline

8.3.1. Different treatment targets

At the moment, the focus treatment was PVI using IRE-ablation. Due to the circular design of the catheter, the catheter can be adjusted to the diameter of the pulmonary veins and is therefore particularly suitable for PVI. However, IRE-ablation could be suitable for the treatment of different arrhythmias or different procedures. An important property of IRE-ablation is that it is possible to create a deep and transmural lesion, and an advantage of IRE-ablation over RF-ablation is the preservation of nerves and coronary arteries[2–4,7,8]. Therefore, IRE-ablation might be suitable for ablation procedures in which transmural lesions are required, e.g. ablation of ventricular tachycardia substrates. In a study of Neven *et al.*[8], the suitability of IRE-ablation for epicardial ablation procedures was confirmed, hereby suggesting that IRE-ablation might be used as replacement for epicardial ablation modalities as RF-ablation or cryoablation. IRE-ablation is not suitable for all ablation procedures, since the amount of ablated tissue cannot directly be controlled. The application of a single IRE-pulse might be enough to create transmural damage, but subsequently one IRE-pulse might also create undesired damage. Therefore, it might be risky to perform IRE-ablation near valuable structures as e.g. the bundle of His or the AV-node. For these type of procedures, RF-ablation is still preferred.

8.3.2. Pulse modalities

As described in the introduction and **chapter 7**, a single monophasic IRE-pulse is used. These parameters were based on the early DC-ablation with the use of a monophasic defibrillator[13]. In **chapter 7** we discussed the possibility of using biphasic pulses to induce IRE.

Nowadays, IRE-ablation is mostly applied for the treatment of tumors, using e.g. bipolar needles with multiple electrodes, pairs of monopolar needles or plate electrodes[14,15]. Depending on the type of electrodes, a pulse train of different IRE-pulses is applied using a specific field intensity, pulse duration and frequency. Lavee *et al.*[16] used a pulse train 8-32 pulses of 100 µs with a frequency of 5 pulses per second to produce epicardial ablations. They found that IRE-pulses using these parameters resulted in transmural lesions. Zager *et al.*[17] investigated the difference in myocardial decellularization between different protocols, using different pulse durations, number of pulses, frequencies and intensities. They found that longer, more and higher intensity pulses led to an increase in myocardial damage, while a higher frequency led to a decrease in myocardial damage. Both of these studies used intra-myocardial needles as electrodes and therefore these studies are not directly comparable to our method.

A disadvantage of the use of DC-current is the stimulation of skeletal muscles during delivery of an IRE-pulse[15,18,19]. Therefore, general anaesthesia is required during the procedure. Both Arena *et al.*[18] and Sano *et al.*[19] investigated high-frequency (HF) IRE-ablation using bipolar pulses with a frequency up to 500 kHz, and demonstrated elimination of muscle contractions. Another advantages of HF IRE-ablation might be the reduction of bubble gas formation, due to the fast alternation between the different polarities[18,20–22]. A disadvantage of HF IRE-pulses is the decreased ablation volume, suggesting that the creation of transmural lesion might not be a suitable treatment goal. On the other hand, a more specific and controllable ablation volume might be used for specific ablation procedures, in which lesion control is important.

In light of the bubble gas formation and heat production, there might be a difference between the above mentioned modalities and protocols. Gas formation is thought to be reduced by the use of bipolar pulses instead of monopolar pulses[23] and by the use of HF IRE-pulses as explained above, however most of these studies are based on *in vitro* experiments using different set ups. It would be beneficial to perform a comparative study, comparing the bubble gas formation as produced by the different modalities, using an *in vivo* model. The amount of thermal damaging is dependent on the tissue characteristics, pulse duration and intensities, and might therefore be different in cardiac ablation compared to tumor ablation[24].

Further studies should be performed to find the optimal IRE-ablation settings, considering the efficacy and safety of the therapy, but also the intended use of the therapy in order to meet the specific requirements.

8.4. References

1. Cappato, R., Calkins, H., Chen, S. A., Davies, W., Iesaka, Y., Kalman, J., *et al.* Updated worldwide survey on the methods, efficacy, and safety of catheter ablation for human atrial fibrillation. *Circ. Arrhythmia Electrophysiol.* **3** (1), 32–38 (2010).
2. Neven, K., Van Driel, V., Van Wessel, H., Van Es, R., Doevendans, P. A. & Wittkampf, F. Myocardial Lesion Size After Epicardial Electroporation Catheter Ablation After Subxiphoid Puncture. *Circ. Arrhythmia Electrophysiol.* **7** (4), 728–733 (2014).
3. Wittkampf, F. H., Van Driel, V. J., Van Wessel, H., Vink, A., Hof, I. E., Gründeman, P. F., *et al.* Feasibility of electroporation for the creation of pulmonary vein ostial lesions. *J. Cardiovasc. Electrophysiol.* **22** (3), 302–309 (2011).
4. Van Driel, V. J. H. M., Neven, K., Van Wessel, H., Vink, A., Doevendans, P. A. F. M. & Wittkampf, F. H. M. Low vulnerability of the right phrenic nerve to electroporation ablation. *Hear. Rhythm* **12** (8), 1838–1844 (2015).
5. van Es, R., van Driel, V. J. H. M., Neven, K., van Wessel, H., Doevendans, P. A. F. M. & Wittkampf, F. H. M. Feasibility of multi-electrode contact measurement as a predictor of long-term success with circular pulmonary vein electroporation ablation (abstract). *Eur. J. Clin. Invest.* **47** (Supplement S1), (2017).
6. Neven, K., Driel, V. Van, Wessel, H. Van, Es, R. Van, Pré, B. Du, Doevendans, P. A., *et al.* Safety and feasibility of closed chest epicardial catheter ablation using electroporation. *Circ. Arrhythmia Electrophysiol.* **7** (5), 913–919 (2014).
7. Du Pré, B. C., Van Driel, V. J., Van Wessel, H., Loh, P., Doevendans, P. A., Goldschmeding, R., *et al.* Minimal coronary artery damage by myocardial electroporation ablation. *Europace* **15** (1), 144–149 (2013).
8. Neven, K., Van Driel, V., Van Wessel, H., Van Es, R., Doevendans, P. A. & Wittkampf, F. Epicardial linear electroporation ablation and lesion size. *Hear. Rhythm* **11** (8), 1465–1470 (2014).

9. Neven, K., Van Es, R., Van Driel, V., Van Wessel, H., Fidder, H., Vink, A., *et al.* Acute and Long-Term Effects of Full-Power Electroporation Ablation Directly on the Porcine Esophagus. *Circ. Arrhythmia Electrophysiol.* **10** (5), e004672 (2017).
10. Wittkampf, F. H. M., Van Driel, V. J., Van Wessel, H., Neven, K. G. E. J., Gründeman, P. F., Vink, A., *et al.* Myocardial lesion depth with circular electroporation ablation. *Circ. Arrhythmia Electrophysiol.* **5** (3), 581–586 (2012).
11. Van Driel, V. J. H. M., Neven, K. G. E. J., Van Wessel, H., Du Pré, B. C., Vink, A., Doevendans, P. A. F. M., *et al.* Pulmonary vein stenosis after catheter ablation electroporation versus radiofrequency. *Circ. Arrhythmia Electrophysiol.* **7** (4), 734–738 (2014).
12. Crick, S. J., Sheppard, M. N., Ho, S. Y., Gebstein, L. & Anderson, R. H. Anatomy of the pig heart: Comparisons with normal human cardiac structure. *J. Anat.* **193** (1), 105–119 (1998).
13. Haissaguerre, M., Montserrat, P., Warin, J. F., Donzeau, J. P., Le Metayer, P. & Massiere, J. P. Catheter ablation of left posteroseptal accessory pathways and of long RP' tachycardias with a right endocardial approach. *Eur. Heart J.* **12** (8), 845–859 (1991).
14. Yarmush, M. L., Golberg, A., Serša, G., Kotnik, T. & Miklavčič, D. Electroporation-Based Technologies for Medicine: Principles, Applications, and Challenges. *Annu. Rev. Biomed. Eng.* **16** (1), 295–320 (2014).
15. Golberg, A. & Yarmush, M. L. Nonthermal irreversible electroporation: Fundamentals, applications, and challenges. *IEEE Trans. Biomed. Eng.* **60** (3), 707–714 (2013).
16. Lavee, J., Onik, G., Mikus, P. & Rubinsky, B. A novel nonthermal energy source for surgical epicardial atrial ablation: Irreversible electroporation. *Heart Surg. Forum* **10** (2), 96–101 (2007).
17. Zager, Y., Kain, D., Landa, N., Leor, J. & Maor, E. Optimization of irreversible electroporation protocols for in-vivo myocardial decellularization. *PLoS One* **11** (11), (2016).
18. Arena, C. B., Sano, M. B., Rossmeisl, J. H., Caldwell, J. L., Garcia, P. A., Rylander, M. N., *et al.* High-frequency irreversible electroporation (H-FIRE) for non-thermal ablation without muscle contraction. *Biomed. Eng. Online* **10** , 102 (2011).
19. Sano, M. B., DeWitt, M. R., Teeter, S. D. & Xing, L. Optimization of a single insertion electrode array for the creation of clinically relevant ablations using high-frequency irreversible electroporation. *Comput. Biol. Med.* **95** , 107–117 (2018).
20. Saulis, G., Lape, R., Pranevičiute, R. & Mickevičius, D. Changes of the solution pH due to exposure by high-voltage electric pulses. *Bioelectrochemistry* **67** (1), 101–108 (2005).
21. Postnikov, A. V, Uvarov, I. V, Lokhanin, M. V & Svetovoy, V. B. Highly energetic phenomena in water electrolysis. *Sci. Rep.* **6** , (2016).
22. Ziv, R., Steinhardt, Y., Pelled, G., Gazit, D. & Rubinsky, B. Micro-electroporation of mesenchymal stem cells with alternating electrical current pulses. *Biomed. Microdevices* **11** (1), 95–101 (2009).
23. Kotnik, T., Mir, L. M., Flsar, K., Puc, M. & Miklavcic, D. Cell membrane electropermeabilization by simmetrical bipolar rectangular pulses. Part II. Reduced electrolytic contamination. *Bioelectrochemistry* **54** , 83–90 (2001).
24. Garcia, P. A., Davalos, R. V & Miklavcic, D. A numerical investigation of the electric and thermal cell kill distributions in electroporation-based therapies in tissue. *PLoS One* **9** (8), (2014).

9. Conclusion

In this thesis several safety aspect of IRE-ablation for the use of catheter ablation are investigated. We found that cathodal IRE-pulses produce significantly more gas as compared to anodal IRE-pulses (**chapter 2 and 3**), while no difference in heat development was found (**chapter 4**). No significant difference in lesion depth was measured between anodal and cathodal IRE-pulses (**chapter 5**). The arcing threshold for anodal IRE-pulses is lower as compared to cathodal IRE-pulses (**chapter 6**). These results suggest that anodal IRE-pulses are preferred over cathodal IRE-pulses.

The results of the studies in this thesis are crucial in the further development of IRE-ablation as a modality for catheter ablation. In combination with the previous studies, the efficacy and safety of IRE-ablation is thoroughly studied to pave the way to the first patient study. IRE-ablation using the circular multi-electrode catheter is thought to be safe and effective. The first patient safety and feasibility study should prove the feasibility of IRE-ablation for PVI, after which the system can be optimized for full scale clinical use.

Important objectives of further research would be the development of a method to precisely predict the lesion area and the adjustment of the electrode and catheter design such way the delivery of the current is optimized and risk on arcing is limited. In an optimal set up, the currently used monophasic defibrillator would be replaced by a modality in which more precise energy levels could be selected and settings could be adjusted to deliver optimal energy based on patient properties (such as resistance) and the therapy goal. It would be beneficial to be able to monitor the resistance instantly, to stop the delivery if an arc might be expected. Also, direct monitoring of lesion formation during delivery of the IRE-pulses would be beneficial for optimal treatment. By combining all these features, in the future the IRE-modality might replace part of the currently used ablation modalities.

10. Acknowledgements

This thesis is the result of one year of hard work at the department of Cardiology at the University Medical Center Utrecht. This result would not have been possible without the help of my supervisors, colleagues, friends and family. Therefore, I would like to thank everyone who helped me the past year during my research.

I would like to specially say thanks to some crucial persons. René van Es, thank you for your collaboration, daily support and the valuable feedback throughout the entire project. Rutger Hassink and Ciska Heida, thank you for the advice and critical notes on my research. Rian Haarman, thank you for stimulating me to gain more insight about myself and my professional development. Marlijn Jansen, Joyce Visser, Martijn van Nieuwburg and Evelyn Velema, thanks for your work during the animal experiments. Marco Stehouwer, thank you for your help during the bubble measurements.

11. Appendix A – JoVE manuscript

TITLE: Pulmonary Vein Isolation with Irreversible Electroporation

AUTHORS & AFFILIATIONS:

René van Es*[1] PhD, Marijn HA Groen*[1,2] BSc, Kars Neven[1,3,4] MD PhD, Vincent JHM van Driel[1,5] MD PhD, Harry van Wessel[6] BSc, Pieter A Doevendans[1,7] MD PhD, Fred HM Wittkampf PhD

*=Authors contributed equally

1. Department of Cardiology, Division Heart and Lungs, University Medical Center Utrecht, The Netherlands
2. Technical Medicine, University of Twente, Enschede, The Netherlands
3. Department of Electrophysiology, Alfried Krupp Krankenhaus, Essen, Germany
4. Witten/Herdecke University, Witten, Germany
5. Department of Cardiology, Haga Teaching Hospital, The Hague, The Netherlands
6. St. Jude Medical, Veenendaal, The Netherlands
7. Netherlands Heart Institute, Utrecht, The Netherlands

KEYWORDS:

Atrial fibrillation, pulmonary vein isolation, irreversible electroporation, contact measurement

SHORT ABSTRACT:

This protocol describes pulmonary vein isolation using irreversible electroporation (IRE) in combination with a method for electrode-tissue contact measurements. IRE may be a better alternative for the commonly used radiofrequency ablation, since IRE is shown to be safer and more effective in experimental studies.

LONG ABSTRACT:

A standard method for treatment of atrial fibrillation (AF) is pulmonary vein isolation (PVI); with this therapy the pulmonary veins are electrically isolated from the atria, to prevent erratic electrical impulses originating at the PVs from reaching the left atrium. Radiofrequency (RF) ablation is the most commonly used method for PVI.

The long-term success of PVI with RF-ablation is limited and multiple procedures are often required, particularly in patients with longstanding persistent AF. The delivery of thermal energy, on which RF-ablation is based, can lead to serious complications such as PV stenosis, phrenic nerve damage, esophageal injury and formation of blood clots by endothelial damage and protein aggregation; in

addition lesion formation is unpredictable due to cooling by the blood flow (heat sink effect) or development of steam pops.

Recently, irreversible electroporation (IRE) has been studied as an alternative modality for PVI. With IRE, the application of a high electrical current between a circular multi-electrode catheter and a skin patch ensues non-thermal irreversible permeabilization of the cell membrane and cell death. Multiple porcine studies have demonstrated the feasibility and safety of IRE for PVI. IRE-ablation therefore may be a better alternative for RF-ablation to perform PVI and ultimately even for other ablation procedures.

Electrode-tissue contact is important for the efficacy of IRE ablation. For multi-electrode catheter it is difficult to use the commonly used contact force measurements. Therefore a novel method, multi-electrode impedance system (MEIS), developed to measure electrode-tissue contact.

In this protocol, a PVI by the use of IRE in combination with MEIS is presented in a porcine model.

INTRODUCTION:

Atrial fibrillation (AF) is the most common cardiac arrhythmia and results in an irregular heart rhythm and insufficient atrial contraction[1]. This may lead to complaints of palpitations, fatigue, atrial thrombi, stroke and left ventricular dysfunction that can ultimately result in heart failure[2].

Initially, AF is treated medically by lowering the ventricular rate for rate control, for example with beta blockers or calcium channel blockers or digoxin. Depending on different patient characteristics e.g. degree of symptoms, presence of a structural heart disease, type of AF etc., in addition on, or as an alternative for rate control, rhythm control strategies are preferred[3]. Rhythm control can be achieved by electrical or pharmacological cardioversion, or by catheter ablation.

The cause of atrial fibrillation often are erratic electrical signals, originating from the pulmonary veins (PV)[4]. These erratic signals can be blocked by electrically isolating the pulmonary veins from the left atrium (LA). Several energy modalities are available to perform pulmonary vein isolation (PVI), with the most common method being radiofrequency (RF) ablation[5]. RF-ablation uses an alternating high frequency electrical current to heat and ablate target tissue. Isolation of the PVs is accomplished by creating a continuous circumferential lesion in both PV antrums. The long-term success remains limited and often multiple procedures are required, particularly in longstanding persistent AF[6–10]. In addition, several complications can occur as a result of the thermal energy used with RF-ablation[11,12]. Blood clots can be formed by protein aggregation and may lead to neurological complications[13,14]. Excessive heating may cause collateral damage to surrounding tissue, e.g. causing damage to the phrenic nerves[15], coronary arteries[16], esophagus[11,17,18] and can lead to PV stenosis[12,19]. Furthermore, lesion formation with RF-ablation is influenced by blood flow by means of a heat sink effect, limiting lesion size [13,20].

Up until the development of RF-ablation in the early 1990s, direct current (DC) catheter ablation was the only available method for cardiac catheter ablation[21]. With DC-ablation, a high current is applied between a catheter electrode and a skin plate. Lesion formation was caused by electroporation of the membranes of the cardiomyocytes and perhaps also by pressure waves caused by arcing at the catheter electrode, possibly also leading to severe complications[22,23]. In the late 1980s, Ahsan *et al.* developed low-energy DC ablation, which resulted in adequate lesion formation without arcing[24–26]. Even though low-energy DC-ablation was successful, it was abandoned after the introduction of RF-ablation.

Recently, low-energy DC ablation or irreversible electroporation (IRE) was reinvestigated as an alternative method to perform PVI[27]. By delivering the current via multiple electrodes on a circular catheter, current density per electrode is decreased such that arcing and spark formation does not occur while the lesion depth is maintained, due to a linear decay in current density with increasing distance from the catheter, compared with an exponential decay for a single-electrode catheter[28]. In contrast to RF-ablation, IRE is capable of producing permanent non-thermal damage to tissue within a fraction of a second[29]. Porcine studies showed that IRE is a safe and effective method for PVI, while no high temperature related complications have been observed[23,27–33]. Wittkampf *et al.*[27] showed that IRE is able to create adequate lesions in the PV ostia[27]. Subsequent studies focused on investigating the possible complications of IRE. In a comparative study, occurrence of PV stenosis was studied for both RF and IRE-ablation. After a 3-month follow up, results showed that IRE-ablation did not affect the PV diameter, while RF-ablation showed immediate PV stenosis persisting for at least 3 months[19]. Another study showed no, or only transient damage to the phrenic nerve after IRE-ablation in the superior vena cava, with an energy level that was able to create transmural lesions[32]. A more recent study investigated the effects of IRE-ablation directly on the exterior esophagus and showed no damage to the esophagus after 2 months follow up[34]. Furthermore, RF-ablation near coronary arteries may lead to stenosis[35]. Porcine studies also showed undamaged coronary arteries 3 weeks and 3 months after epicardial IRE-ablation[16,36].

Besides safety, also the efficacy of IRE was assessed in several studies. With IRE, lesion size is directly related to the magnitude of delivered energy, both endo- and epicardially, the latter for both linear and circular electrodes[28,30,31]. The findings of these studies indicate that IRE is able to create continuous lesions that are deep enough to create PV isolation.

As with RF, IRE-ablation is based on the delivery of electrical energy from catheter electrode(s) to target tissue. Since lesion formation is dependent on current density that decreases with distance from the electrode. Therefore, the quality of contact between catheter and target tissue is equally important for the effectiveness and safety of RF- as well as for IRE-ablation[37,38]. With RF-ablation catheters, force sensors have recently been incorporated in the catheter tip[38–40]. However, contact force (CF) measurements are technically challenging if not impossible with circular multi-electrode catheters. Therefore a multi-electrode impedance system (MEIS) that allows electrical measurement of circular electrode-tissue contact without the need for special pressure sensors was developed[41]. Several studies suggested electrode impedance as a good indicator for contact between the electrode and tissue[37,42,43]. Increasing the amount of contact between electrode and tissue results in an increase in impedance because the impedance of healthy myocardium is higher than that of blood[44]. MEIS can be used for impedance based contact measurements[41,45]. With MEIS, the voltage is measured between this same electrode and an indifferent skin patch, while a current is applied between this same electrode and an adjacent electrode. The impedance is calculated by dividing the measured voltage by the applied current. The localized electrical field reduces the influence of remote high-impedance structures as e.g. pulmonary tissue[41]. A porcine study showed similar clinical outcome using MEIS values and local electrogram signals, indicating MEIS is as least as good as current methods[45].

In this protocol we describe the procedure for performing PVI with IRE in combination with MEIS in a large porcine model.

PROTOCOL:

All methods were approved by the Animal Experimentation Committee of the University Medical Center Utrecht and were performed in compliance with the Guide for the Care and Use of Laboratory Animals.

1 Preparation of the procedure

1.1 Pre-medication and anesthesia.

1.1.1 Start amiodarone (1200 mg per day), seven days before the procedure.

1.1.2 Start carbasalate calcium (80 mg per day) and clopidogrel (300 mg on the first day, then 75 mg per day), three days before the procedure.

1.1.3 Before surgery, administer ketamine 10 mg/kg, midazolam 0.4 mg/kg and atropine 0.5 mg intra muscular to sedate the animal.

1.1.4 Insert an intravenous line in the ear vein.

1.1.5 Induce the anesthesia using thiopental sodium 4mg/kg injected using the intravenous line in the ear vein.

1.1.6 Intubate the animal and start ventilation using a tidal volume of 10 ml/kg and 12 breaths per minute with a O_2/air ratio of 1:2.

1.1.7 Administer midazolam 10 mg and sufentanil 0.25 mg intra venous and start with midazolam 0.5 mg/kg/h intravenously, sufentanil 2.5 µg/kg/h and pancuronium bromide 0.1 mg/kg/h.

1.1.8 Administer heparin 100 IE/kg intravenous, maintain an activated clotting time of >300 seconds throughout the procedure.

1.2 Positioning of the animal

1.2.1 Shave the lower back and place two indifferent patch electrodes (7506, Valley Lab Inc, Boulder, CO, USA) and the NavX-back patch.

1.2.2 Move the animal into supine position and secure to the operating table.

1.2.3 Shave and place the ECG electrodes and the five remaining NavX-patches.

1.2.4 Disinfect the neck and the left groin region.

1.3 Connection of the equipment (Figure 10.1)

1.3.1 Start up the NavX system, the MEIS system, the EP-4 cardiac stimulator, the external defibrillator (Lifepak9, Physio-Control Inc, Redmond, WA), and the oscilloscope.

1.3.2 Connect the NavX system with the EP-4 cardiac stimulator using the Breakout box of NavX.

1.3.3 Connect the ECG electrodes to the NavLink.

1.3.4 Connect one of the indifferent patch electrodes as a reference to the junction box, connect the other indifferent patch to the MEIS system.

1.3.5 Connect the junction box and the MEIS system using a catheter cable with 10 connectors.

1.3.6 Connect the defibrillator to the IV box.

1.3.7 Connect the oscilloscope to the IV box.

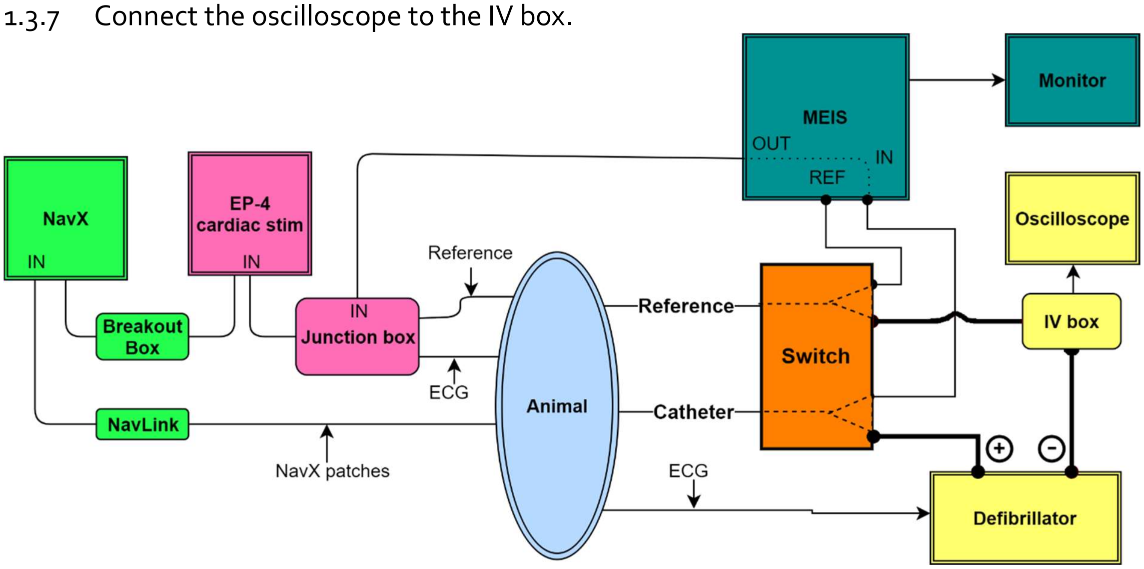

Figure 10.1 Schematic overview of the used equipment. ECG = electrocardiogram cables, Reference = connection to the indifferent patch electrodes, Catheter = decapolar ablation catheter. Light green = Ensite NavX navigation system which can be used to visualize the heart using a 3D model (St. Jude Medical). NavLink and the Breakout box are used for connection with the NavX patches and EP-4 cardiac stimulator resp. Pink = cardiac stimulator which is used for the recording of both ECG and catheter signals, the junction box is used for connection with the reference and the MEIS system. Dark green = Multi-electrode impedance system which is used to measure contact between electrode and tissue, Yellow = defibrillator which is used for delivery of the ablation shock. The IV box is a current and voltage sensor to measure the delivered current and voltage which are displayed on the oscilloscope. Orange = the switch between the MEIS system and the ablation system.

2 Start of the procedure

2.1 Insert introducers

2.1.1 Prepare the right jugular vein, insert a 6F introducer and position the sheath.

2.1.2 Prepare the right carotid artery and insert a 6F introducer.

2.1.3 Prepare the right femoral vein and insert a 14F introducer.

2.1.4 Prepare the left femoral vein and insert a 6F introducer.

2.2 Insert the catheters under fluoroscopic guidance

2.2.1 Aspirate and flush the 6F sheath in the carotid artery with heparinized saline.

2.2.2 Connect the invasive blood pressure measurement to the 6F sheath in the carotid artery.

2.2.3 Flush the 5F octapolar steerable catheter (Inquiry™, St. Jude Medical) with heparinized saline and wipe the outside with a wet gauss.

2.2.4 Introduce the coronary sinus (CS) catheter into the CS using the 6F introducer in the Jugular vein.

2.2.5 Connect the CS catheter to the EP-4 junction box.

2.2.6 Insert a screw-in pacing catheter (6416, Medtronic Inc, Minneapolis, MN) in the high right atrium (HRA) using the 6F introducer in the left Femoral vein.

2.2.7 Connect the catheter to the EP-4 junction box

2.2.8 Introduce a 0.0014”guidewire into the right atrium (RA) through the 14F sheath in the right femoral vein.

2.2.9 Flush the 8.5F steerable sheath (Agilis; St. Jude Medical, Minnetonka, MN, USA) with heparinized saline and wipe with a wet gauss.

2.2.10 Introduce and advance the steerable sheath over the guidewire into the RA

2.2.11 Remove the guidewire and position the sheath against the atrial septum just above the CS catheter (Figure 10.2).

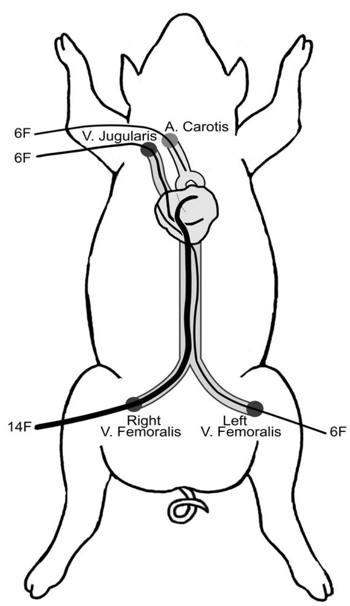

Figure 10.2 Schematic overview of the insertion of the sheaths. A. Carotis = 6F introducer *for the invasive blood pressure* measurement; V. Jugularis = 6F introducer for the coronary sinus catheter, V. Femoralis left = 6F introducer for the HRA catheter and V. Femoralis right = 14F introducer for the ablation catheter

2.2.12 Perform a transseptal puncture to gain access to the LA.
2.2.13 Remove the dilator from the transseptal sheath.
2.2.14 Aspirate the saline from the sheath until blood appears to remove any air bubbles, subsequently flush the transseptal sheath with heparinized saline to prevent the formation of blood cloths.

2.3 Visualize the right pulmonary vein[46]
2.3.1 Position the transseptal sheath towards the right pulmonary vein.
2.3.2 Perform contrast angiography using contrast bolus injection (20mL) in the left atrium (Figure 10.3 C).
2.3.3 Demarcate the position of the right and inferior pulmonary veins
2.3.4 Repeat procedure for inferior pulmonary vein

3 Preparation of the mapping/navigation system and the contact measurement system

3.1 Preparing the EnSite NavX system (St. Jude Medical, Minneapolis, MN)
3.1.1 Use the same reference patch as the reference indifferent electrode patch of the EP-4 cardiac stimulator, by connecting NavX to the break out box.
3.1.2 Introduce the circular decapolar catheter into the LA through the trans septal sheath.
3.1.3 Reconstruct the LA and parts of the PVs geometry using NavX by maneuvering the catheter through the LA.

3.2 Preparing the MEIS system
3.2.1 Connect the second indifferent patch electrode to the MEIS system as a reference.
3.2.2 Connect the decapolar catheter to the MEIS system.
3.2.3 Calibrate the MEIS system according to the manual.
3.2.4 Perform a no-contact measurement for 10 seconds with the catheter floating in the LA, under fluoroscopic guidance.
3.2.5 Determine the reference value for no-contact as previously described[41].

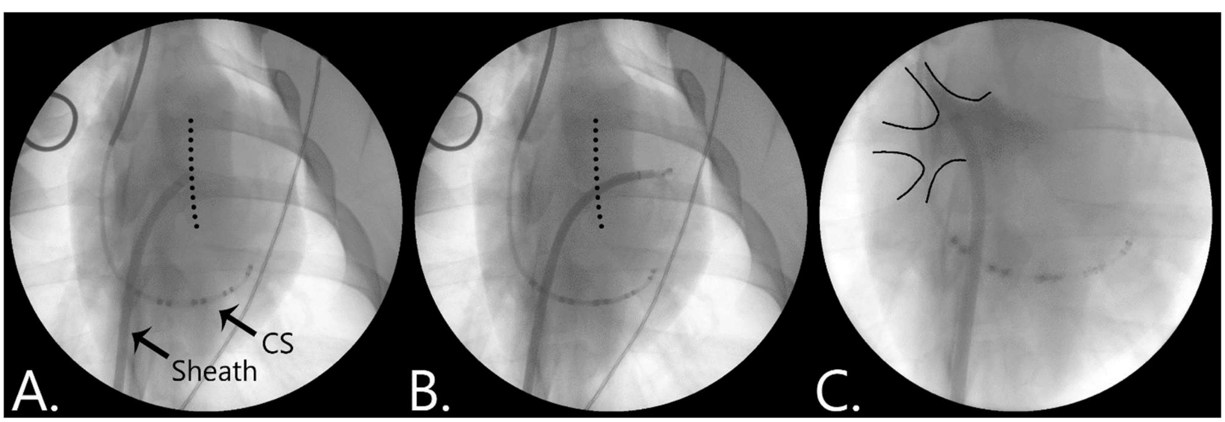

Figure 10.3 Fluoroscopic images of position of the CS catheter and the steerable sheath prior (A) and after the Transseptal puncture (B). The dotted line indicates the position of the atrial septum. (C) Injection of a contrast bolus into the right pulmonary vein, the superimposed lines indicate the border of the pulmonary vein. CS = coronary sinus.

3.2.6 Position the catheter in the left atrial appendage, to assure the catheter is in contact with myocardial wall.
3.2.7 Set the reference value for good contact to the highest measured value in this position.

4 Ablation

4.1 Determine ablation resistance

4.1.1 Switch the catheter and the indifferent patch electrode to the external defibrillator.
4.1.2 Adjust the settings of the oscilloscope so it is suitable for a 100-J test-pulse.
4.1.3 Set the ablation device to the synchronized mode.
4.1.4 With the catheter positioned in the PV ostium, deliver an anodal 100-J pulse and store the oscilloscope current (I) and voltage (V) recordings.
4.1.5 Calculate total system resistance by dividing the measured voltage by the measured current; adjust the serial R so the total system impedance is within the desired range of 55-65 Ohms.

4.2 Positioning the catheter in the PV

4.2.1 Switch the catheter and the indifferent patch electrode to the MEIS system.
4.2.2 Move the decapolar catheter into the common tubular part of the inferior pulmonary vein, using both fluoroscopic guidance, EP-signals and NavX.
4.2.3 Using the MEIS system, position the catheter in the PV antrum in such a position that as many electrodes are in good contact with the wall.
4.2.4 Using NavX, mark the position of the electrodes that are in good contact.

4.3 Performing IRE-ablation

4.3.1 Adjust the settings of the oscilloscope so it is suitable for 200-J pulse.
4.3.2 Reposition the catheter in the PV, as described in 4.2.
4.3.3 Switch the catheter and the indifferent patch electrode to the external defibrillator.
4.3.4 Deliver a synchronized anodal 200-J shock between the catheter and the indifferent patch electrode.
4.3.5 Store the oscilloscope I/V traces and check the tracings for signs of arcing.
4.3.6 Switch the multi-electrode catheter to the MEIS system.
4.3.7 Repeat the procedure from 4.2 until the entire circumference of the PV antrum has covered with good contact ablation.
4.3.8 Then repeat step 4.3 for all PVs.

4.4 Confirming PV isolation

4.4.1 Wait thirty minutes before testing PV isolation.
4.4.2 Start adenosine (20 mg bolus).
4.4.3 Switch the catheter and the indifferent patch to the MEIS system.
4.4.4 Mark and log the MEIS impedance values measured at the ablation position.
4.4.5 Test for bidirectional electrical isolation by positioning the decapolar catheter distally to the ablation line.
4.4.6 Assess the presence of PV potentials using the EP-4 cardiac stimulator.
4.4.7 Apply bipolar stimulation of 10 mA via all electrode pairs of the decapolar catheter and check for LA capture.
4.4.8 Repeat the procedure for all other PVs.

REPRESENTATIVE RESULTS:

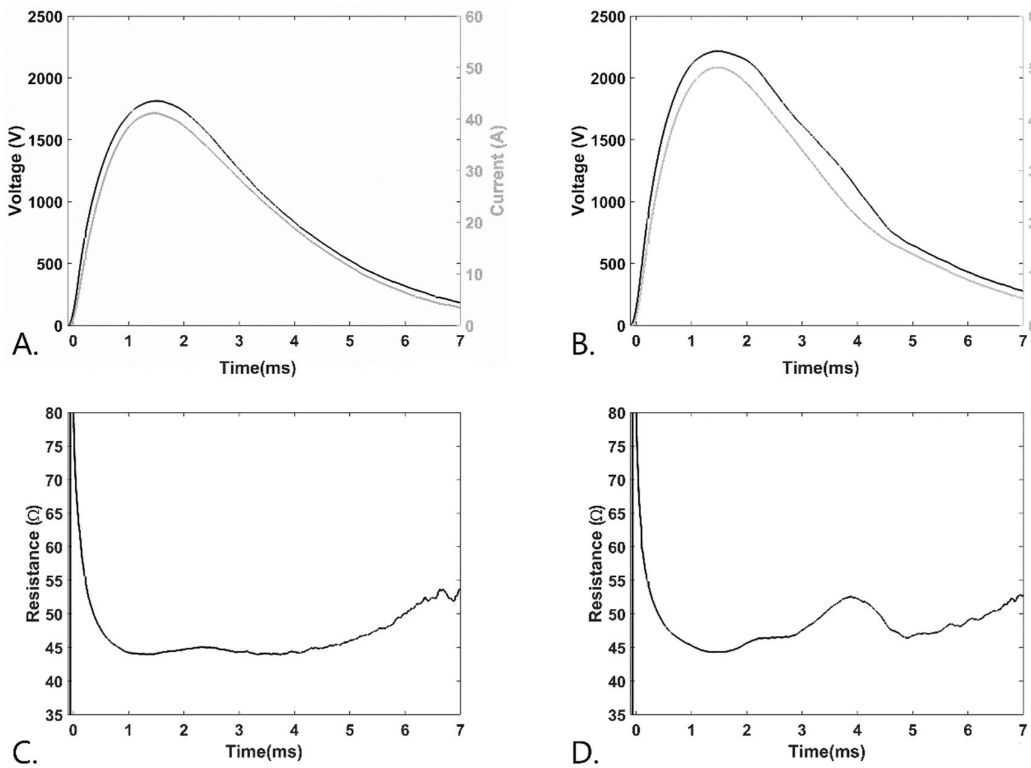

Figure 10.4 Measured voltage and current wave forms during (A) 200J and (B) 300J IRE applications, the resistance (voltage divided by current) of these applications are shown in C and D, respectively. Arcing occurs after applying 300J (B), both the voltage and current waveforms are clearly distorted compared to the 200J application. The occurrence of arcing is also clearly visible as a temporary rise in resistance in figure D.

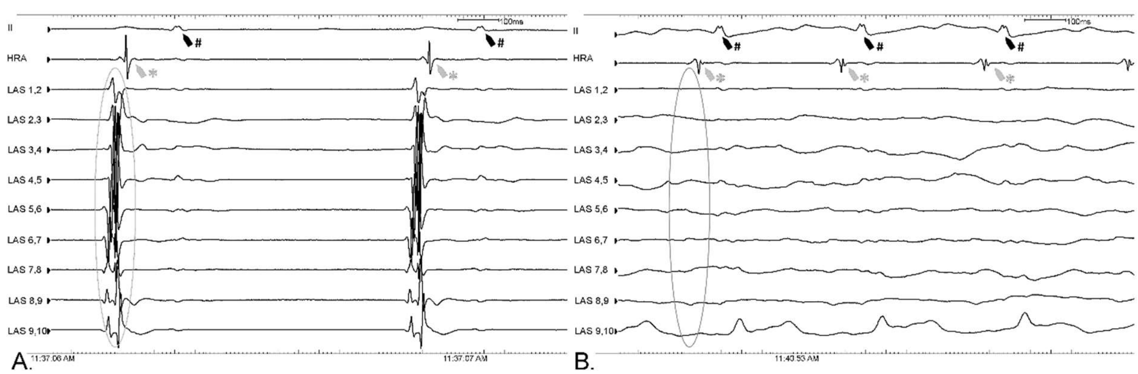

Figure 10.5 Electrogram signals of (A) pre-ablation and (B) post-ablation. Sharp atrial signals are measured pre-ablation, marked in the grey circle (A), while no atrial signals were seen post-ablation (B), indicating ablation was successful. II = electrode of the surface ECG, ventricular signals marked with black (#) arrows, HRA = high right atrium, atrial electrograms marked with grey (*) arrows, LAS = circular decapolar ablation catheter with bipolar electrograms.

FIGURE AND TABLE LEGENDS:

1. Schematic overview equipment (methods)
ECG = electrocardiogram cables, Reference = connection to the indifferent patch electrodes, NavX =Ensite NavX navigation system which can be used to visualize the heart using a 3D model (St. Jude Medical), EP-4 cardiac stim = cardiac stimulator which is used for the recording of both ECG and catheter signals, MEIS = Multi-electrode impedance system which is used to measure contact between electrode and tissue, IV box = current and voltage sensor for display on the oscilloscope and both the NavLink, Breakout box and junction box are used for connection between the catheter and ECG cables and the used equipment.

2. Schematic overview of sheath placement (methods)
Schematic overview of the insertion of the sheaths. A. Carotis = 6F introducer for the invasive blood pressure measurement; V. Jugularis = 6F introducer for the coronary sinus catheter, V. Femoralis left = 6F introducer for the HRA catheter and V. Femoralis right = 14F introducer for the ablation catheter.

3. Fluoroscopic image of TSP site (methods)
Fluoroscopic images of position of the CS catheter and the steerable sheath prior (A) and after the Transseptal puncture (B). The dotted line indicates the position of the atrial septum. (C) Injection of a contrast bolus into the right pulmonary vein, the superimposed lines indicate the border of the pulmonary vein. CS= *coronary sinus.*

4. IV curves (results)
Measured voltage and current wave forms during (A) 200J and (B) 300J IRE applications, the resistance (voltage divided by current) of these applications are shown in C and D, respectively. Arcing occurs after applying 300J (B), both the voltage and current waveforms are clearly distorted compared to the 200J application. The occurrence of arcing is also clearly visible as a temporary rise in resistance in figure D.

5. Pre-post ablation electrograms
Electrogram signals of (A) pre-ablation and (B) post-ablation. Sharp atrial signals are measured pre-ablation, marked in the red circle (A), while no atrial signals were seen post-ablation (B) indicating ablation was successful. II = electrode of the surface ECG, ventricular signals marked with blue arrows, HRA = high right atrium, atrial electrograms marked with green arrows, LAS = circular decapolar ablation catheter with bipolar electrograms.

DISCUSSION:

In this protocol we present a method for PVI using IRE-ablation combined with electrode-tissue contact measurement. During previous porcine studies sufficient lesions could be created without complications related to high temperatures[23–34]. IRE could be a fast and safe alternative for the current ablation techniques such as RF-ablation.

Critical steps

The measurement of the total patient resistance, as mentioned in step 4.1, is important since it affects the delivered current and therefore lesion formation and safety of the procedure. A higher resistance results in a lower delivered current and a higher voltage and vice versa. While lesion formation is dependent on the amount of current delivered, a high current also increases the risk of arcing, therefore the total resistance should be within certain limits. The total resistance is calculated by delivering an initial pulse of 100 J in the PV ostium. By adding a serial resistance, the total resistance can be increased to meet the preset criteria. Furthermore, prior research has shown that an anodal pulse (catheter is the positive pole) poses a smaller risk of arcing compared to a cathodal pulse at the same energy level. It is therefore important connect the setup as shown in figure 1.

Contact between electrodes and tissue is critical for the efficacy of the ablation. In this protocol the MEIS measurement, in combination with both fluoroscopic guidance, electrogram signals and NavX, is used to maneuver the catheter in an optimal position at the target area. Fluoroscopic guidance, electrograms signals and NavX are commonly used methods for positioning the catheter and confirmation of electrode-tissue contact. The MEIS system offers real time intuitive feedback on electrode tissue contact, and can in combination with NavX, ensure complete circumferential ablation of the PVs.

Finally, the confirmation of isolation of the PV is of great importance, since the procedure would not be successful without isolation. In this protocol both MEIS values, electrogram signals and adenosine testing are used for the conformation of electrical isolation, whereby adenosine is commonly used to evaluate the permanent character of isolation and therefore is leading[38,47].

Limitations

Both IRE and MEIS have only been investigated using *in vitro* and porcine studies and therefore the results may not be directly translatable to *human* subjects. Both catheter design and energy level settings should be assessed in a first human feasibility study. Currently, a standard external monophasic defibrillator with specific discrete energy levels is used. Further studies should focus on methods for different energy generation, for example by using a biphasic defibrillator, or a dedicated IRE-ablation system

MEIS contact measurements are based on the difference in impedance between blood and healthy myocardium, however no studies have been performed on fibrotic tissue, as is present in previously ablated hearts. Cinca *et al.* showed significant differences in impedances between healthy and fibrotic tissue, where fibrotic tissue has a lower impedance[44]. No research has been performed on these differences and the influence on the MEIS values.

Clinical implications

Several studies suggested that IRE-ablation is safer and more effective than RF-ablation for PVI. With IRE-ablation a circular catheter is used, that is able to create a continuous circumferential lesion in a fraction of a second. Therefore, the use of IRE-ablation could reduce procedure time of PVI significantly. Since IRE is non-thermal, lesion formation is not hampered by blood flow along the catheter electrodes or through vessels in the target tissue. Therefore, IRE is expected to lead to fewer reconnections and thus, a higher long term success rate.

ACKNOWLEDGMENTS:

We would like to thank Evelyn Velema, Marlijn Jansen, Martijn van Nieuwburg and Joyce Visser for their work during the animal studies.

DISCLOSURES:

The authors Harry van Wessel and Fred Wittkampf are the inventors of the IRE-ablation technology and are currently employees of St. Jude Medical. Kars Neven is consultant for St. Jude Medical.

REFERENCES:

1. Go, A. *et al.* Prevalence of diagnosed atrial fibrillation in adults: National implications for rhythm management and stroke prevention: the anticoagulation and risk factors in atrial fibrillation (atria) study. *JAMA* **285** (18), 2370–2375 (2001).
2. Kirchhof, P. *et al.* 2016 ESC Guidelines for the management of atrial fibrillation developed in collaboration with EACTS. *Eur. Heart J.* **37** (38), 2893 LP-2962 (2016).
3. January, C. T. *et al.* 2014 AHA/ACC/HRS Guideline for the Management of Patients With Atrial Fibrillation. *Circulation* **129** , (2014).
4. Haïssaguerre, M. *et al.* Spontaneous Initiation of Atrial Fibrillation by Ectopic Beats Originating in the Pulmonary Veins. *N. Engl. J. Med.* **339** (10), 659–666 (1998).
5. Cappato, R. *et al.* Updated worldwide survey on the methods, efficacy, and safety of catheter ablation for human atrial fibrillation. *Circ. Arrhythmia Electrophysiol.* **3** (1), 32–38 (2010).
6. Rostock, T. *et al.* Long-term single- and multiple-procedure outcome and predictors of success after catheter ablation for persistent atrial fibrillation. *Hear. Rhythm* **8** (9), 1391–1397 (2011).
7. Katritsis, D. *et al.* Long-term follow-up after radiofrequency catheter ablation for atrial fibrillation. *Europace* **10** (4), 419 LP-424 (2008).
8. Bertaglia, E. *et al.* Does catheter ablation cure atrial fibrillation? Single-procedure outcome of drug-refractory atrial fibrillation ablation: a 6-year multicentre experience. *Europace* **12** (2), 181 LP-187 (2010).
9. Kumar, S. *et al.* Better lesion creation and assessment during catheter ablation. *J. Atr. Fibrillation* **8** (3), (2015).

10. Teunissen, C. *et al.* Five-year efficacy of pulmonary vein antrum isolation as a primary ablation strategy for atrial fibrillation: A single-centre cohort study. *Europace* **18** (9), 1335–1342 (2016).
11. Scanavacca, M. I., D'Ávila, A., Parga, J. & Sosa, E. Left atrial-esophageal fistula following radiofrequency catheter ablation of atrial fibrillation. *J. Cardiovasc. Electrophysiol.* **15** (8), 960–962 (2004).
12. Robbins, I. M. *et al.* Pulmonary Vein Stenosis after Catheter Ablation of Atrial Fibrillation: Emergence of a New Clinical Syndrome. *Ann. Intern. Med.* **138** (8), 1769–1775 (2003).
13. Yokoyama, K. *et al.* Comparison of Electrode Cooling Between Internal and Open Irrigation in Radiofrequency Ablation Lesion Depth and Incidence of Thrombus and Steam Pop. *Circulation* **113** (1), 11 LP-19 (2006).
14. Sauren, L. D. *et al.* Transcranial measurement of cerebral microembolic signals during endocardial pulmonary vein isolation: Comparison of three different ablation techniques. *J. Cardiovasc. Electrophysiol.* **20** (10), 1102–1107 (2009).
15. Sacher, F. *et al.* Phrenic Nerve Injury After Atrial Fibrillation Catheter Ablation. *J. Am. Coll. Cardiol.* **47** (12), 2498–2503 (2006).
16. Du Pré, B. C. *et al.* Minimal coronary artery damage by myocardial electroporation ablation. *Europace* **15** (1), 144–149 (2013).
17. Hirata, K. *et al.* Atrio-Esophageal Fistula as a Complication of Percutaneous Transcatheter Ablation of Atrial Fibrillation. *Circulation* **109** , 2724–2726 (2004).
18. Doll, N. *et al.* Esophageal perforation during left atrial radiofrequency ablation: Is the risk too high? *J. Thorac. Cardiovasc. Surg.* **125** (4), 836–842 (2003).
19. Van Driel, V. J. H. M. *et al.* Pulmonary vein stenosis after catheter ablation electroporation versus radiofrequency. *Circ. Arrhythmia Electrophysiol.* **7** (4), 734–738 (2014).
20. Pardo Meo, J. *et al.* Atrial Coronary Arteries in Areas Involved in Atrial Fibrillation Catheter AblationClinical Perspective. *Circ. Arrhythmia Electrophysiol.* **3** (6), (2010).
21. Gallagher, J. J. *et al.* Catheter Technique for Closed-Chest Ablation of the Atrioventricular Conduction System. *N. Engl. J. Med.* **306** (4), 194–200 (1982).
22. Bardy, G. H. *et al.* Catheter Mediated Electrical Ablation - the Relation between Current and Pulse Width on Voltage Breakdown and Shock-Wave Generation. *J. Am. Coll. Cardiol.* **7** (2), A99–A99 (1986).
23. Davalos, R. V., Mir, L. M. & Rubinsky, B. Tissue ablation with irreversible electroporation. *Ann. Biomed. Eng.* **33** (2), 223–231 (2005).
24. Ahsan, A. J., Cunningham, D., Rowland, E. & Rickards, A. F. Catheter ablation without fulguration: design and performance of a new system. *Pacing Clin. Electrophysiol.* **12** (9), 1557–61 (1989).
25. Rowland, E., Cunningham, D., Ahsan, A. & Rickards, A. Transvenous ablation of atrioventricular conduction with a low energy power source. *Br. Heart J.* **62** (5), 361 LP-366 (1989).
26. Ahsan, A. J., Cunningham, D. & Rowland, E. Low energy catheter ablation of right ventricular outlfow tract tachycardia. *Br. Heart J.* **65** (3), 231–233 (1991).
27. Wittkampf, F. H. *et al.* Feasibility of electroporation for the creation of pulmonary vein ostial lesions. *J. Cardiovasc. Electrophysiol.* **22** (3), 302–309 (2011).
28. Neven, K. *et al.* Myocardial Lesion Size After Epicardial Electroporation Catheter Ablation After Subxiphoid Puncture. *Circ. Arrhythmia Electrophysiol.* **7** (4), 728–733 (2014).
29. Lavee, J., Onik, G., Mikus, P. & Rubinsky, B. A novel nonthermal energy source for surgical epicardial atrial ablation: Irreversible electroporation. *Heart Surg. Forum* **10** (2), 96–101 (2007).
30. Wittkampf, F. H. M. *et al.* Myocardial lesion depth with circular electroporation ablation. *Circ. Arrhythmia Electrophysiol.* **5** (3), 581–586 (2012).
31. Neven, K. *et al.* Epicardial linear electroporation ablation and lesion size. *Hear. Rhythm* **11** (8), 1465–1470 (2014).
32. van Driel, V. J. H. M. *et al.* Low vulnerability of the right phrenic nerve to electroporation ablation. *Heart Rhythm* **12** (8), 1838–44 (2015).
33. Davalos, R. V, Rubinsky, B. & Mir, L. M. Theoretical analysis of the thermal effects during in vivo tissue electroporation. *Bioelectrochemistry* **61** , 99–107 (2003).
34. Neven, K. *et al.* Acute and Long-Term Effects of Full-Power Electroporation Ablation Directly on the Porcine Esophagus. *Circ. Arrhythmia Electrophysiol.* **10** (5), e004672 (2017).
35. Paul, T., Bokenkamp, R., Mahnert, B. & Trappe, H.-J. Coronary artery involvement early and late after radiofrequency current application in young pigs. *Am. Heart J.* **133** (4), 436–440 (1997).
36. Neven, K. *et al.* Safety and feasibility of closed chest epicardial catheter ablation using electroporation. *Circ. Arrhythmia Electrophysiol.* **7** (5), 913–919 (2014).
37. Piorkowski, C. *et al.* First in human validation of impedance-based catheter tip-to-tissue contact assessment in the left atrium. *J. Cardiovasc. Electrophysiol.* **20** (12), 1366–1373 (2009).
38. Andrade, J. G. *et al.* Pulmonary vein isolation using 'contact force' ablation: The effect on dormant conduction and long-term freedom from recurrent atrial fibrillation — A prospective study. *Hear. Rhythm* **11** (11), 1919–1924 (2014).
39. Ikeda, A. *et al.* Relationship between catheter contact force and radiofrequency lesion size and incidence of steam pop in the beating canine heart. *Circ. Arrhythmia Electrophysiol.* **7** (6), 1174–1180 (2014).
40. Rosso, R., Chorin, E., Levi, Y., Rogowski, O. & Viskin, S. Radiofrequency Ablation of Atrial Fibrillation: Nonrandomized Comparison of Circular versus Point-by-Point 'Smart' Ablation for Achieving Circumferential Pulmonary Vein Isolation and Curing Arrhythmic Symptoms. *J. Cardiovasc. Electrophysiol.* 1–6 (2016). doi:10.1111/jce.13058
41. van Es, R. *et al.* Novel method for electrode-tissue contact measurement with multi-electrode catheters. *Europace* 1–8 (2017). doi:10.1093/cercor/bhw393
42. Zheng, X. *et al.* Electrode impedance: An indicator of electrode-tissue contact and lesion dimensions during linear ablation. *J. Interv. Card. Electrophysiol.* **4** , 645–654 (2000).

43. Deno, D. C., Sih, H. J., Miller, S. P., Teplitsky, L. R. & Kuenzi, R. Measurement of electrical coupling between cardiac ablation catheters and tissue. *IEEE Trans. Biomed. Eng.* **61** (3), 765–774 (2014).
44. Cinca, J. *et al.* Passive transmission of ischemic ST segment changes in low electrical resistance myocardial infarct scar in the pig. *Cardiovasc. Res.* **40** (1), 103–112 (1998).
45. van Es, R. *et al.* Feasibility of multi-electrode contact measurement as a predictor of long-term success with circular pulmonary vein electroporation ablation (abstract). *Eur. J. Clin. Invest.* **47** (Supplement S1), (2017).
46. Crick, S. J., Sheppard, M. N., Ho, S. Y. E. N., Gebstein, L. & Anderson, R. H. Anatomy of the pig heart: comparisons with normal human cardiac structure. *J. Anat.* **193** (1), 105–119 (1998).
47. Miyazaki, S. *et al.* Clinical Implication of Adenosine Test at Repeat Atrial Fibrillation Ablation. *Circ. Arrhythmia Electrophysiol.* **5** , 1117–1123 (2012).